An investigation op the electrical resistance of thin films of rare earth metals

Lodge, F. M. K.

AN INVESTIGATION OF THE ELECTRICAL RESISTANCE OF THIN FILMS OF RARE EARTH METALS.

by

F.M.K. LODGE B.Sc.

Presented in candidature for the degree of Doctor of Philosophy.

August 1969.

ABSTRACT

Measurements have been made of the electrical resistivity in the film plane of rare earth metal films over a thickness range of 130 Å to 2500 Å. The films are deposited onto glass substrates by high vacuum evaporation at pressures better than 10^{-6} torr and are protected by an over coating of silicon monoxide. The resistivity has been examined between $4.2^{\circ}K$ and room temperature; the magnetoresistance has also been studied in the presence of applied transverse fields up to 15 KOe and longitudinal fields up to 10 KOe.

The variation of resistance with temperature is similar in form to that obtained for bulk specimens for all film thicknesses. However, in films less than about 400 Å thick, the spin-disorder resistivity shows a pronounced decrease in magnitude but the degree of variation did not appear to be consistent with thickness. The spin-disorder resistivity is obtained by computing a least-squares fit to the linear high temperature part of the resistance curve and extrapolating to $0^{\circ}K$.

The results show that in the temperature region where spin-wave theory is applicable, at very low

temperatures $\rho_{spin} \propto T^2$, in accordance with spin-wave theory but at higher temperatures, this falls off, so that $\rho_{spin} \propto T^{3/2}$. It is found that in the first case, the variation of $\rho_{spin}(T)$ can be better explained in terms of an anisotropy energy gap and the change to a $T^{3/2}$ proportionality has been related to the behaviour of the spontaneous magnetization and the anomalous Hall effect.

In addition, the variation of ρ_{spin} of dysprosium is examined in detail and it is suggested that the observed fall off of spin resistivity with thickness, which can be extrapolated to zero at zero thickness, is related to the variation of magnetization with thickness in the film.

Finally, magnetoresistive studies detected negative effects with fields applied transversely to the electric field. The anomalous peak at the Néel point is suppressed in dysprosium and terbium and a small demagnetizing field effect is observed in dysprosium.

CONTENTS

INTRODUCTION

Over the past decade, there has been a fruitful investigation of the properties of the rare earth metals.In particular, neutron diffraction experiments have revealed a variety of complex equilibrium arrangements for the heavy rare earth metals gadolinium through thulium. Gadolinium appears to be a normal ferromagnet, but the other five elements exhibit antiferromagnetism in a certain characteristic range of temperature, and in this region, the ordering assumes a structure which is periodic about the c-axis, either helicoidal or sinusoidal.

In contrast to the iron-group transition metals, theoretical attempts at interpretation of the properties of rare earth metals has met with a good deal of success, with the possible exception of electrical resistivity where, apart from gadolinium, a reliable quantitative treatment is still awaited.

Electrical resistivity is one of the most sensitive and yet one of the most complex physical properties of metals and alloys. It is known to be dependent upon electronic structure, elastic constants and magnetic interactions but the nature of this dependence is not completely understood. In the heavy rare earth metals, magnetic ordering has a profound effect on the resistivity, but while the bulk metals have been extensively researched, comparitively little attention has been paid to thin films. It is proposed to report here some electrical measurements carried out on thin films of the heavy rare earth metals.

CHAPTER ONE

THE MOLECULAR FIELD THEORY OF FERROMAGNETISM

The electrons which cause the magnetic properties of the rare earth metals are in 4f states and are probably tightly bound and localized on parent nuclei. In iron, cobalt and nickel the electrons responsible for ferromagnetism are those which are derived from the 3d states of free ions and are relatively unscreened from neighbouring atoms. They therefore probably exist in states which are itinerant. Molecular field models have been developed for the two limiting cases and the original Weiss model is applicable to electrons which are localized within the positive ions forming the lattice while the collective-electron model due originally to Stoner (1)* and Slater (2) deals with almost-free itinerant electrons. The Weiss model is based on the hypothesis that, when atoms which contain localized, incompletely populated shells condense to form metallic solids, these shells retain their localized character, so that ions at the crystal lattice sites constitute the elementary dipoles which are ordered by exchange forces between them. The use of a molecular field model is equivalent to the neglect of any fluctuations in the degree of order among groups of n neighbouring ions, from point to point in the sample at any one instant or from time to time at a particular point.

* Numbers in brackets indicate references on page 100.

This leads to the field acting on each ionic dipole being written as

$$\underline{H} = \underline{H}_a + \lambda \underline{M} \qquad 1.1$$

where $\underline{H}_a$ is the applied field and $\lambda \underline{M}$ is the molecular field, being proportional to the magnetization $\underline{M}$, with λ the molecular field constant.

It is recalled that the relation between the intensity of magnetization of a paramagnetic sample and the applied field $\underline{H}$ which induces it is

$$M = M_m B_J(\mu_m H/kT) \qquad 1.2$$

M_m is the saturation magnetization which could be attained in an infinite field with all the dipoles of moment μ_m aligned and $B_J(x)$ is the Brillouin function

$$B_J(x) = \frac{2J+1}{2J} \coth \frac{2J+1}{2J} x - \frac{1}{2J} \coth \frac{1}{2J} x$$

where $x = \mu_m H/kT$ and J is the total angular momentum.

The molecular field in a ferromagnetic body is very much greater than any realisable applied field and so neglecting $\underline{H}_a$, from equations 1.1 and 1.2 the expression

$$M_s/M_m = B_J(\mu_m \lambda M_s/kT) \qquad 1.3$$

is obtained, where M_s is the spontaneous magnetization due to the molecular field.

Since M_s appears on both sides of equation 1.3, it is not possible to display M_s as a simple function of T. Instead the variation maybe derived graphically by plotting both sides of equation 1.3 against ($\mu_m \lambda M_s/kT$) and finding the points at which the curves intersect.

It is found that a critical temperature exists above which the only solution is $M_s=0$. This is identified as the ferromagnetic Curie temperature T_c. For temperatures below T_c a plot of M_{s/M_m} versus T/T_c yields a universal curve for a given value of J.

It is found that the Brillouin curve for $J=\frac{1}{2}$ represents the general shape of the experimental variation well, but that it is incorrect in several details. For low temperatures, expansion of the Brillouin function yields (for $J=\frac{1}{2}$, $g=2$) (where g is the Landé factor)

$$M_{s/M_m} = 1 - 2e^{-2x}$$

while the best fit with the experimental data is given by

$$M_{s/M_m} = 1 - \text{const.}T \qquad \text{for } 0 < T/T_c < 0.3$$

The molecular field approach may be extended to cover the behaviour of a ferromagnetic material above its Curie temperature, when it behaves paramagnetically. When M_s falls to zero at T_c, the internal field also falls to zero and remains so, above T_c, unless a magnetic field is applied, which will give a magnetization given by equation 1.2. In this case however, since M_s is small, λM is no longer very much smaller than H_a and only the initial linear portion of the Brillouin function is required, where it has a slope $(J+1)/3J$. Then it follows from equation 1.2 that

$$M = M_m \frac{J+1}{3J} \cdot \frac{\mu_m H}{kT} \qquad 1.4$$

$$\text{ie.} \quad M = M_m \frac{J+1}{3J} \cdot \frac{\mu_m (H_a + \lambda M)}{kT} \qquad \text{since } H = H_a + \lambda M \qquad 1.5$$

so that for the volume susceptibility $\chi = M/H_a = \dfrac{C}{T - T_c}$ 1.6

where $C = \dfrac{M_m \mu_m}{3k} \dfrac{J+1}{3J}$ and $T_c = \lambda C$

Equation 1.6 is known as the Curie-Weiss law and it is found experimentally that from a few degrees above T_c, $1/\chi$ is linear with T, so that the data are in excellent agreement with the Curie-Weiss law.

The origin of the Weiss molecular field was obscure until 1928 when Heisenberg put forward the first theory of ferromagnetism based on exchange interactions. It is assumed that the electrons mainly involved are localized, and the Hamiltonian is then written as

$$\mathcal{H} = -2 \sum_{ij} J_{ij} \, \underline{s}_i \cdot \underline{s}_j \qquad 1.7$$

where the summation is over pairs ij, of interacting ions with a single electron each. When this is generalised to the entire crystal, we have the Heisenberg Hamiltonian

$$\mathcal{H} = -2 \sum_{ij} J_{ij} \, \underline{S}_i \cdot \underline{S}_j \qquad 1.8$$

where J_{ij} is the exchange integral and $\underline{S}_i$ is the total spin of atom i.

Three types of exchange are usually distinguished in the metallic state. Firstly, direct exchange, which is the coupling of spins of atoms which are far enough apart to have almost free atom characteristics. Secondly, itinerant exchange, which is applied to the transition metals, where the itinerant d electrons are likely to form a wide energy band. In these two mechanisms it is the d-d coupling which is of prime importance and the effect of the conduction electrons is considered as a secondary effect. In the third type of exchange, the s-d (or f) interaction, the coupling of inner shells via their conduction electrons is considered explicitly, and it is this interaction which is most clearly applicable to the rare earth metals.

CHAPTER TWO

THE RARE EARTH METALS

2.1 Magnetic Ordering Characteristics.

Neutron diffraction has revealed a variety of complex spin configurations in the magnetically ordered phases of the rare earths. Gadolinium and the heavier rare earth metals crystallise in a simple hexagonal close-packed form and all possess a resultant spontaneous magnetization at sufficiently low temperatures.

In the ferromagnetic phase, the spontaneous moment is parallel to the hexagonal axis in gadolinium and perpendicular to the axis in dysprosium and terbium (Figure 2f). In each case the ordering is a simple parallel alignment of the ions. Below $20^{\circ}K$, erbium possesses a spontaneous magnetization which is parallel to the hexagonal axis and it is due to the more complicated arrangement shown in Figure 2d in which there is a helical distribution of the transverse components of the ionic moments. Holmium has a similar structure below $19^{\circ}K$. Thulium has yet another configuration and at low temperatures possesses an antiphase structure with four layers pointing one way, then three the other (Figure 2a).

In the antiferromagnetic phase, Tb, Dy, and Ho possess the helical, or screw, structure illustrated in Figure 2e. There is ferromagnetic alignment within each layer of ions perpendicular to the hexagonal axis but the direction of alignment changes from one layer to the next.

The antiferromagnetic phases of erbium and thulium are less simple. Above the Curie temperature of 20°K the conical structure of erbium gives way to a structure which has no resultant magnetization (Figure 2c). The transverse moments remain helically ordered but the magnetic scattering amplitude along the hexagonal axis, which measures the moment at an ion over the time of flight of a neutron past it (10^{-13} seconds) varies periodically, reversing every eighth layer. Thulium, in its antiferromagnetic phase, has a simple longitudinal wave structure along the hexagonal axis, reversing every seven layers, and no transverse ordered moments(Figure 2b).

Neutron investigations have also revealed that the lighter rare earth metals Ce, Nd and Eu exhibit helical antiferromagnetism below 4.2°K, 12.5°K and 87°K respectively.

2.2 Electronic Structure.

The elements of the rare earth group have the electronic configuration $(4f)^n 6s^2 5d$, with the exception of europium and ytterbium, which have $(4f)^7 6s^2$ and $(4f)^{14} 6s^2$ respectively. As n increases, the relative stability of the 4f levels is enhanced and they fall increasingly below the outer electrons, both energetically and radially. From neutron diffraction it has been concluded that the root-mean square radius of the 4f charge distribution is about 0.3Å, i.e. of the order of 0.1 of the inter-atomic distance of 3.6Å in the metallic state. Thus the metals can be considered as consisting of tri-positive ions surrounded by a sea of conduction electrons. This view is borne

out by measurements of the high temperature susceptibilities which follow a Curie-Weiss law and possess effective moments extremely close to the free 3+ ion values. Therefore, in calculating the properties of the rare earth metals, it is justifiable to consider an isolated ion initially and subsequently introduce the additional effects due to the metallic environment.

The energy levels are calculated in the usual Hartree-Fock approximation (3-8). The most important contribution is due to the central potential which gives the $4f^n$ configuration. The f-f coulomb interaction is then introduced, which partially removes the degeneracy of the configuration and the resulting terms are specified by the total moments $\underline{L}$ and $\underline{S}$. The term with the lowest energy is given by Hund's Rules (i.e. maximum S and maximum L consistent with this value). In practice this is the only term which it is necessary to consider. The spin-orbit coupling lifts the term degeneracy and the resulting multiplets are specified by the total angular momentum $\underline{J}$. For all the rare earths except Sm^{3+} and Eu^{3+} the spin-orbit coupling is so large that $E_{LS} \gg kT$, where E_{LS} is the multiplet separation, and it is therefore necessary only to consider the ground state J value ($J=L \pm S$).

In a crystal, each rare earth ion is surrounded by other ions on a regular lattice and this gives rise to an electric field (termed the crystal field) of the appropriate symmetry on the ion. The effect of the crystal field is to partially remove the $(2J + 1)$ fold degeneracy of each J level of the free ion so that new levels

occur. For the rare earth metals however, this crystal field splitting E_c is less than kT as is evidenced by the success of the ionic model in accounting for the susceptibilities. The susceptibility is the main effect depending only on the isolated ion and all other properties (magnetic coupling, electrical resistivity) are concerned with the interactions of the ions themselves and the conduction electrons.

2.3 The s-f Exchange Interaction.

This exchange interaction has been studied in detail by several authors (9-12) and for the case of a conduction electron of spin $\underline{S}_e$ and an ion of spin $\underline{S}_j$ it is usually written in the scalar form

$$\mathcal{H} = - G(\underline{S}_j . \underline{S}_e) \qquad 2.1$$

The conduction electrons are scattered under the influence of this interaction and strictly, the exchange energy G should depend on the initial and final k states. The effect of exchange of this type was first examined by Rudermann and Kittel (13) for the coupling of nuclei, by Yosida (14) for the Cu-Mn alloys and by Kasuya (9) for gadolinium, and is called, in consequence, the R-K-K-Y interaction.

As a result of the scattering produced by equation 2.1, the conduction electrons in the neighbourhood of the ion (n) become polarised. This polarisation $P_n(\underline{R})$ is given by

$$P_n(R) = \frac{9\pi Z^2}{4V^2} \frac{G}{E_F} S_n . F(2k_F R) \qquad 2.2$$

where Z is the number of conduction electrons per atom, V is the atomic volume, E_F is the Fermi energy, k_F is the Fermi wave vector,

R is the distance from the ion and

$$F(x) = \frac{(x.\cos x - \sin x)}{x^4}$$

The function F(x), and hence the polarisation, is long range and oscillatory. This polarisation acts on a second spin $\underline{S}_m$ at position $\underline{R}_m$ as : $-G\,\underline{S}_m.P_n(\underline{R}_m)$ and this is equivalent to the coupling

$$\mathcal{H}_{n,m} = -I_{n,m}\underline{S}_n.\underline{S}_m$$

where $I_{n,m} = \frac{9\pi}{4}\left(\frac{Z^2}{V^2}\right)\frac{G^2}{E_F}.F(2k_FR_m)$

Thus the indirect interaction is long-range and oscillatory, a property which derives from the singularity in k at k_F.

The principal problem in applying the R-K-K-Y interaction to the rare earth metals is to correctly include the effect of the spin-orbit coupling on the spins $\underline{S}_n$, $\underline{S}_m$; de Gennes has shown (15) that for $E_{LS} \gg kT$, it is necessary only to make the substitution

$$S_i = (g_J - 1)J_i$$

The model accounts well for the magnetic ordering behaviour of the rare earth metals (15,16,17) with approximately constant values of G, k_F and $\sum_{m\neq n} F(2k_FR_m)$.

The main features of this model have remained intact, despite many attempts to improve upon it. Perhaps the most fundamental improvement is the generalisation of the interaction for a non-spherical Fermi surface (18). In general, the interaction is found to fall off as $1/R^3$ and to oscillate with a period corresponding to a calipering of the Fermi surface in the R-direction.

CHAPTER THREE

METALLIC CONDUCTION

3.1 The Bloch Transport Equation.

The development of the quantitative theory of electron transport by Bloch (19) led to the derivation of the Boltzmann transport equation, which is obtained when an electronic system is described by means of a distribution function $f(\underline{K},\underline{r},t)$, where $\underline{K}$ is the electron wave vector, which is defined such that the number of electrons in the six-dimensional volume element $d\underline{K}.d\underline{s}$ at time t is given by

$$\frac{1}{4\pi^3} f(\underline{K},\underline{r},t)d\underline{K}.d\underline{s}$$

The Boltzmann transport equation is then written as

$$\frac{df}{dt} = -\dot{\underline{K}}\cdot\nabla_K f - \underline{v}\cdot\nabla_r f + \frac{\partial f}{\partial t} + \left(\frac{\partial f}{\partial t}\right)_c \qquad 3.1$$

where $\left(\frac{\partial f}{\partial t}\right)_c$ denotes the rate of accretion of electrons in $d\underline{s}.d\underline{K}$ due to scattering events and $\underline{v}$ is the electron velocity.

In steady-state conditions under the influence of time-independent forces, $\frac{\partial f}{\partial t}=0$ and equation 3.1 becomes

$$\dot{\underline{K}}\cdot\nabla_K f + \underline{v}\cdot\nabla_r f = \left(\frac{\partial f}{\partial t}\right)_c \qquad 3.2$$

The distribution function can be written as the sum of two terms

$$f(\underline{K},\underline{r}) = f_0(\varepsilon) + f_1(\underline{K},\underline{r}) \qquad 3.3$$

where $f_0(\varepsilon)$ is the equilibrium Fermi distribution, $f_1(\underline{K},\underline{r})$ is the deviation of the true distribution from equilibrium, and ε is the electron energy. It is also convenient to write

$$f_1 = -\varphi(\underline{K},\underline{r})\frac{\partial f_0}{\partial \varepsilon} \qquad 3.4$$

Then, linearization in f_1 of the Boltzmann equation leads to an integral equation

$$e\left[\underline{E} + \frac{1}{c\hbar}\underline{\nabla}_K \epsilon \times \underline{H}\right].\frac{1}{\hbar}\underline{\nabla}_K f(\underline{K},\underline{r}) + \frac{1}{\hbar}\underline{\nabla}_K \epsilon . \nabla f(\underline{K},\underline{r})$$

$$= \frac{1}{kT}\int \mathcal{S}(\underline{K},\underline{K}').f_o(\epsilon).\left[1 - f_o(\epsilon')\right].\left[\varphi(\underline{K}') - \varphi(\underline{K})\right] d\underline{K}' \qquad 3.5$$

where e is the electronic charge, c is the velocity of light and $\mathcal{S}(\underline{K},\underline{K}')$ is the probability per unit time that an electron in the state $\underline{K}$ will be scattered into the state $\underline{K}'$.

$e\left[\underline{E} + \frac{1}{c\hbar}\underline{\nabla}_K \epsilon \times \underline{H}\right]$ is the force acting on an electron as a result of an electric field $\underline{E}$ and a magnetic field $\underline{H}$.

Equation 3.5 is known as the Bloch equation and in general, a solution cannot be obtained in a closed form. The Bloch equation may be solved by two methods. Firstly, by a relaxation time approximation and secondly, by a variational principle.

3.2 Solution of the Bloch Equation.

a) The relaxation time approximation.

This method relies on the use of a relaxation time τ, defined by

$$\left(\frac{\partial f}{\partial t}\right)_c = -\frac{f - f_o}{\tau} = -\frac{f_1}{\tau} \qquad 3.6$$

By means of equation 3.6, the Bloch integral equation can be reduced to the steady-state distribution function

$$\varphi = \tau \underline{P}.\underline{v} + \frac{e\tau}{c\hbar^2}\left(\underline{H}.\underline{\Omega}\varphi\right) \qquad 3.7$$

where $\underline{\Omega}$ is the operator $\underline{\nabla}_K \epsilon \times \underline{\nabla}_K$ and $\underline{P} = e\underline{E} - (\epsilon - E_F)\underline{\nabla} \ln T$ where T is the absolute temperature.

For the simplest case of $\underline{H} = 0$, the solution of equation 3.7 is

$$\varphi = \tau \underline{P}.\underline{v} \qquad 3.8$$

Examination of the validity of equation 3.6 in order to justify the simplification which it allows reveals that a meaningful relaxation time $\tau(\underline{K})$ can be defined whenever the energy change of an electron per collision is small compared to kT i.e. in the limit of elastic scattering. Application of this criterion to electron-phonon (e-p) scattering has shown that this relaxation mechanism is quasi-elastic only at high temperature, when $kT > k\Theta_D$. At $T < \Theta_D$, phonon energy is comparable to kT and consequently e-p scattering is inelastic. Here, Θ_D is the Debye temperature.

In collision processes, the transition probability for scattering is generally proportional to the number of scattering centres. In the case of e-p scattering, the number of scattering centres is the number of phonons which exist in the lattice at thermal equilibrium. At high temperatures, the number of phonons is proportional to the absolute temperature. Consequently in that temperature range $\tau \propto 1/T$, which follows from equation 3.6.

Analysis of the electrical conductivity based on a relaxation time approximation and assuming a spherical energy surface, gives, from equation 3.8

$$\sigma = \frac{\underline{J}}{\underline{E}} = \frac{n_o e^2 \tau_\sigma(E_F)}{m^*} \qquad 3.9$$

where n_o is the density of conduction electrons, $\underline{J}$ is the current density, $\underline{E}$ is the electric field, m^* is the effective mass and E_F is the Fermi energy.

Therefore, in the high temperature range, the electrical conductivity $\sigma \propto 1/_T$. This prediction is substantiated experimentally.

In order to derive any meaningful prediction of conductivity when $T < \Theta_D$, the conductivity relaxation rate is modified to allow for small angle inelastic scattering of electrons, which is caused by the vibrational spectrum being dominated by phonons with wave vectors $q << q_o$, where q_o is the Debye wave vector, and of average energy $\simeq kT$. This leads to an electrical conductivity inversely proportional to T^5, which again is experimentally confirmed in pure metals.

At extremely low temperatures, even in the purest specimen, the relaxation mechanism which arises from elastic scattering of electrons by impurities, ultimately takes pre-eminence over the diminishing e-p scattering. Thus, at sufficiently low temperatures, elastic scattering is once again the dominating mechanism and the collision integral can again be characterised by a meaningful relaxation time.

b) <u>The variational method.</u>

Although the relaxation time approximation appears attractive, it has been shown that situations exist in which it is inapplicable. Here, the more general variational method is used (20,21,22) to solve the Bloch equation.

The first step in a proper variational calculation of the resistivity is the selection of a trial function. At high temperatures, and also at sufficiently low temperatures where impurity scattering dominates, from equation 3.8

$$\varphi(\underline{K}) = \tau \underline{P}.\underline{v}_K \qquad 3.10$$

The assumption of a spherical Fermi surface enables $\underline{v}_K$, the electron velocity in state $\underline{K}$, to be replaced by $\hbar\underline{K}/m^*$ and the trial function then takes the form

$$\varphi(\underline{K}) = \underline{K}.\underline{E} = EK_x \qquad 3.11$$

where the electric field E is along the x-direction.

The analytic calculation of the resistivity has been dealt with in detail (23,24) and the derived expression for the resistivity is

$$\rho_i(T) = 4\mathcal{R}\left(\frac{T}{\Theta}\right)^5 \mathcal{J}_5\left(\frac{\Theta}{T}\right) \qquad 3.12$$

Here $\mathcal{R} = \dfrac{3\hbar q_o^6 G(0)}{16.e^2 k\Theta_D k_F^4 \upsilon_F^2}$ where $G(0) = \dfrac{4}{9}\pi \dfrac{E_F^2}{N_P M_C}$

and $\mathcal{J}_5(x) = \displaystyle\int_o^x \frac{z^5 dz}{(e^z - 1)(1 - e^{-z})}$ is the transport integral of order 5.

υ_F is the Fermi velocity, k_F is the Fermi wave vector, k is Boltzmann's constant, N_P is the number of scattering processes, M_C is the mass of the crystal ion and Θ is the Debye temperature derived from the resistivity. It is assumed that $\rho_i(T)$, the ideal resistivity, is given by Matthiessen's rule

$$\rho(T) = \rho_i(T) + \rho_r \qquad 3.13$$

where $\rho(T)$ and ρ_r are the total and residual resistivities.
The equations 3.12 comprise the Bloch-Gruneisen formulae, which reproduce the temperature dependence of the ideal resistivity of many metals with surprising accuracy.

At high temperatures, $\Theta/T = x \ll 1$ and $\mathcal{J}_5(x) = \frac{1}{4}x^4$

and from equation 3.12 $\rho_i(T) = \mathcal{R}\dfrac{T}{\Theta} \qquad T \gg \Theta \qquad 3.14$

Equation 3.14 predicts the linear increase of $\rho_i(T)$ with T at high temperature.

At low temperatures, $x \gg 1$ and $\mathcal{J}_5(x)$ is evaluated at 124.4,

then $$\rho_i(T) = 497.6\,\mathcal{R}\left(\frac{T}{\Theta}\right)^5 \qquad T \ll \Theta \qquad 3.15$$

Here the Bloch theory predicts a T^5 law for the ideal resistivity. This, as well as the linear dependence of $\rho_i(T)$ at high temperatures confirms the results obtained from the relaxation process using much simpler physical arguments.

3.3 Ferromagnetic Metals.

The electrical behaviour of ferromagnetic metals reveals a variety of peculiarities that appear to be intimately related to their unusual magnetic properties. The electrical resistivity is believed to come from two main sources. The first is due to the scattering of conduction electrons by the lattice vibrations, which is the principal cause of the linear increase of $\rho(T)$ above the Curie temperature T_c. Unlike normal metals, extrapolation of this line to $T = 0^{\circ}K$ does not intersect the ordinate at $\rho \simeq 0$, which points to an additional resistance contribution associated with the interaction of the conduction electrons with the magnetic spin system. In the disordered paramagnetic region, ρ_{spin} is constant with temperature. Matthiessen's rule (equation 3.13) acquires an additional term and becomes,

$$\rho(T) = \rho_i(T) + \rho_r + \rho_{spin} \qquad 3.16$$

A further classification arises because these metals have two overlapping bands at the Fermi energy, an s band and a d band. Thus, in both the phonon case and the spin-wave case the scattering may take place within a single band or may involve s-d transitions.

The single band phonon scattering has been described by the Bloch theory and leads to a T^5 dependence at low temperatures and a T dependence above the Debye temperature. Less well understood however, is the phonon scattering involving s–d transitions. This mechanism was first suggested by Mott (25), who considered a metal in which a fairly broad 4s conduction band overlaps a much narrower 3d band. Under the influence of lattice vibrations, an s electron may be scattered into an empty state in the s or d band. Since lattice scattering cannot induce spin flips in lowest perturbation theory, an s↑ electron is considered to scatter into either an empty s↑ or d↑ state, and similarly for an s↓ electron. The principal influence on the resistivity is through the magnetization-dependent relaxation rates $\tau_{sd}^{\uparrow}$ and $\tau_{sd}^{\downarrow}$ and Wilson (26) has shown that the resistivity due to s–d scattering varies as T^3 at low temperatures but, like the single band case, varies as T above the Debye temperature. In its simplest form, the band model cannot account for the occurrence of an antiferromagnetic arrangement, nor a Curie–Weiss law in the paramagnetic region.

An alternative explanation for the resistivity of ferromagnetic metals is based on the Heisenberg model. The additional resistivity is now a consequence of scattering of s electrons by localized spins through the mechanism of exchange interaction. At high temperatures, i.e. near T_c , the theory relies on a molecular field approximation, whereas at low temperatures the process can be discussed in terms of scattering of conduction electrons by spin-waves.

In contrast to the s–d interaction mechanisms, where the basic

electron-phonon or electron-impurity interactions are not altered, spin-disorder scattering is a new interaction, and in this theory the resistivity is increased not by the enhancement of an existing relaxation rate, but by the addition of an altogether new one. Vonsovski (27) appears to have been the first person to recognise that an additional contribution to the resistivity would occur in ferromagnets as a result of the exchange interaction. Subsequently, Turov (28) used a spin-wave treatment to show that the s-d interaction leads to a T^2 variation of the magnetization resistivity at low temperatures.

A qualitative description of the temperature dependence of the spin-wave resistivity was given independently by Kasuya (29). Representing the s-d interaction by a molecular field, he obtained an expression

$$\rho_{spin} = \left(\frac{3\pi Nm^*}{2\hbar e^2 E_F}\right).G^2(g - 1)^2 J(J + 1) \qquad 3.17$$

where N is the number of atoms per unit volume and G is the exchange energy, which predicts a constant spin-disorder term at high temperatures. A similar approach was developed by de Gennes and Friedel (30), who examined the effects of short range order in the vicinity of the Curie temperature.

Kasuya (31) later employed a spin-wave description of the interaction to derive a low temperature expression for ρ_{spin}. He obtained the expression

$$\rho_{spin} = \frac{\pi^2}{8}\frac{Z}{N}\frac{m^*}{e^2}\frac{G^2}{\hbar E_F}(g - 1)^2 J.\left(\frac{kT}{k_F^2 \mathcal{D}}\right)^2 \qquad 3.18$$

where Z is the number of conduction electrons per atom, $\mathcal{D}$ is a constant

and the other symbols have their usual meaning. Exactly the same result was obtained by Mannari (32) for the case of zero-orbital angular momentum (g=2, J=S). However, while the Kasuya-Mannari result may explain the behaviour of ρ_{spin} at temperatures very small compared with the Curie temperature, it fails to account for the linear behaviour which sets in at temperatures low enough for spin-wave theory still to be a good approximation.

Dekker and van Peski-Tinbergen (33) developed the molecular field model further from that of Kasuya and de Gennes and Friedel by including the effect of the energy transfer between the conduction electrons and the spin system. They obtain the expression

$$\rho_{spin}(T) = \frac{3\pi N m^* G^2}{2e^2\hbar E_F}\left\{S(S+1) - \varkappa^2 - \varkappa \tanh\left[\frac{3T_c\varkappa}{2T.S(S+1)}\right]\right\} \qquad 3.19$$

where $\varkappa$ is the average atomic spin. This differs from the corresponding formula of de Gennes and Friedel in the final term, which includes the energy transfer effect.

3.4 Metallic Thin Films.

The concept of resistivity as an intrinsic property of a metal is meaningful only under the assumption that the electrical properties of a given specimen are independent of its shape and size. However, the resistivity may still be defined as

$$\rho = \frac{A}{L}.R \qquad 3.20$$

where A is the cross-sectional area, L is the length and R is the resistance of the specimen, even though ρ proves to be a function of A and/or L.

Experimentally, the conditions under which the resistivity becomes a function of the sample dimensions are obvious. As long as the distance between the boundaries of the sample are very much greater than the electronic mean free path (l_f) in the bulk material, the presence of these boundaries will not significantly influence the intrinsic transport properties. However, when one or more dimension approaches l_f, a significant fraction of the electrons will strike and be scattered at the surface rather than in the bulk. If the surface of the film scatters conduction electrons inelastically, thereby artificially limiting l_f, the resistivity is increased above the bulk value and is a function of thickness. On the other hand, if electrons are specularly reflected from the surface, the resistivity of the film is the same as that of the corresponding bulk material and is independent of film thickness for an isotropic Fermi surface.

Surface scattering is very rarely specular since this type of wave reflection requires that surface irregularities be smaller than the wavelength. The de Broglie wavelength of electrons on the Fermi surface $\lambda_F = 2\pi/k_F$ is of the order of one inter-atomic distance in metals. It is obviously impossible to meet such a stringent requirement macroscopically. Chopra and Bobb (34) have obtained a value of $p = 0.8$, where p is the fraction of electrons specularly scattered at the surface, for single crystal gold films grown on mica.

It is interesting to note however, that specular reflection has been observed by Ennos (35) who obtained resistivity values close to that of bulk for annealed gold films grown on bismuth oxide at

thicknesses of only 60 Å. Lucas (36) has extended this work and has shown that it is possible to affect the resistance of a 'single crystal' film by depositing other metals or insulators on top of them.

The theory or transport in thin films rests on the solution of the Boltzmann equation (3.1) subject to appropriate boundary conditions. The strict analysis was first given by Fuchs (37) and elaborated by Sondheimer (38). The problem is essentially a one-dimensional one and for the case of diffuse scattering the solution must be such that the distribution function for electrons immediately adjacent to and travelling away from the surface is the equilibrium distribution. Using this boundary condition, the Boltzmann equation is solved to give, for very thin films

$$\frac{\sigma}{\sigma_o} = \frac{3}{4}\xi . \log \frac{1}{\xi} \qquad \xi = a/l_f \ll 1 \qquad 3.21$$

where σ_o is the bulk conductivity and a is the film thickness.

In the limiting case for thick films

$$\frac{\sigma}{\sigma_o} = 1 - \frac{3}{8\xi} \qquad \xi \gg 1 \qquad 3.22$$

These expressions can be interpreted simply in terms of a reduction of the mean free path due to surface scattering. Mayer (39) has compromised these two extremes with the equation

$$\frac{\sigma}{\sigma_o} = \frac{3}{4}\xi . \left(\log \frac{1}{\xi} + 0.4228\right) \qquad 3.23$$

When one considers practical values, l_f is of order of 100 Å, so that a film with $\xi = 0.1$ will be one which it may be just possible to realize as a continuous sheet. It can certainly be stated that lower values of ξ will give a film with an island structure. In this case,

the conduction mechanism is now that between discontinuous islands so that the above equations no longer apply. Equation 3.23 is the most satisfactory approximation for practical cases.

The situation described above has assumed that electrons will be diffusely scattered from the inside surfaces of the film. It is possible to modify the results by introducing the specular scattering parameter p. Consideration of this parameter modifies the boundary condition of the distribution function and Sondheimer has shown that the equations 3.21 and 3.22 become

$$\frac{\sigma}{\sigma_o} = \frac{3}{4} \cdot \frac{1+p}{1-p} \cdot \xi \cdot \log \frac{1}{\xi} \qquad \xi \ll 1 \qquad 3.24$$

$$\frac{\sigma}{\sigma_o} = 1 - \frac{3(1-p)}{8\xi} \qquad \xi \gg 1 \qquad 3.25$$

and Mayer's equation (3.23) becomes

$$\frac{\sigma}{\sigma_o} = \frac{3}{4}\xi \left(1 + 2p\right)\left(\log \frac{1}{\xi} + 0.4228\right) \qquad 3.26$$

This allows for specular reflection but has assumed that the value of p is the same for both surfaces. If this is not the case, so that p = p at one surface and q at the other, then the equations are further modified as has been shown by Lucas (36). The complete equation for the conductivity ratio then becomes

$$\frac{\sigma}{\sigma_o} = 1 - \frac{3}{4\xi}\int_0^1 \frac{(T - T^3)\{1 - \exp(-\xi/T)\}}{1 - pq\{\exp(-2\xi/T)\}} \cdot \left[2 - p - q + (p+q-2pq)e^{-\xi/T}\right] dT \qquad 3.27$$

for the case of $\xi \gg 1$, this equation can be approximated to

$$\frac{\sigma}{\sigma_o} = 1 - \frac{3(2 - p - q)}{16\xi} \qquad 3.28$$

but there is no satisfactory expression for $\xi \ll 1$.

3.5 Ferromagnetic Thin Films.

The theory of ferromagnetism in thin films was proposed in 1946 by Kittel (40), who showed that for thicknesses smaller than approximately 3000 Å, a stable, energetically favourable situation occurs for magnetization parallel to the film. The relation of the saturation magnetization of such a domain to the structure, thickness and temperature of a thin film is an important problem, the more so because these relations intrinsically affect the resistivity of a ferromagnetic film. The principal models of thin film magnetization are described here and their predictions summarised.

a) The Heisenberg Trace Method.

This model is more suitable at high temperatures and leads in first order approximation to the molecular field model, whose basis is the replacement of the exchange spin-spin interaction by an interaction of each spin with a molecular field given by the whole set of other spins. This method was fully developed for thin films by Valenta (41). The model predicts that the Curie temperature and therefore the magnetization at a given temperature,

is reduced. However, while the molecular field approximation gives a qualitatively correct explanation for the temperature dependence of the bulk magnetization, it predicts a Curie temperature which is too high by 60%. The next higher approximation, the Bethe - Peierls - Weiss (B.P.W.) approximation, which essentially eliminates this error, has been successfully used by Pearson (42) in improving the molecular field approach by making the B.P.W. theory suitable for thin films. In the B.P.W. approximation, each spin-carrying atom interacts with its nearest neighbours and the effect of the other spins is represented as a molecular field effect. Pearson found that the Curie point is reduced by only a small percent from the bulk value, even for 8-layer films. For a film of twenty layers, the magnetization falls off quickly at the surface to 60% of its value at the centre of the film.

Corciovei (43) has added another improvement to the molecular field theory. He has developed the Heisenberg trace method for thin films, calculating the second-order approximation of the partition function. The main result of the second-order approximation using an isotropic exchange Hamiltonian was that an ideal monatomic film cannot support ferromagnetism.

b) Spin-Wave Theory.

Low temperature theoretical studies of spontaneous magnetization were initiated by Bloch. He predicted that a

two-dimensional lattice would be non-ferromagnetic while the bulk material would be ferromagnetic, with the decrease of magnetization with temperature being proportional to $T^{3/2}$. The transition between the two-dimensional and three-dimensional case in cubic lattices was first examined by Klein and Smith (44), using a spin-wave approach. They calculated the magnetization to fall off as T^n, with $n < 3/2$. Later, Glass and Klein (45) applied this theory to lattices other than simple cubic ones. Their calculation of relative magnetization as a function of temperature and film thickness predicted strong deviations from the Bloch $T^{3/2}$ law and these deviations were appreciable in films thinner than about 100 atomic layers.

Qualitatively, the results obtained from the simple spin-wave theory are the same as those from the molecular field approach. Bulk magnetization is retained to well below 1000 Å thickness at low temperatures. The Curie temperature may be expected to decrease as the thickness decreases.

Doring (46) was the first to apply the proper boundary conditions in a spin-wave treatment. He allowed for a small anisotropy field uniform through the sample. In the case of a simple cubic lattice, he maintained that as the anisotropy field goes to zero, the thin-film magnetization still falls off more rapidly than $T^{3/2}$ but not so rapidly as that of Klein and Smith; the dominant cause of the difference arising in the boundary

conditions.

In contrast to the Bloch theory modifications above, Corciovei (47) has developed the spin-wave theory for thin ferromagnetic films by the more sophisticated Holstein-Primakoff approach (48). Wojtczak (49) and Davis (50) have furthered this theory and have shown that under certain conditions, the theoretical thin-film magnetization may

a) fall off essentially as $T^{3/2}$

b) fall off faster than $T^{3/2}$ and show a thickness dependence

c) fall off slower than $T^{3/2}$, again with a thickness dependence.

Most recently, Szczeniowski and Wojtczak (51) have introduced a more sophisticated theory, based on Valenta's model of the sublattices (52). The thin film is considered as a superposition of monatomic layers and the assumptions made are that the periodicity conditions are satisfied in the plane of a layer and that the lack of a part of nearest neighbours for the boundary layers is taken into account in the direction perpendicular to the surface. The decrease in Curie temperature occurs for very thin films with the increasing role of the surface states, whose strong influence leads to the fact that the ferromagnetic properties can only appear beginning from about five layers.

3.6 The Rare Earth Metals.

The heavy rare earth elements Tb - Tm have been shown to (53) display a complex ordering of their magnetic moments at low temperatures. Below a Néel point, they all exhibit an antiferromagnetic structure with a wave-like variation of one or more of the components and at a lower Curie point there is a transition to a structure with a ferromagnetic moment.

These structures have been shown (54,55,56) to be a consequence of a long-range exchange interaction via the conduction electrons, which imposes the wave variation on the moments and a large anisotropy arising from the crystalline electric field. Resistivity measurements (57-61) show that the transport properties can reflect these transitions in a complex way. There is normally a sharp rise in the resistivity as the temperature decreases through the Néel point, followed by a maximum at a lower temperature and a sudden decrease at the Curie point. These effects are very anisotropic, being large only in the direction of the hexagonal c-axis. In the plane perpendicular to this axis, the resistivity decreases as the magnetic order increases.

Boas and Mackenzie (62) have shown that the resistivity at any temperature of a hexagonal polycrystalline sample can be related to the single crystal resistivities by the relationship

$$\rho_{poly} = (2\rho_{\perp} + \rho_{\parallel})/3 \qquad 3.29$$

where $\rho_{\perp}$ and $\rho_{\parallel}$ are the resistivity values perpendicular and parallel to the c-axis.

The anomalies in the resistivity have been discussed by Elliott and Wedgewood (63) in terms of two types of ordering which may occur together in the rare earth metals. Along the c-axis, the moment variation is a longitudinal wave and the moment on an atom at $\underline{R}_n$ is

$$\mu_n^z = g\mu_B JM'.\sin(\underline{q}.\underline{R}_n + \delta) \qquad 3.30$$

where g is the Lande factor, μ_B is the Bohr magneton, $\underline{q}$ is the spin-wave vector, J is the total angular momentum and $JM' = \langle J_z \rangle$. This structure occurs in the high temperature phase of Er and Tm. For moments in the basal plane, the structure is a helix and

$$\mu_n^x = g\mu_B JM.\cos(\underline{q}.\underline{R}_n) \qquad 3.31$$

where $JM = \langle J_{\perp} \rangle$

$$\mu_n^y = g\mu_B JM.\sin(\underline{q}.\underline{R}_n) \qquad 3.32$$

This structure occurs in the high temperature phase of Dy, Tb and Ho. M and M' determine the degree of order and are functions of temperature.

This type of ordering produces an exchange field for the conduction electrons of lower symmetry than the lattice, introducing new boundaries into the Brillouin zone perpendicular

to the c-axis. As a result of this, the Fermi surface is distorted and on this basis, the essential features of the $\rho(T)$ curves for Tb, Dy, Ho and Er have been reproduced with various degrees of accuracy. Recently, the resistivity of single crystal thulium has also been interpreted in this way (64).

Finally, Rocher (65) has pointed out that the s-f interaction (equation 2.2) can be combined with the molecular field model expression for ρ_{spin} (equation 3.17) to give an expression for θ_p , the paramagnetic Curie temperature

$$k\theta_p = \frac{3\pi Z^2 G^2 (g-1)\, J(J+1)}{E_F V^2} \sum_{n \neq o} F(2k_F R_{on}) \qquad 3.33$$

Rocher has calculated the sum in equation 3.33 for various structures. With Z=3 and for a hexagonal structure with a lattice ratio of $c/_a = 1.58$, this sum is equal to $-6.5.10^3$. It is then possible to derive the effective mass and exchange energy as

$$m^*/_{m_o} = 7.7\left[\rho_{spin}/\theta_p\right] \qquad 3.34$$

and

$$G = \frac{m_o}{m^*}\left[\frac{9.6\ \rho_{spin}}{(g-1)^2 (J+1)}\right]^{\frac{1}{2}} \qquad 3.35$$

where m_o is the free electron mass and the other symbols have their usual meaning.

3.7 The Anomalous Hall Effect.

It is well known that if a metal sample in which a primary current $\underline{j}_y$ is flowing, is subjected to a magnetic field $\underline{B}_z$, a potential $\underline{E}_x$ is created such that

$$\underline{E}_x = -R_o(\underline{j}_y \wedge \underline{B}_z) \qquad 3.36$$

where R_o is the normal Hall coefficient (66).

The Hall resistivity ρ_H, is defined as the transverse Hall electric field per unit longitudinal current density

$$\text{i.e.} \qquad (\rho_H)_{xy} = E_x/j_y \qquad 3.37$$

$$\text{and} \qquad \rho_H = R_o B \qquad 3.38$$

Studies of the Hall effect in ferromagnetic materials (67) have indicated the presence of a term dependent on the magnetization, as well as the ordinary term linear in the magnetic field. This additional term has been identified as the 'anomalous' or 'spontaneous' Hall coefficient and it is now well established that for a ferromagnetic metal, the Hall resistivity can be written

$$\rho_H = R_o B + R_s 4\pi M \qquad 3.39$$

where R_s is the anomalous Hall coefficient and M is the spontaneous magnetization.

Initial attempts to explain the anomalous Hall effect were made by Karplus and Luttinger (68), based on an intrinsic spin-orbit

coupling of the magnetic electrons which are also charge carriers. In their model, this interaction led to an asymmetric scattering of the electrons and a resulting Hall-type transverse electric field. Such a model would not be expected to explain the anomalous Hall effect in the rare earths, due to the highly localized magnetic electrons which do not participate in conduction.

More recently, Kondo (69) has shown that an anomalous Hall effect can result from the s-d (or s-f) electron spin-spin interaction, which in principle also describes the resistivity of the rare earths. Maranzana (70) has also given a very thorough treatment of the Hall effect based on Kondo's model.

Using a molecular field approximation, Irkhin and Abel'skii (71) have calculated the anomalous Hall effect considering both the intrinsic spin-orbit coupling of the magnetic electrons and the s-d 'mixed' coupling. They obtain for both mechanisms an expression for R_s:

$$R_s = \frac{9\pi}{64}\left(\frac{J_o}{E_F}\right)^2 \frac{m^* \lambda^{eff}}{e^2 N\hbar M_s(0)} \cdot \left[\frac{1}{4} - \gamma^2\right] \qquad 3.40$$

where λ^{eff} is the effective spin-orbit coupling constant, m* is the effective mass, J_o is the exchange integral, E_F is the Fermi energy, N is the number of atoms per unit volume, $M_s(0)$ is the zero degree magnetization and $\gamma = \frac{1}{2}\left[\frac{M_s(T)}{M_s(0)}\right]$ where $M_s(T)$ is the

spontaneous magnetization at a given temperature.

By making use of the expression for the spin-disorder resistivity (ρ_{spin}) from the Kasuya-Mannari theory (31,32), equation 3.40 is reduced to

$$R_s = \pm \frac{3}{16} \frac{\lambda^{eff}}{E_F} \frac{\rho_{spin}}{M_s(0)} \qquad 3.41$$

which predicts R_s proportional to ρ_{spin}.

Also, by further simplifying equation 3.40, Irkhin and Abel'skii have derived the expression

$$R_s = C\left[M_s^2(0) - M_s^2(T) \right] \qquad 3.42$$

where C is a constant. This relationship has also been proposed by other authors (72,73) and Kikoin and Igosheva (74) have used equations 3.41 and 3.42 to make the identification

$$\rho_{spin} = B\left[M_s^2(0) - M_s^2(T) \right] \qquad 3.43$$

where B is a constant.

Using a spin-wave approximation, Kagan and Maksimov (73) have calculated a T^4 dependence for R_s at low temperatures with a transition to a T^2 dependence at higher temperatures. The region of transition from T^4 to T^2 depends to a considerable degree on the nature of the Fermi surface. The presence of 'protuberances' in the Fermi surface will result in the transition to the T^2 dependence at comparitively low temperatures. Rhyne (75) has found that for the

rare earths the T^2 dependence is realized at very low temperatures, owing to the complexity of the Fermi surface and that equation 3.41 is satisfied at low temperatures. Rhyne also found that equation 3.42 is obeyed over the same low-temperature range as the T^2 dependence found from spin-wave theory.

CHAPTER FOUR

THIN FILM PREPARATION

4.1 Choice of Method.

Thin solid films may be prepared by several different methods, the principal techniques for the deposition of metallic films being:

a) Electrodeposition.

b) Chemical precipitation.

c) Thermal decomposition on a heated substrate of a metal halide or of a metal carbonyl gas.

d) Explosion of metal wires in an inert gas.

e) Chemical reaction of a metal halide and water vapour to form a metal oxide.

f) Cathodic sputtering of metal or metal oxides in a low pressure glow discharge.

g) Vacuum evaporation of metals and thermally stable compounds.

Of these methods, only the last two are capable of being controlled so that high quality films having thicknesses ranging between 100 Å and 3000 Å can be produced. The choice between the two rests largely on the substance to be deposited. Cathodic sputtering is very suitable for the preparation of complex compounds in thin film form, since, as the temperature is low,

they sputter without decomposing. Low vapour pressure metals may also be more easily deposited by sputtering because of the practical difficulties of providing very high temperature sources. However, it is not easy to prepare metal films free from oxide contamination by cathodic sputtering unless great care is taken to exclude all traces of oxygen from the sputtering atmosphere. The pressure range for cathodic sputtering is 10^{-2} torr to 10^{-1} torr and for vacuum evaporation 5.10^{-4} torr and less. Providing the required low pressure can be attained, film deposition is more rapid by vacuum evaporation and a higher quality film is obtained.

The heavy rare earth metals have a high affinity for oxygen, even in the bulk form, and since their melting points are only in the region of 1500°C, it appears that evaporation is the more suitable method of the two, where speed of evaporation in high vacuum will most effectively reduce contamination by oxygen and water vapour.

4.2 Factors affecting the growth of films.

a) Film nucleation.

The nucleation of thin films condensed from the vapour phase onto substrates held at temperatures lower than that of the evaporating source has been treated by Pound et al. (76), Sears

and Cahn (77), Walton (78) and Rhodin and Walton (79). Just after impingement, an atom can either stick permanently to the substrate or re-evaporate in a finite time or, far less frequently, bounce off the substrate on impingement. The probability that an adsorbed atom re-evaporates is

$$W = \psi \exp\left(Q_{ad}/kT\right) \qquad 4.1$$

where ψ is the frequency factor for the adsorbed atom ($\sim 10^{14}$ sec^{-1}), Q_{ad} is the binding energy of the atom to the substrate and T is the temperature of the adsorbed atom. The relative size of Q_{ad} to kT determines the residence time of the adsorbed atom. If the adsorbed atoms equilibriate thermally with the substrate immediately on impingement, T would be the substrate temperature. This is assumed to be the case in the following treatment.

If Q_{ad} is very large compared to kT, re-evaporation is very unlikely. This situation is encountered for very low substrate temperatures or for metal substrates. However, if the substrate is inert towards the film atoms, and this is frequently the case for substrates such as glass or plastics, Q_{ad} will be small and the probability of re-evaporation will be high.

The number of atoms returning to the vapour phase per second for a certain coverage of adsorbed atoms will be the product of the number of adsorbed atoms and the probability of evaporation,

$$N\uparrow = N_{ad}\,\psi \exp\left(Q_{ad}/kT\right) \qquad 4.2$$

where $N\uparrow$ is the number of re-evaporating atoms/cm^2/sec and N_{ad} is the number of adsorbed atoms/cm^2.

A steady state exists if the number of re-evaporating atoms equals the number of impinging atoms

$$N\downarrow = N\uparrow \qquad 4.3$$

Under this steady state condition, the substrate coverage is therefore a function of the deposition rate $N\downarrow$ and

$$N_{ad} = \frac{N\downarrow}{\psi} \exp\left(-Q_{ad}/kT\right) \qquad 4.4$$

Condensation of a permanent deposit may thus be impossible even if the substrate temperature is so low that the evaporation rate of the film material in its bulk form at that temperature is negligible. However, condensation of a permanent deposit on the substrate does occur at sufficiently high impingement rates because of the interaction between adsorbed single atoms. Adsorbed atoms can migrate over the surface, giving rise to collisions with other atoms, and aggregates of adsorbed atoms are formed. These aggregates should be more stable towards re-evaporation than single adsorbed atoms, since they are bound together by the condensation energy. As long as the aggregates are very small, their surface-to-volume ratio is very high and the resulting high total surface energy makes the aggregates less stable and the probability

of re-evaporation is high. Consequently, there is a point where the aggregate has reached a critical size of minimum stability when the addition of another atom will make it more stable.

Nucleation theory states that there will be a barrier to the condensation of a permanent deposit if the size of the critical nucleus is at least two atoms. If there is a nucleation barrier, the film will show an island structure in the initial stages of growth. A film grown under the conditions of a large nucleation barrier will consist of a few large aggregates and will be discontinuous up to relatively high average film thickness. On the other hand, a small nucleation barrier produces a film which consists of many small aggregates which will become continuous at relatively low thickness.

The size of the critical nucleus is dependent on temperature and so increasing the substrate temperature at a constant deposition rate will increase the size of the critical nucleus. Furthermore, an island structure will persist to a higher average coverage than at low temperatures.

b) The melting point of the deposit.

Levinstein (80) has shown that both the size and orientation of the crystals in evaporated metal deposits can be correlated to their melting points. Films formed from high melting point metals consist of micro-crystals with no specific orientation,

whilst films of low melting point metals produce large crystals which are orientated preferentially to the substrate. This agrees well with the theoretical prediction that high boiling point metals have a smaller critical nucleus than low boiling point metals and should therefore become continuous at smaller average film thickness.

c) The adsorption of residual gases.

The residual gases present during evaporation may have an important effect on both the structure and purity of the condensed surface. Stahl (81) studied the oxidation of a number of metals deposited onto a specimen surface inside an electron diffraction camera at a gas pressure of 10^{-5} torr. Stahl concluded that oxidation may occur either while the metal is in transit or during condensation. Other tests showed that a substrate temperature in excess of 300°C is generally required to oxidise a metal film after condensation, whereas the substrate temperature in Stahl's measurements was never greater than 70-100°C. Intense oxidation was not likely to be due to gas molecules colliding with the vapour molecules in the source-substrate space (~ 1 cm in Stahl's study) because the mean free path of the vapour atoms at 10^{-5} torr is greater than 100 cm. However, the second possibility of vapour atoms combining with oxygen molecules on the substrate surface is very probable. It follows that the more the film formation rate

is prolonged, the greater will be the number of gas molecules impinging on the substrate during condensation. The impinging gas molecules may combine with the condensed atoms to form oxides or be trapped in the film by the condensing vapour atoms. Thus it can be stated as a general rule that a vacuum evaporated metal film will be more pure and less granular the more rapid its growth.

d) The distance from the source to the substrate.

Conventionally, this distance varies roughly between 10 cm and 50 cm. Too short a distance will cause the source to overheat the substrate but too long a distance will increase the evaporation time and will involve wastage of source material. Moreover, a large source-substrate separation may cause 'soft' films to be formed with poor adherence.

e) Crystalline structure and orientation of films.

According to Evans and Wilman (82), many electron diffraction results have shown that the deposits on amorphous or 'inactive' crystalline substrates tend to grow in preferred orientations. On the average, the crystals have a densely populated net plane of a certain type parallel to the macroscopic substrate surface, but there is a spread about the mean direction of orientation. The interpretation now generally accepted is that such a 'one-degree' orientation originates from the tendency of the atoms to aggregate first in close packing to form plane sheets of

monatomic thickness on the substrate, when their mobility is sufficient on the substrate at the condensation temperature.

The 'one-degree' orientation referred to by Evans and Wilman is one in which the deposit crystals tend to be aligned with one principal axis in a common direction; the orientation about the preferred direction being random. The orientation axis is usually normal to the plane of the film but it may be inclined depending on the incidence angle of the impinging vapour atoms.

f) The effects of the vapour incidence angle.

It has been shown by Koenig and Helwig (83) and Holland (84) that evaporated films deposited with the vapour atoms impinging at high incidence angles may develop a coarse texture. The reason for this is that at high incidence angles, the vapour atoms are unable to penetrate the interstices between the nuclei growing on the substrate surface. Thus, condensation is confined to the peaks of the most prominent grains which grow at the expense of their neighbours and in a direction which tends towards that of the vapour beam.

Various workers have noted that the orientation of the crystals in evaporated films is dependent on the vapour incidence angle. Evans and Wilman (82) found that materials (Fe, Al, NaF) whose atoms have a low mobility both on the deposit and on the substrate had little or no orientation in thin layers but as the

deposit thickness increased they developed a one-degree orientation with the orientation axis inclined away from the surface normal towards the vapour stream. They considered that the tilting of the orientation axis was due to the deposit forming a coarse texture and growing in a preferred direction, as described above. Further, that as the oblique deposit grew, its temperature was raised by radiation from the source, which caused a sufficient increase in atomic mobility on the deposit crystals for the arriving atoms to take up preferred positions on suitably disposed crystals.

Summary.

From the several factors which can influence the growth, structure and physical properties of an evaporated film, a number of conclusions can immediately be drawn about the way in which a high quality film of a rare earth metal can be produced.

Firstly, the rate of deposition must be high, in order to assist aggregation and reduce oxidation. Secondly, the substrate temperature must be kept as low as possible in order to minimize the size of the critical nucleus and assist continuous formation. Finally, the substrate should be mounted vertically above the source so that an even growth is obtained.

CHAPTER FIVE

EXPERIMENTAL DETAILS

5.1 Apparatus

a) The vacuum system.

The system (Figure 5.1) has a conventional lay-out, employing electromagnetic valves which are operated by microswitches on the baffle valve spindle. The rotary pump is a two-stage unit, having a displacement of 110 litres/minute and an ultimate vacuum of 2.10^{-4} torr. It is protected from electrical failure by an electromagnetic air-admittance valve which is normally closed when the pump is in operation.

The main diffusion pump is a three-inch, water-cooled, three stage fractionating pump with a specified baffle pumping speed of 85 litres/second and, in order to reduce the pressure gradient down the barrel of this pump, it is supported by a one inch diffusion pump. Pumping speed is thus increased at low pressures.

Above the diffusion pumps is a liquid nitrogen cold-trap. This is connected to the work chamber via a combined water-cooled oil baffle and isolation valve. Another isolation valve is situated between the diffusion pumps and the rotary pump so that the diffusion pumps can be separately kept under vacuum when this valve

and the baffle valve are closed. This permits the diffusion pumps to be kept at operating temperature when the work chamber is at atmospheric pressure. Without this facility, considerable time would be wasted in waiting for the pumps to cool so that they could be exposed to the atmosphere and attain working temperature again on a subsequent cycle. The diffusion pumps are protected from water failure by a thermal sensing switch which opens if the pump barrel temperature rises above a critical level.

All the interconnecting vacuum line is one-inch copper tube and the distance between components is kept as short as possible to ensure maximum pumping speed. A short piece of flexible tubing is included in the roughing line to reduce vibrations from the rotary pump. All the components are easily demountable by bolt or screw seals, which compress an elastomer O-ring.

Pressures in the region 1 to 10^{-3} torr are indicated by two thermocouple gauges, one in the roughing line and one in the base-plate wall. A hot-cathode ionization gauge, located in the baffle valve unit, directly measures pressure in the region 10^{-2} to 10^{-7} torr.

b) Ultimate pressure.

The major factors which determine the ultimate pressure obtained by an oil diffusion pump may be listed as follows:

1. Leakage of air into the vacuum chamber.

2. Outgassing of the inner walls of the chamber.
3. Outgassing of the sealing materials.
4. Gases or vapours which have been returned to the foreside of the pump by back-diffusion through the vapour jets; added to this, there will be gas or vapour which has gone into solution at the forepressure in the condensed pumping fluid returning to the boiler and subsequently being liberated through the jets.
5. Gases produced by the continuous decomposition in the boiler of some of the pumping fluid and afterwards liberated through the jets.
6. Vapour of the pumping fluid itself, or of its constituents.

It is observed that the rate of rise of the pressure in the chamber when it is isolated from the diffusion pumps is greatest in the early stages of pumping and is very small in comparison after many hours of pumping. It is assumed in the light of this that the system is air-tight and that the residual gas in the system is a result of factors 2-6.

The outgassing of internal surfaces in the vacuum chamber is reduced by baking the chamber for several hours inside an oven at about 200^{o}C. It is not possible to bake out the baffle valve unit because of the proximity of micro-switches in its casing. Seals made of Viton-A, an elastomer with a very low vapour pressure,

are used in the fore-line but these may only be safely baked to 200°C. Factor 4. is reduced to an insignificantly low level because back-diffusion is very small in a multi-stage pump, with dense ejector stages for the second and third stages.

Factors 5. and 6. can play a big part in limiting the ultimate pressure obtainable by an oil diffusion pump. If the pumping fluid is a mixture of chemical compounds, as is the Silicone 705 fluid which is used in the present system, then the vapour pressure of interest is that of the most volatile component. At baffle (or cold-trap) temperatures below about 20°C, the decomposition products of the pumping fluid are the most important contribution to the ultimate vacuum. As these products certainly contain non-condensable permanent gases, even a cold-trap filled with liquid nitrogen is incapable of reducing the ultimate pressure due to these gaseous products.

A cold-trap is a very effective vapour pump however, because when full, at a sufficiently low temperature, it may be assumed that all the molecules of vapour which impinge on the trap walls are condensed, provided that the pressure of this vapour at the trap temperature is negligible compared with the total gas pressure in the vacuum chamber at room temperature. This is the case for almost all vapours if liquid nitrogen is used as a coolant. Cold-traps have the great disadvantage that they inevitably have considerable

impedance to gas flow, and so reduce the pumping speed of the system for permanent gases.

In order to obtain an approximate value of the pumping speed of the system, the rate of internal outgassing was determined during the early stages of pumping by isolating the chamber and measuring the time t for the pressure to rise from 10^{-5} torr (p_1) to 10^{-4} torr (p_2).

If at any point in a vacuum circuit, a cross-section plane is considered, then if V is the volume of gas flowing across this plane per unit time and p is the pressure at that plane, then :

$$Q = pV \qquad 5.1$$

where Q is the 'throughput'.

If p_1 is the intake or fine-side pressure provided at the chamber by the diffusion pump (including the impedance of the inter-connecting system) and the pumping speed of the diffusion pump is S, then :

$$Q = p_1 S \qquad 5.2$$

so $$S = \frac{Q}{p_1} = \frac{p_2 V_{chamber}}{p_1 t} = \frac{25.10^{-4}}{5.10^{-5}} = 50 \text{ litres/sec.}$$

where $V_{chamber}$ is estimated at 25 litres and the time t = 5 sec.

Throughput is often defined in terms of the lusec. This is the throughput in litre-micron/sec. At 10^{-5} torr, the volumetric

speed is 50 litres/sec. At 10^{-3} torr (1 micron) this volume would be (from Boyle's law) : $\frac{10^{-5}}{10^{-3}}.50$ i.e. 0.5 lusec.

Owing to this rather modest pumping speed, the region of 10^{-6} torr is the most practical working pressure for the system because reducing the pressure much further below this involves very much more time spent in baking out the system as the ultimate limiting pressure is approached. The lowest pressure ever achieved was 2.10^{-7} torr, after 72 hours bake-out at $200^{o}C$.

c) The base-plate and vacuum chamber apparatus.

Located on top of the baffle-valve, the base-plate (Figure 5.2) was turned from rolled non-magnetic Austenitic stainless steel. The finished surface was passivated in nitric acid to prevent the formation of an oxide coating which would outgas in vacuo.

The O-ring groove in the top of the base-plate has a trapezium cross-section of a type first described by Barton (85). This design has the advantage of straight-forward machining and compression of the O-ring without distortion.

The weight of the bell-jar alone supplies sufficient compression on the O-ring to make a seal at the start of evacuation. The sealing surfaces of the O-ring and the bell-jar are totally grease-free and are thoroughly cleaned before every use.

In addition to carrying the air-admittance valve for the

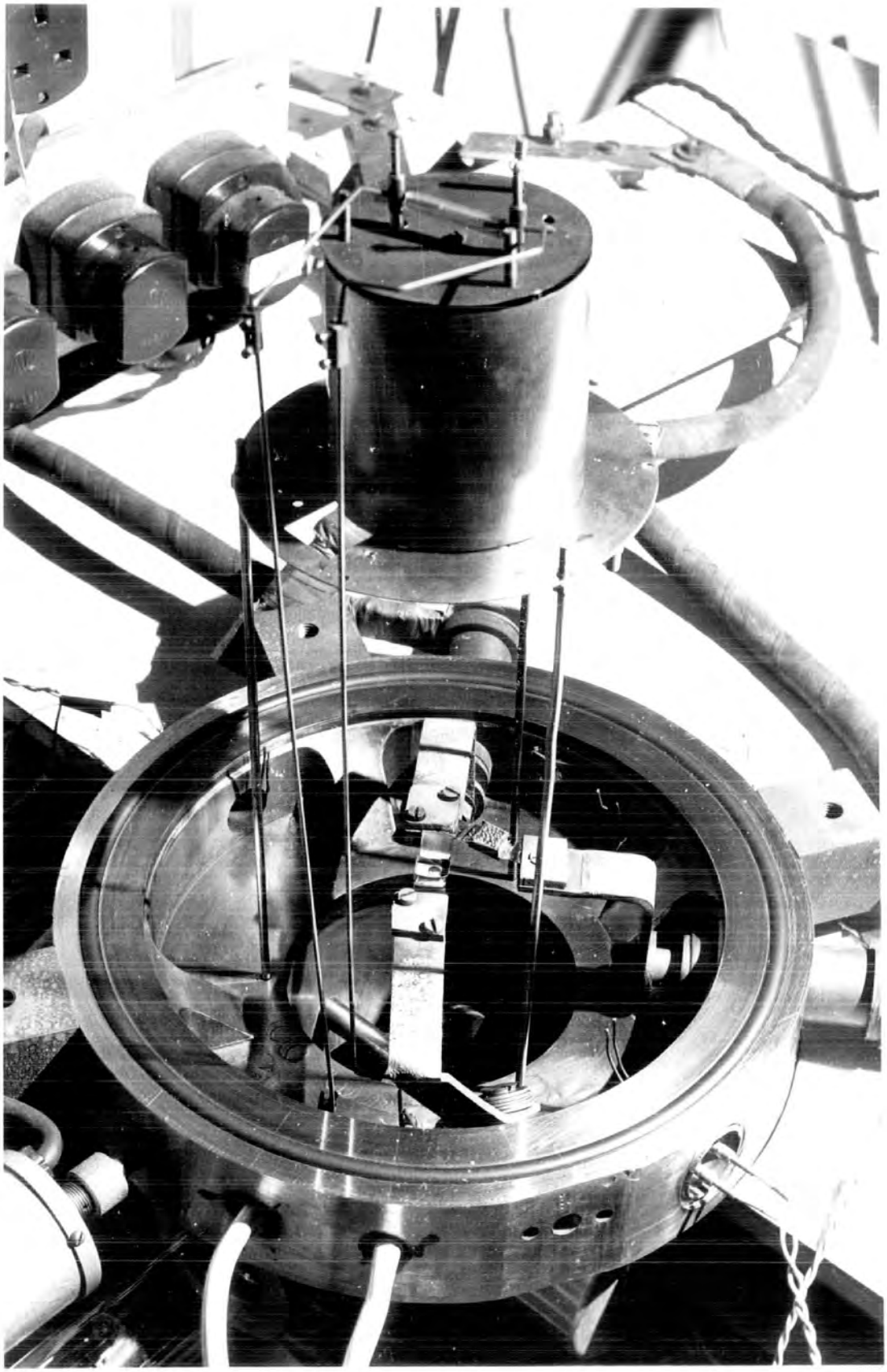

Fig.5.2 The base-plate and evaporator assembly.

chamber, the base-plate also accommodates the various electrical leads-through for the system. These comprise three pairs of metal-ceramic low-current leads mounted on stainless steel flanges and brazed into the base-plate wall. These are suitable for thermocouple outputs or instrumentation connections. There are also two medium-current (30 Amps) metal-ceramic leads, also brazed into the base-plate wall and which are used to carry the power for the substrate heater. Finally, there are two heavy-current (200 Amps) demountable leads which carry a low-tension power supply to the evaporators.

The lay-out of the evaporators can be clearly seen in Figure 5.2. Two boats are used, one for the source material and one for silicon monoxide, which is deposited on to the films as a protective overcoat. The substrate is located on a tripod vertically above the source and 17cm. away from it.

A 200 watt quartz-iodine bulb is mounted just above the substrate in a stainless steel heat shield and by this means, the temperature of the substrate can be raised to approximately 400^{o}C. The bulb is controlled by a variac, so that any temperature may be selected. The temperature of the substrate is measured by a copper-constantan thermocouple which touches the substrate surface and can be continuously monitored by a chart recorder.

5.2 Vacuum Evaporation.

a) The evaporator.

The chosen method of evaporation is by resistive heating of foil boats. The melting points of the heavy rare earth metals lie between 1300°C and 1700°C, excluding ytterbium at 824°C. Allowing for a margin of 300°C, the probable maximum temperature needed to evaporate a rare earth metal by this method was taken to be 2000°C.

The power source is a low-tension transformer with a rating of 200 Amps. at 5 volts and this is controlled by a linear variac in the mains supply. The boats were to be made from tantalum or molybdenum sheet, the thickness of which was 0.1 mm. and the boat length was required to be 4 cm. It was necessary that the boat width should be such that a temperature of 2000°C could be attained in the boat at full power.

Now, the power consumption of the heater, in watts, is :

$$W = I^2 R \qquad 5.3$$

where I is the current, and the resistance $R = \frac{\rho\beta}{\zeta}$, where ρ is the resistivity, β is the length of the heater and ζ is the cross-section of the heater.

Whence $$I = \left(\frac{W\zeta}{\rho\beta}\right)^{1/2} \qquad 5.4$$

Tungsten, which has physical and electrical properties very similar to those of tantalum and molybdenum, has values of $W \approx 50$ watts/cm^2 of surface and $\rho = 0.65\ 10^{-4}$ ohm-cm. at 2000°C. These values are used as being the closest obtainable. So, for a current of 200 Amps., from equation 5.4, a value of 1.5 cm. is obtained as the final dimension of the heater for the attainment of temperatures in the region of 2000°C. Allowing a further margin, the boats are constructed with the dimensions of 4 cm.× 1 cm.× 0.01 cm. in the shape as shown in Figure 5.2.

In early tests on this design, at full power, surface temperatures in the region of 2400°C were recorded using a tungsten/tungsten-rhenium thermocouple.

b) The evaporant.

Of the two possible types of boat metal, it has been found that the heavy rare earth metals evaporate preferentially from boats made of tantalum because they do not 'wet' this metal in their molten states, while in molybdenum boats, they tend to run over the surface of the boat, increasing the conductivity and thus necessitating that much more power be supplied before evaporation takes place. In order to prevent contamination of the evaporants themselves, the boats are ultrasonically cleaned before use.

Rare earths are best evaporated in the form of small chips or filings, which need less power to melt them than larger lumps.

The evaporant charge is prepared in an argon atmosphere in a glove-box, where it is either filed or sawn from the parent block, using tools which are only used for the metal in question.

c) The film mask.

The usual four-probe method is used to measure the resistance of the films. In this method two extra probes are used to eliminate errors due to contact resistance. In general, the separation of the potential probes on the sample replaces the sample length. In the case of a bulk specimen the probes are very fine point contacts but in the case of a thin film, the potential contacts must necessarily have a finite area because they must be evaporated at the same time as the specimen by means of a mask. The shape of the film mask which was used to grow the films can be seen in Figure 5.3 ; the probes on the films are 0.25 inches apart and 0.012 inches in width. The width of the strip is 0.125 inches. Two pairs of contacts are evaporated, one pair acting as a spare or for other measurements.

d) The substrate.

Glass substrates are used primarily because of the high electrical insulation properties of glass, which is so essential to the measurement of the resistance of the films but also because glass is in itself an excellent substrate material and can be

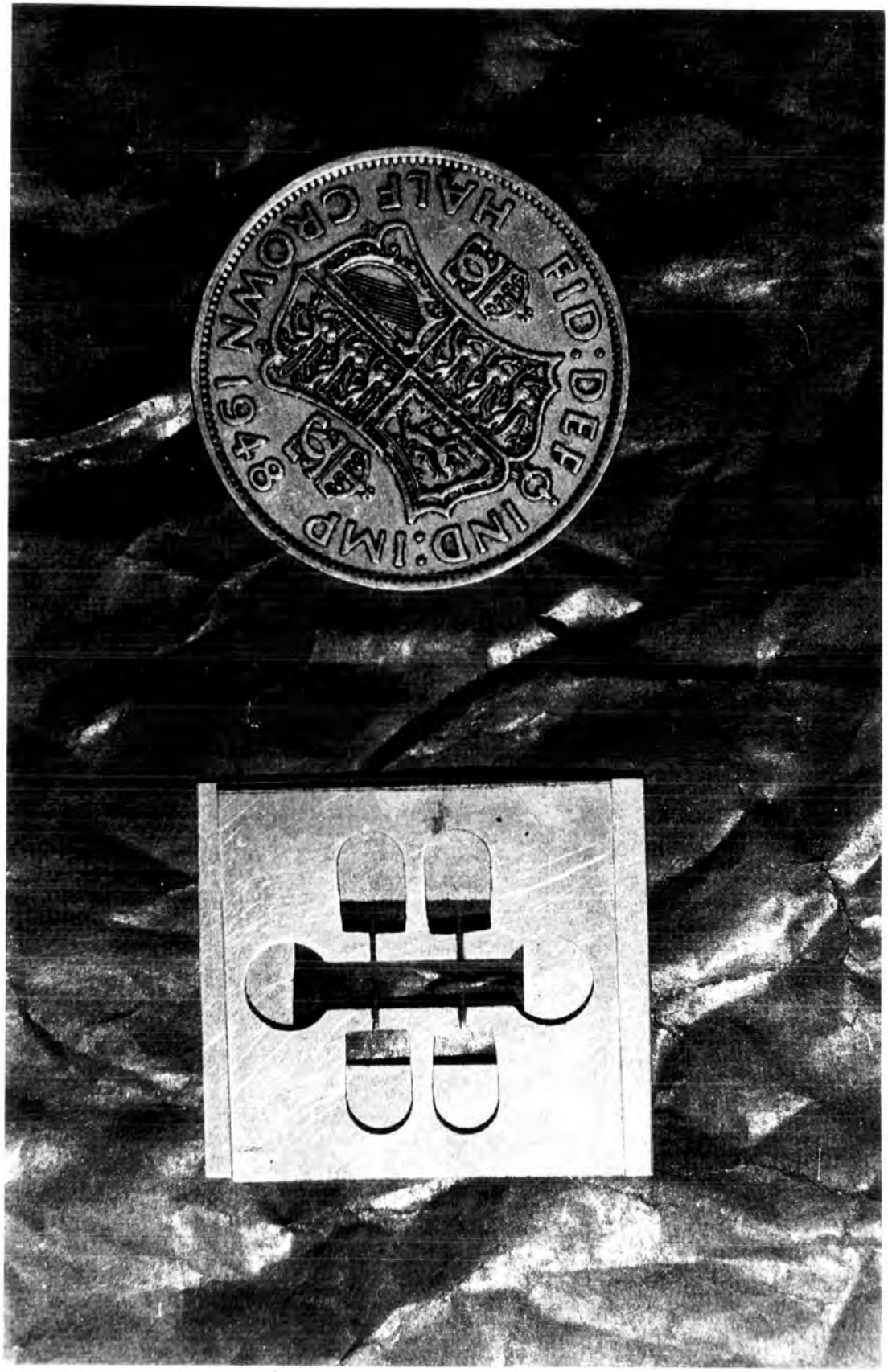

Fig.5.3 The film mask.

cleaned to a higher degree than is possible with most 'active' or metal substrates. The substrates themselves measure 1× 0.75× 0.032 inches.

The cleanliness of the substrate surface is extremely important in order to prevent both dust particles from roughening the surface and grease-like materials, adsorbed water etc. from contaminating the film. Various chemical techniques have been devised for the cleaning of base materials ; these methods are all satisfactory for removing gross surface contamination but they are not capable of freeing the substrate surface from mono-molecular films of water or hydrocarbon etc. Also, a cleaned surface rapidly becomes dirty when exposed for even a short period in a normal atmosphere.

Fortunately, surface contamination condensed from the atmosphere or remaining after chemical cleaning can be removed from the substrate prior to deposition by raising the temperature of the substrate in vacuum or by exposing the receiving surface to the bombardment of high velocity ions.

Several of the chemical methods were tried initially, including vapour de-greasing in iso-propyl alcohol and a technique developed by Colbert and Weinrich (86) and used in the aluminizing of large telescope mirrors, which involves rubbing a thin protective film of toluene dissolved in a mineral oil onto the

substrate surface and subsequently evaporating this film in vacuo. It is claimed that the film protects the surface during atmospheric exposure. These cleaning processes were abandoned however because of residual smears, which they seemed to cause.

The cleaning method which was finally adopted is a modification of a technique first used by Fuller and Adamski and reported by Prutton (87). The glass substrate is swabbed alternately first with a strong hot teepol solution and then with iso-propyl alcohol until the majority of contaminants have been removed. For the second part of the process, the substrate is twice cleaned ultrasonically ; first in a 1:1000 solution of teepol in hot distilled water and secondly in iso-propyl alcohol. It is then immediately inserted in the substrate-holder of the evaporation system and evacuation is commenced. The reason for this is to avoid a final drying of the substrate (e.g. by a silk cloth) during which the glass would develop an electrostatic charge, which firmly holds minute particles on the cleaned surface. These particles, once introduced, are subsequently responsible for pin-holes in the condensed film. Microscopic examination of a substrate cleaned in this manner has shown that a very clean, relatively particle-free surface is obtained. A water-drop spread evenly across the surface when deposited upon it, indicating the total absence of grease-like contaminants.

During the early stages of the pump-down period to the working pressure, the substrate is heated to approximately 300°C by the quartz-iodine bulb. This removes the remaining alcohol and also bakes out any residual adsorbed gases from the substrate, leaving it fully prepared for deposition.

e) Film protection.

The rare earth metals possess a high affinity for oxygen, and in the form of a thin film, will rapidly deteriorate to the oxide when exposed to the atmosphere. Since work carried out with the films after growth involves removing them from vacuum, it is very necessary that they should be protected against oxidation. This is achieved by over-depositing an insulating substance onto the film while it is still in vacuo. Several materials fulfill the requirements of insulation and durability (e.g. bismuth oxide, zinc sulphide, silicon monoxide) and of these, silicon monoxide (SiO) was chosen because it is relatively easy to evaporate, highly insulating and very durable.

The influence of over-depositing SiO on thin metal films has been thoroughly investigated by Dean (88) and by Milgram and Lu (89). Both report that the resistance of vacuum-deposited metal films decreased when over-coated with SiO. Milgram and Lu explained this effect as being due to a change in the surface tension of

the metallic film. Dean also found that a protective over-coating of SiO enhanced the stability of the film resistance during extended storage. Indeed, in the present measurements, a dysprosium film which was re-examined eight months after it had been grown, was found to have the identical electrical resistance as it possessed immediately after its growth.

f) Electrical contacts.

The means of making reliable electrical contacts to the film caused some difficulty at first, when various types of pressure contacts were tried, with only intermittent success, before an ultrasonic bonder became available. This machine, designed primarily to effect contacts onto integrated circuits, will bond a fine aluminium wire onto almost any clean metal surface and was found to be ideal for the purpose of effecting contacts to the films. However, it is not possible to make a contact through the SiO over-coat with the bonder, so it is necessary to have exposed areas of metal film which protrude from underneath the SiO and which are in contact with the rare earth film.

g) The procedure of film growth.

Immediately after cleaning, the substrate is placed on a stainless steel mask which will allow six small areas of metal to be deposited on the substrate. These are the contact spots for the

rare earth metal film and to produce them, silver powder is evaporated from a molybdenum boat. Silver is used for this purpose because it is slow to oxidise and it is easy to bond the aluminium wire onto it. Once the substrate has been baked out at 300°C, the silver evaporation is carried out, normally in the region of 10^{-6} torr, since high perfection is not a rigid criterion for the contact spots.

Following this deposition, the substrate is removed from the chamber and placed on another mask, the shape of which has already been described. This mask partially covers the silver spots, allowing the rare earth film to join up with the contacts by over-laying them while part of the silver remains shielded from the over-coating. Once it is under high vacuum, the temperature of the substrate is raised to about 300°C and maintained at this temperature for approximately two hours to free the substrate from gas which may be adsorbed during the atmospheric exposure. At the end of this time the substrate temperature is reduced to about 200°C at which it is held until shortly before evaporation.

The cold-trap is kept topped up with liquid nitrogen during the pumping time by an automatic replenisher which senses the level of the liquid by means of gas-bulb thermometers.

Prior to evaporation, the boats and their charges are thoroughly outgassed by passing a moderate current through them,

insufficient to cause evaporation but enough to drive off all residual gas. During this, the substrate is shielded from the source by a stainless steel shutter, which can be removed magnetically from outside the system. Finally, in order to assist aggregation of the film, the substrate temperature is allowed to regain the ambient room temperature. At this point, the shutter is removed and the source is slowly brought up to melting point. When melting occurs, the power is sharply raised and the source material is evaporated in about four seconds. The temperature of the substrate rises to the region of 70°C during this time, owing to radiation from the source. When evaporation is complete, the power is at once transferred to the boat containing SiO, which is covered with a 'pepper pot' lid to prevent decrepitation of the SiO when the boat is heated, and a film of SiO is over-deposited onto the metal film. Following this, the film is annealed at about 200°C for twenty minutes before being left to regain the ambient while in vacuo.

5.3 The Specimen.

a) Film thickness.

No film thickness monitor is available and continuous films of approximately 100 - 3000 Å are required. The most satisfactory solution appeared to be a method of relating the film thickness

to the amount of material evaporated, which can accurately be determined by using a known weight of the evaporant and weighing the boat before and after evaporation. Then from one standard film whose thickness is precisely known, the thickness of any other film can be calculated from the weight of the evaporant which is used, provided that the conditions affecting film growth are the same for all the films.

On this basis, a dysprosium film was grown from 140 m.grams of evaporant and its thickness was measured by the Plessey Company on a Talystep 2, an instrument which can detect increments as small as 50 Å on a surface. Some of the traces obtained from various positions on the film are shown in Figure 5.4, and from these, a thickness value of 1850 Å (± 3%) was obtained.

The mass m_1 of dysprosium which will produce a film 1000 Å thick is immediately obtained, and the required mass m_2 of any other metal for a film of the same thickness is obtained from

$$m_2 = m_1 \frac{d_2}{d_1} \qquad 5.5$$

where d_1 and d_2 are the densities of dysprosium and the second metal respectively.

b) Film purity.

The bulk material from which the films are grown is normally supplied as 99.9% pure. It is desirable to know if this purity

will be appreciably affected during film growth by the effect of residual gas bombardment on the substrate surface.

The number of molecules striking unit area of a surface in the chamber per second can be calculated as (90)

$$N = \frac{3 \cdot 5 \cdot 10^{22} p}{\sqrt{M.T}} \qquad 5.6$$

where p is the pressure in torr and M is the molecular weight of the gas.

At a pressure of 10^{-6} torr, water vapour is the main constituent of the residual gas and for T = 343^{0}K, N is found to be 4.10^{14} molecules/sec.

Now, the number of atoms in a square centimetre film of dysprosium is approximately

$$N' = V.B.A \qquad 5.7$$

where V is the volume of the film in cm^{3}, B is the atomic volume in cm^{3}/gm-atom and A is Avogadro's number. For a film of 1000 Å thickness, this is found to be 6.10^{17} atoms, so that the rate of deposition is approximately 10^{17} atoms/sec.

The rate of deposition is therefore approximately 250 times greater than the rate of residual gas bombardment and so the purity of the film should not be appreciably different from that of the bulk material.

5.4 The Method of Resistance Measurement.

a) The four-probe technique.

In the four-probe method for measurement of resistance, a constant current is passed through the specimen between two probes and the potential drop between two other probes is measured. The potential drop used to obtain the value of the resistance of the specimen between the potential probes is the average value obtained for both directions of current flow. This procedure eliminates as far as possible errors due to thermoelectric or rectification effects which may occur within the film due to inhomogeneities of structure, rectifying boundaries, or other defects. In order to minimize further effects due to rectification at the probes themselves, a potentiometric method is employed. Under these conditions, probe contact resistance will have little effect beyond reducing the sensitivity of the potentiometer.

In order to measure the resistance of the film, a stabilized direct current of 1mA is passed through it and the potential drop between the probes is measured on a vernier potentiometer. The circuit of the current supply is shown in Figure 5.5. The supply is independent of load resistance and is constant to 1 part in 1000. The current is set by passing it through a standard 100 ohm wire-wound resistance and adjusting the potential drop across this

to 100 mV.

The potential drop in the film can be read to ± 1 μV on the vernier potentiometer but it is found to be much easier to monitor the potential to ± 5 μV, from which the film resistance is determined to better than 1 part in 1000.

b) The specimen-holder and Cryostat.

The film is removed from the chamber as soon as it has cooled to room temperature and the aluminium wire contacts are bonded onto the exposed silver areas by means of the ultra-sonic bonder.

The specimen-holder 'A' is depicted in Figure 5.6. It is constructed in two halves of perspex, which can be screwed together. The substrate is placed in a recessed groove in the lower half of the holder, so that it sits flush with the perspex surface and when the upper half is fitted, the substrate is held securely in place. The four contact wires are led to the external connections and soldered into position.

The specimen-holder is now attached to the support 'B', a stainless steel tube approximately three feet in length, which is push-fitted into a hole in one end of the specimen-holder. The thermocouple is also fitted at this time, by passing it through a small hole in the specimen-holder and using the grip of the

two halves of perspex to press it against the surface of the film.

The stainless steel tube is fixed to a brass plate 'C' which forms the cover of the Cryostat when in position. The electrical leads are guided round the tube by spacers and out of 'C' through a six-way ceramic-to-metal seal which has hollow leads-through into which the leads can be fed before soldering.

The specimen-holder assembly is now inserted into a one-inch diameter blind stainless steel tube, which is bolted to 'C' through the flange 'D' at the top of the tube. The whole assembly can be evacuated through a brass tube let into 'C' and an elastomer O-ring makes the seal between 'C' and 'D'.

When in position, the Cryostat top-plate 'C' is located by a clamping ring round its circumference. The remainder of the Cryostat head carries an exhaust pipe for the evacuation of the liquid helium dewar and a recovery pipe for the collection of helium gas. Liquid helium is introduced into the dewar via a syphon which passes through a hole in the Cryostat head. This hole is sealed when not in use. The helium dewar itself is approximately three feet long and four inches in diameter and it fits into the Cryostat head through a short tube. A vacuum seal is made by a tight rubber sleeve which covers the metal/glass junction.

The Cryostat is suspended between the two facing poles of an electromagnet, which can supply a field up to 10 KOe for a pole gap of six inches. When the film is in situ, it is at the centre of the magnet and the direction of the magnetic field is perpendicular to the direction of the constant current in the film, so that transverse magneto-resistance can be examined by this arrangement. The magnetic field is normally applied either perpendicular or parallel to the face of the film and it is possible to rotate the specimen relative to the field at any time except when the helium dewar is under vacuum.

c) Measurement of temperature.

A calibrated copper-constantan thermocouple is used to measure the temperature of the film. One junction is kept immersed in liquid nitrogen while the other junction is inserted between the two halves of the perspex specimen-holder so that it is pressed onto the glass substrate surface, as near to the film as possible.

The thermocouple is monitored by a conventional potentiometer arrangement which can be read to $\pm 2\ \mu V$ when correctly standardised. The response for a $1^{o}K$ change in temperature for a copper-constantan thermocouple is shown in Figure 5.7, from which it can be seen that even in the region of least response

the temperature can be read to $\pm 1^{o}K$, while at $280^{o}K$, a response of 40 μV per ^{o}K enables the temperature to be determined to $\pm 0.05^{o}K$.

d) Experimental procedure.

The liquid helium Cryostat is surrounded by a liquid nitrogen dewar which encloses all but the Cryostat head. The Cryostat is flushed with helium gas and evacuated so that a very slow rate of cooling is obtained. Liquid nitrogen is introduced into the outer dewar and as the film cools down at an almost constant rate of $1^{o}K$ per 40 seconds, the resistance is recorded at intervals of $5^{o}K$, except in the region of the anomalous behaviour, when it is monitored more frequently. The current is reversed at each point and normally, identical values of resistance are observed for both directions of current flow.

A few cc's of helium gas are admitted to the Cryostat from time to time to keep the rate of temperature fall as constant as possible as the temperature of liquid nitrogen is approached. When $77^{o}K$ has been realised, further temperature reduction is achieved by introducing liquid helium into the Cryostat from a storage dewar via a stainless steel transfer tube.

With the introduction of the liquid helium, the temperature of the Cryostat falls rapidly to $4.2^{o}K$. When steady conditions have been reached, the liquid helium is boiled off by means of a

small heating coil which is lowered into the dewar. The Cryostat is allowed to warm slowly to 77°K and the film resistance is recorded in the same way as before.

e) Measurement of magneto-resistance.

Measurement of the transverse magneto-resistance effects in the films is performed in the same way as for the zero field measurements. The largest possible magnetic field is normally used in order to produce the greatest magneto-resistive effect in the specimen.

During measurements at constant field, the film is exposed to the same changes of temperature as for zero field and the measurements are taken at the same temperatures as the zero field readings for ease of comparison between the two.

Isothermal measurements at temperatures between 77°K and room temperature are taken by using a slush bath made from liquid nitrogen and a low freezing point organic liquid such as pentane.

The transverse field is normally applied in a direction perpendicular to the face of the film but it may also be applied parallel to the face of the film by rotation of the film holder. However, in between changes of the magnitude and direction of the applied field, the film is allowed to regain the paramagnetic phase to destroy any remanent effects of magnetization in the

ferromagnetic or anti-ferromagnetic phases.

The longitudinal magneto-resistive effect is studied in a solenoid electro-magnet which will produce a field of about 10 KOe. Owing to the size of the specimen-holder, it is only possible to fit a single dewar into the magnet and so iso-field observations are limited between 77^{o}K and room temperature.

CHAPTER SIX

RESULTS AND DISCUSSION.

6.1 Results.

Proposals about the resistivity of the rare earth metals have been made by Mackintosh (91), Miwa (92) and Elliott (54,63). They state that new boundaries are introduced into the Brillouin zone structure when the magnetic lattice periodicity differs from the ionic lattice periodicity in the c-axis. This causes a large change in the component of the Fermi surface along the c-axis while leaving the component of the basal plane relatively unchanged. These complex magnetic structures exist in the rare earth metals in the anti-ferromagnetic phase and it is reasonably well established that this associated effect is the cause of the peaks in the c-axis resistivity curves of the rare earths and postulated that, if the anti-ferromagnetism could be quenched by the application of a magnetic field, the peaks would disappear.

Measurement of the electrical resistivity of films of varying thickness of the metals gadolinium through thulium have been carried out in the temperature range 4.2^{o}K to 320^{o}K and the results show various differences from those reported for the bulk metals (53).

a) Dysprosium.

Dysprosium was examined in greatest detail partly because it proved to be the easiest of the rare earth metals to evaporate and also because the bulk metal displays very marked anomalies in the electrical resistivity at the magnetic transition points.

Figure 6.1 shows the resistance versus temperature curve for the 1903 Å dysprosium film. The resistance R of the film is described in units of ohms/square of film surface, where one side of the square is parallel to the direction of the primary current. In this form, R is directly proportional to the resistivity through the proportionality factor t, the thickness of the film. The form of this curve is typical of the dysprosium films of thickness greater than 500 Å. Figure 6.2 shows the R(T) curve of the 132 Å film, which typifies the curves of the thinner dysprosium films.

A marked anomaly is observed near the Néel point θ_N in all cases, although the appearance is more definite in the thick films, where a decrease in resistance with increasing temperature is observed. Above the Néel point, the linear increase in R(T) is wholly due to the phonon resistivity. The magnitude of the ferromagnetic Curie point θ_c also appears to decrease as the film thickness decreases.

In dysprosium, the paramagnetic Curie point θ_p lies at

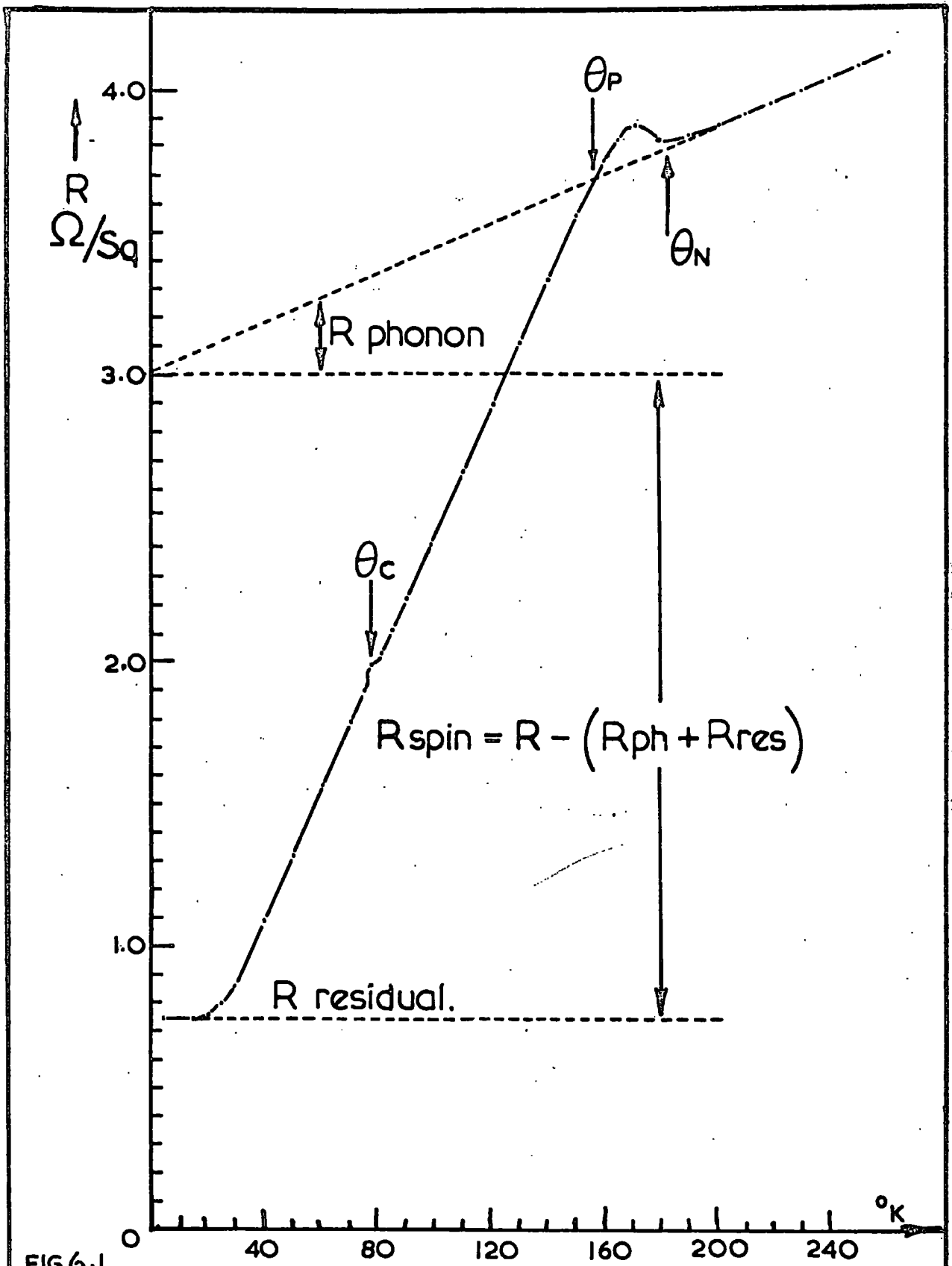

FIG 6.1

Typical example of Resistance vs Temperature Curve as measured on a 1900Å Dy film.

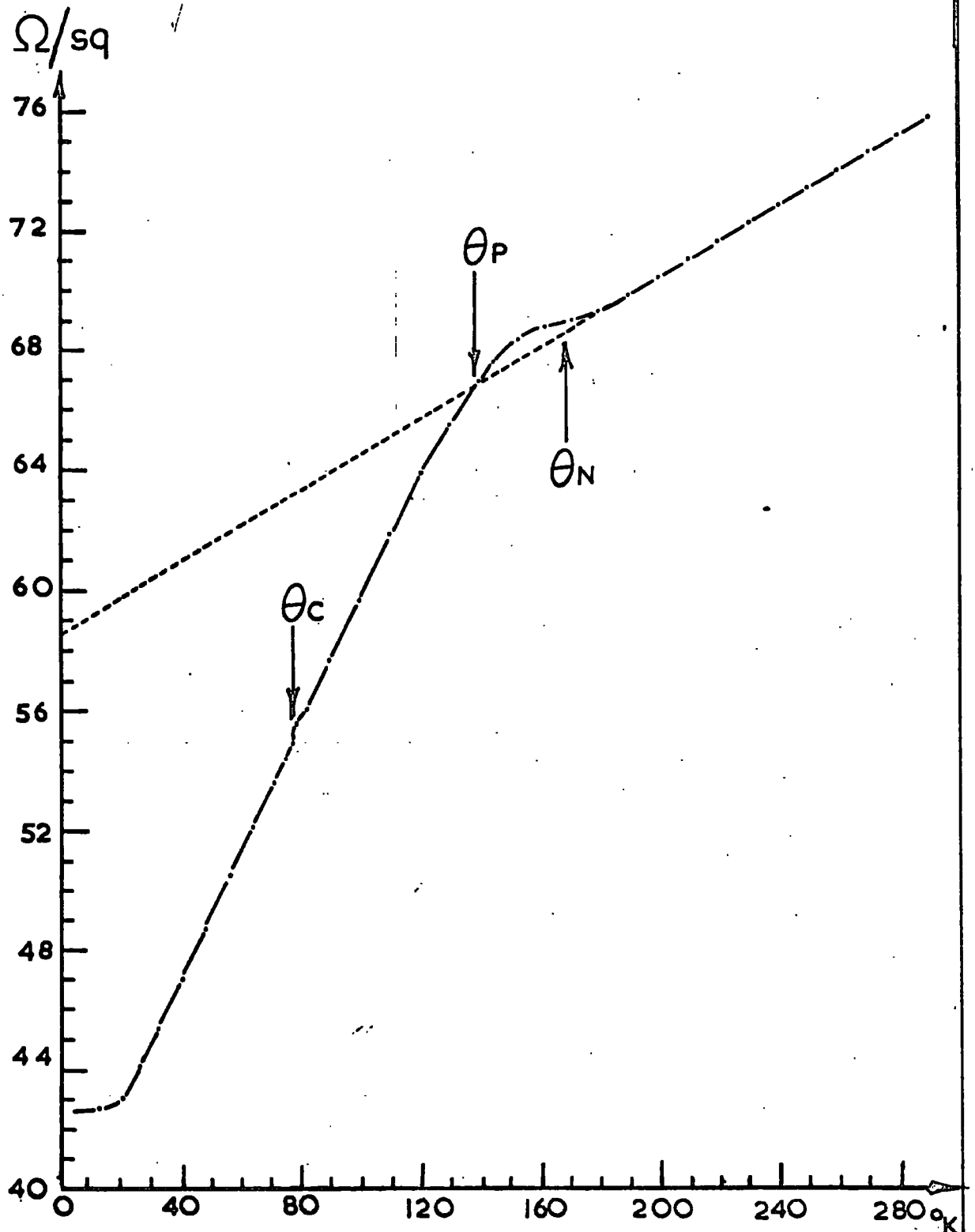

FIG 6.2

Resistance vs. Temperature Curve as measured on a 130Å thick Dy film.

153°K in the bulk metal and it was found that the intersection of the R(T) curve with the extrapolated phonon resistivity term corresponded closely with this value in the thick films. Owing to this agreement in value, this intercept was used as a measure of Θ_ρ for dysprosium. The extrapolation of the phonon resistance from the linear paramagnetic region was carried out by means of a computer fit to the experimental points using a least squares programme.

It has been previously stated from Matthiessen's rule (equation 3.16) that in a ferromagnetic metal the total resistivity is the sum of the contributions from the residual, phonon and magnetic spin-disorder resistivities. In the magnetically ordered temperature region, it is the magnetic spin resistivity which is the dominant and most rapidly changing contribution, and its isolation is achieved (53) as shown in Figure 6.1. The extrapolation of the linear paramagnetic temperature region back to 0°K eliminates the phonon resistivity and subtracting the residual resistivity from the intercept isolates the maximum value of the magnetic spin resistivity. The T^5 dependence of the phonon resistivity at very low temperatures had to be neglected because of the difficulties of experimentally isolating this term.

b) Terbium.

The Néel point and ferromagnetic Curie point lie within $10^{o}K$ of each other in terbium and Figure 6.3a shows the observed R(T) curves in this temperature region for the two terbium films which were examined. The thick film (2120 Å) exhibits anomalies at $231^{o}K$ and $224^{o}K$ before R(T) rapidly decreases in the ferromagnetic temperature region. However, the thin film (405 Å) exhibited no anomalies in this temperature region of the type shown by the thick film and R(T) remains linear until $214^{o}K$. Below this temperature, there is a steady decrease in the resistivity with decreasing temperature throughout the ferromagnetic region.

c) Holmium.

Both of the holmium films were less than 1000 Å thick because irrespective of the amount of evaporant material used, there was always a large residue after the evaporation and although several attempts were made, a thick holmium film was not successfully grown.

The R(T) curves of the holmium films exhibited inflexions at the Néel point, in contrast to the bulk material, which shows a small peak near the Néel point (53). The R(T) curve of the 801 Å film in the region of the Néel point is reproduced in Figure 6.3b.

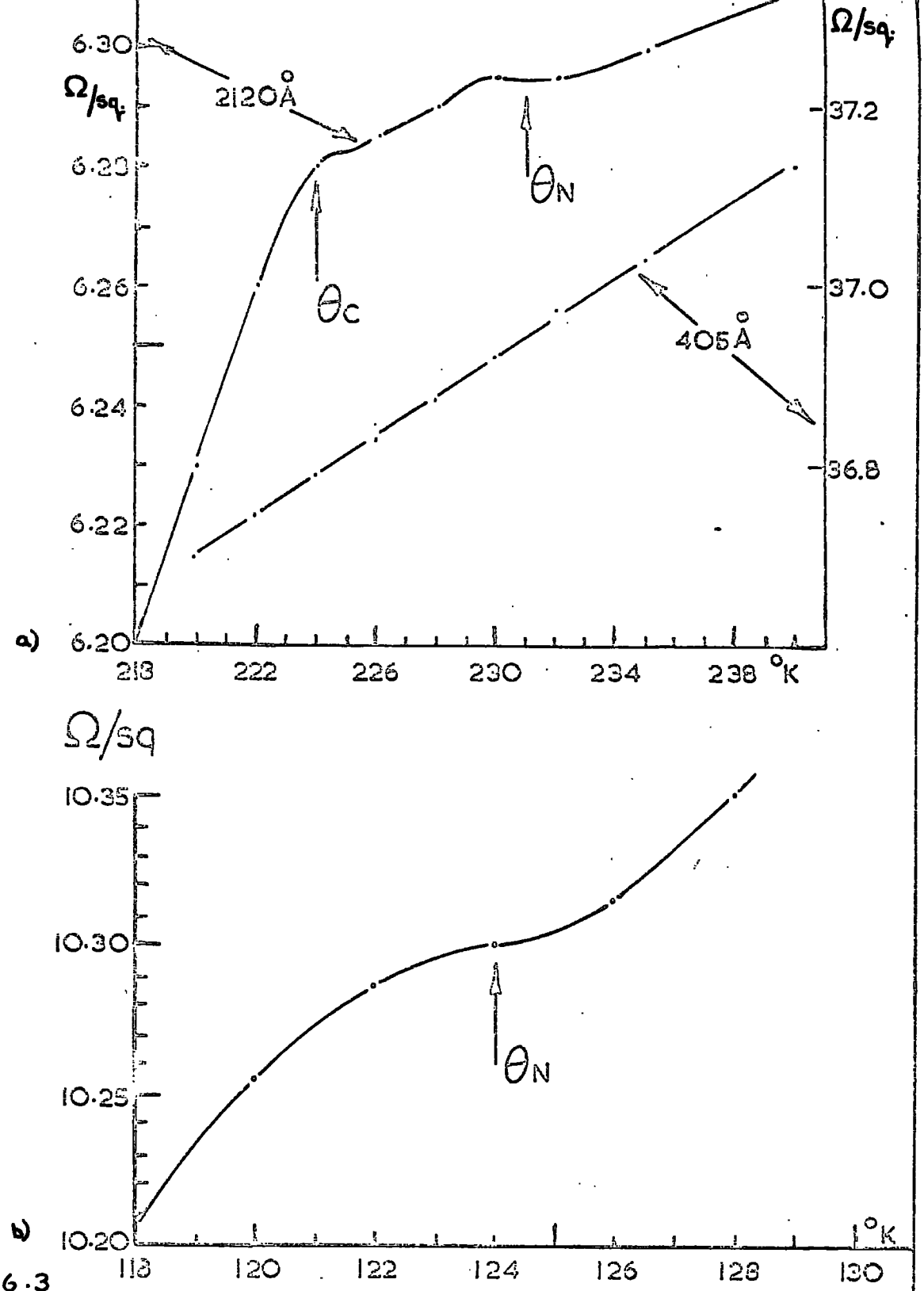

FIG 6·3

Resistance vs Temperature in the neighbourhood of the Neel point for Tb (top) and Ho 8010Å (bottom).

A slight increase of resistance with increasing temperature is observed at the ferromagnetic Curie point and small changes of slope in R(T) are observed in the region $50^{o}K$ - $60^{o}K$, which are associated with the intermediate magnetic structures existing in this temperature region (93).

d) Erbium.

Figure 6.4 shows the R(T) curve for the 1404 Å, which is typical of both of the erbium films in the magnetically ordered region below the Néel point of $85^{o}K$. The ferromagnetic Curie point θ_c is clearly visible between $20^{o}K$ and $25^{o}K$, where the sharp increase in resistivity can be explained by the appearance in the anti-ferromagnetic phase of the new Brillouin zone boundaries. The transition to a modulated sinusoidal anti-ferromagnetic pattern above $50^{o}K$ is also reflected in the R(T) curve by the appearance of the anomalous hump in that temperature region. There is a slight decrease of resistance with increasing temperature just below the Néel point, where a minimum in R(T) is observed. Above θ_N , R(T) is linear with increasing temperature.

The R(T) curve of the 475 Å film is similar in general appearance to that of the 1404 Å film and the Curie point anomaly appears in the region $20^{o}K$ - $25^{o}K$. However, the Néel point anomaly is less marked and the Néel point itself drops to the $60^{o}K$ - $70^{o}K$

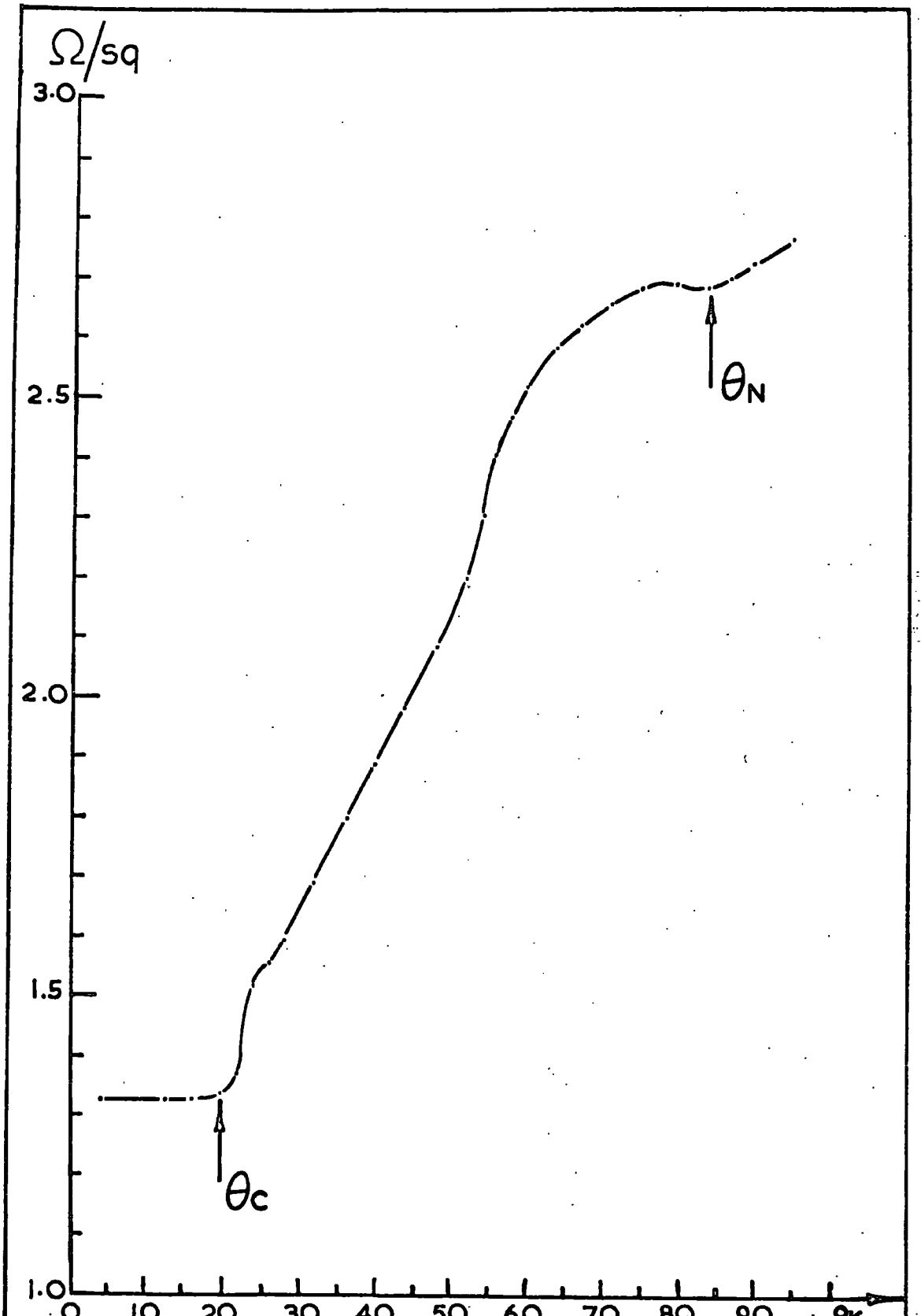

FIG 6.4

Resistance vs Temperature Curve for 1400Å Erbium film.

temperature region.

e) Thulium.

The R(T) curve between 4.2°K and 70°K for the single thulium film of 2180 Å thickness is shown in Figure 6.5. The sharp increase in resistance with temperature through the Curie point θ_c agrees well with the previous reports on thulium (94,95,96).

Unlike erbium, the R(T) curve of thulium does not reflect the transition of the magnetic moment to a sinusoidal modulation, which occurs at 38°K in the bulk metal. However, there is a marked anomaly at the Néel point, which once again has been attributed to the new Brillouin zone boundaries of the anti-ferromagnetic region (64). Above 65°K, R(T) increases linearly with temperature through the paramagnetic region.

f) Gadolinium.

Gadolinium orders into a simple ferromagnetic phase and consequently the R(T) curve is not expected to exhibit the pronounced anomalies such as are shown by the metals with anti-ferromagnetic phases. The R(T) curve of the 1614 Å film is shown in Figure 6.6. Above the Curie point of 298°K, R(T) increases linearly with temperature. Below θ_c , R(T) falls steadily with decreasing temperature.

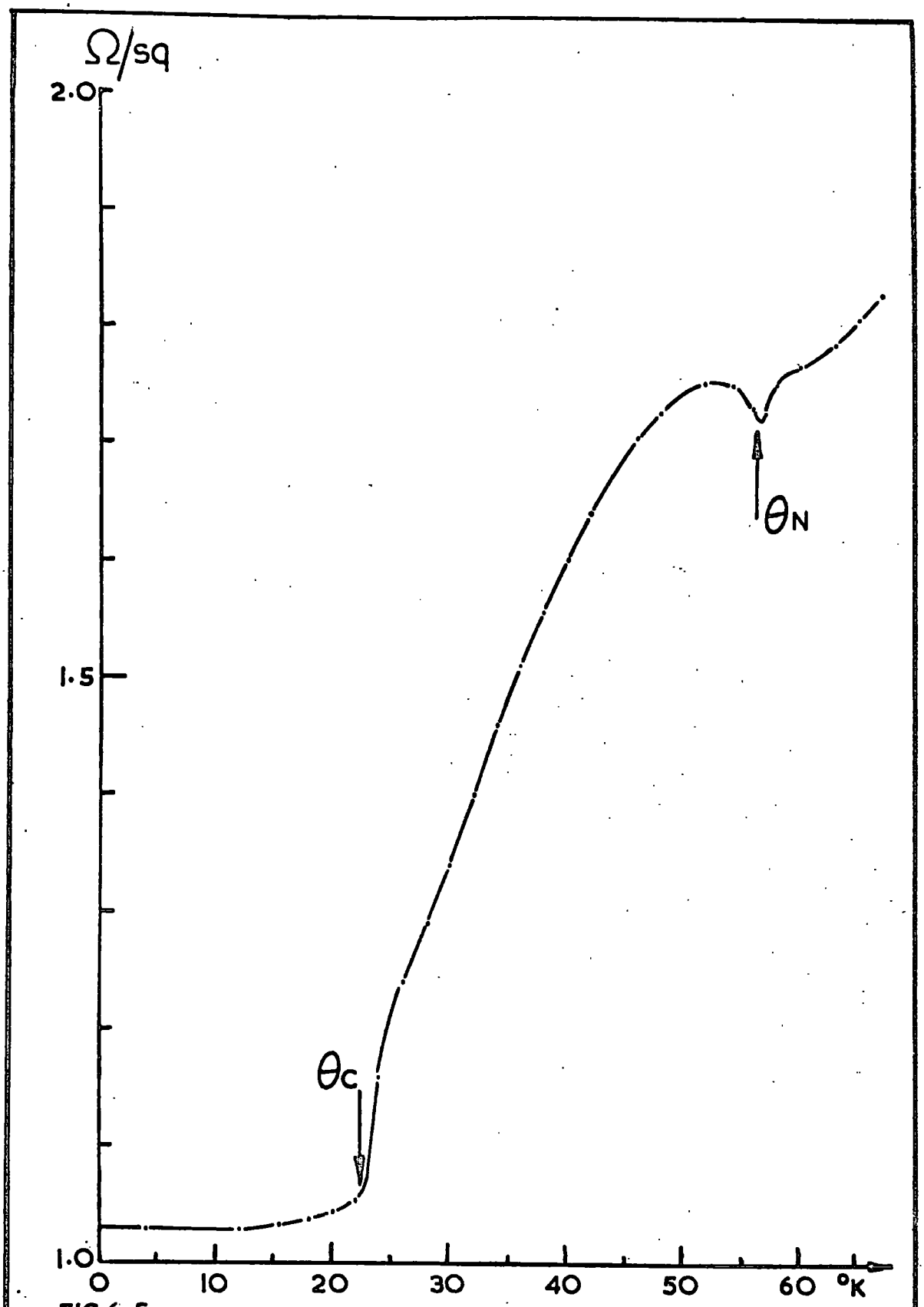

FIG 6.5

Resistance vs. temperature Curve for 2180 Å Thulium film.

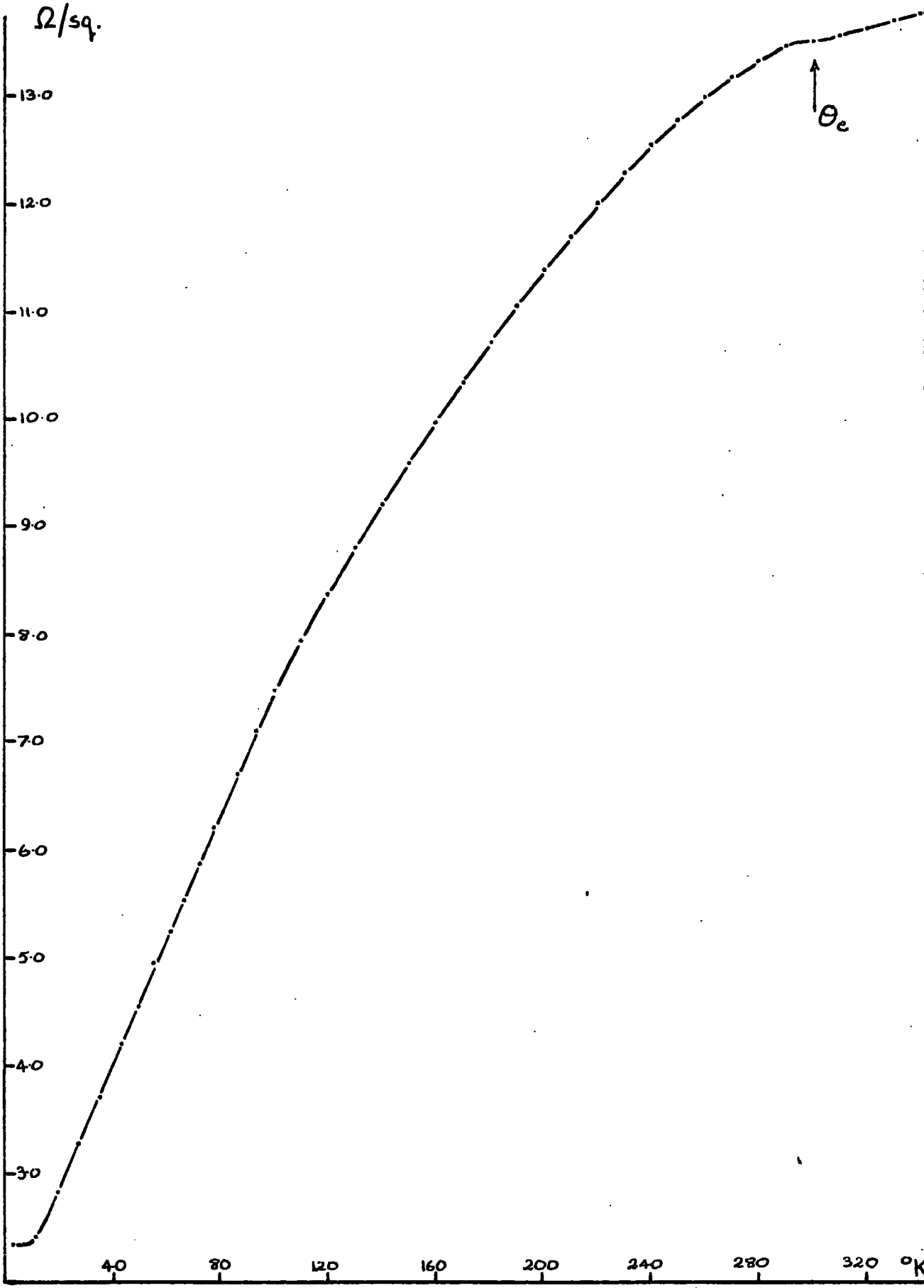

Fig 6·6 R(T) curve of Gd 1614 Å

Gadolinium films proved extremely difficult to deposit because unlike the other metals, gadolinium did not evaporate from the melting point at 1300°C, but only at temperatures approaching the boiling point of 3000°C. Owing to this feature, only one film of 1614 Å thickness was successfully grown.

g) Film parameters.

Table 6.1 presents the various resistivity parameters for all the films used in this study. The corresponding bulk values are given in parenthesis where possible. For the case of dysprosium, a sample was cut from the bulk starting material and the resistivity examined. The results of this sample are given in place of values reported from elsewhere. The remaining figures for the bulk metals are those reported by Colvin et al. (53) from measurements on polycrystalline samples.

The resistance ratios tend to be greater in the thick films and in dysprosium are only approximately a factor of two down on the bulk material. The spin-disorder resistivities ρ_{spin} also show a thickness variation in the metals where both thin and thick films were grown. Gadolinium and terbium even exceed the bulk value of ρ_{spin}, while holmium and dysprosium, except for the Dy 1000 Å film, tend towards the bulk values in the thick films.

Figure 6.7 shows the variation with thickness of the spin-disorder resistivity of dysprosium. There is little change above 500 Å thickness but below this, it falls off sharply with decreasing thickness. However, it is clear from Table 6.1 that the thickness variation of the spin-disorder resistivity observed in dysprosium is not consistent in the films of the other metals. The 'thin' films of the metals Tb, Ho and Er were grown in the 400 - 500 Å range and while at this thickness dysprosium still possesses over 90% of the 'thick' film value of ρ_{spin}, Tb has decreased to 40%, Ho to 75% and Er to 10% of the 'thick' film value. Also, Gd, Tb and Ho apparently possess a spin-disorder resistivity which is greater than the bulk value. In Tb and Ho this is only about 10% greater than bulk but Gd exceeds the bulk value by almost 50%. The thick films of Er and Tm have only 40% and 55% respectively of the bulk spin-disorder resistivity value.

The Néel and paramagnetic Curie temperatures appear to have some thickness dependence, while the ferromagnetic Curie point shows very little fluctuation. The derivatives of the phonon resistivities also show little variation with thickness although those of Ho, Er and Tm are higher than the other metals. However, reasonable agreement is obtained with the bulk measurements of Colvin et al. (53). The phonon resistivities all varied with T in the high temperature region, in accordance with equation 3.14.

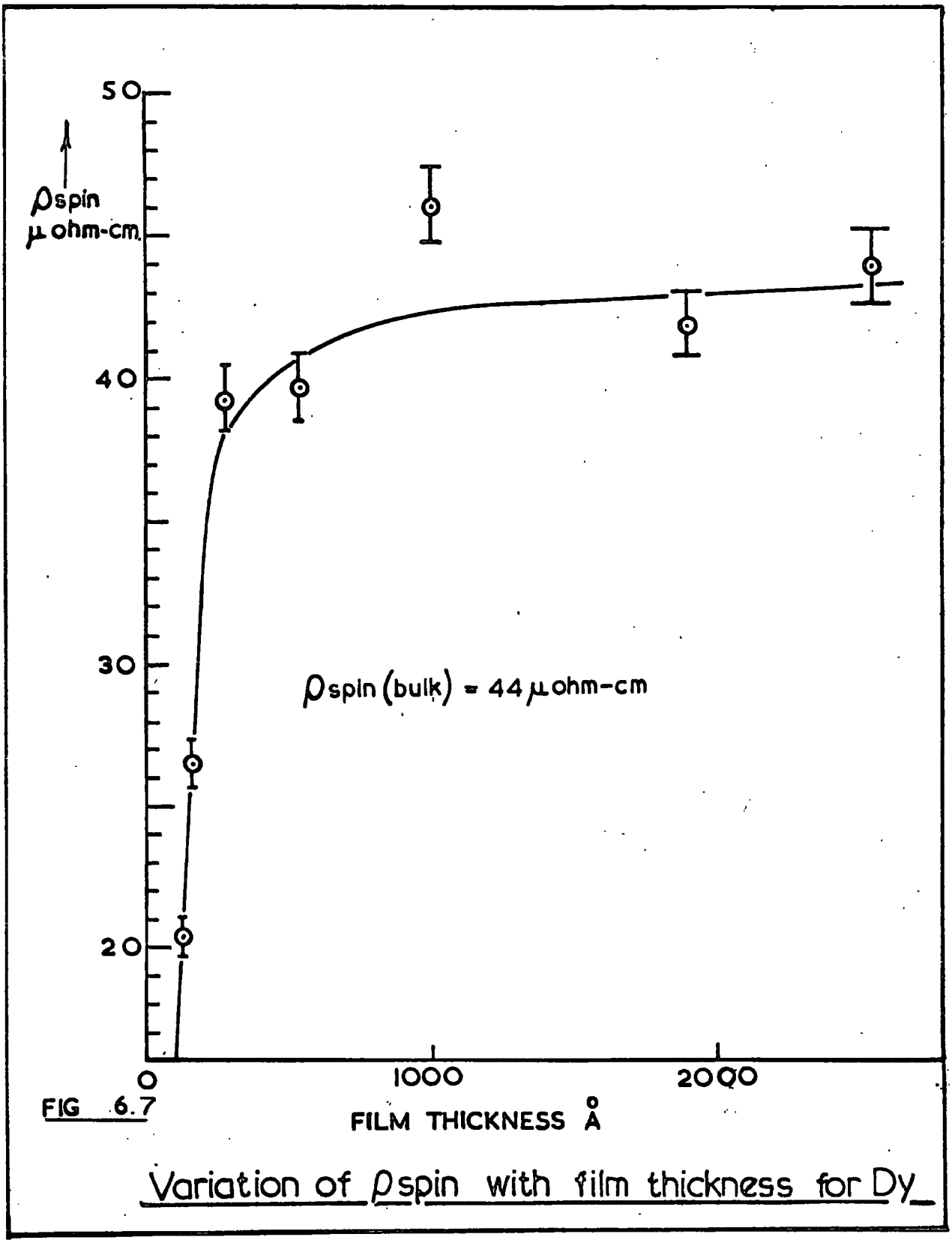

FIG 6.7

Variation of ρspin with film thickness for Dy

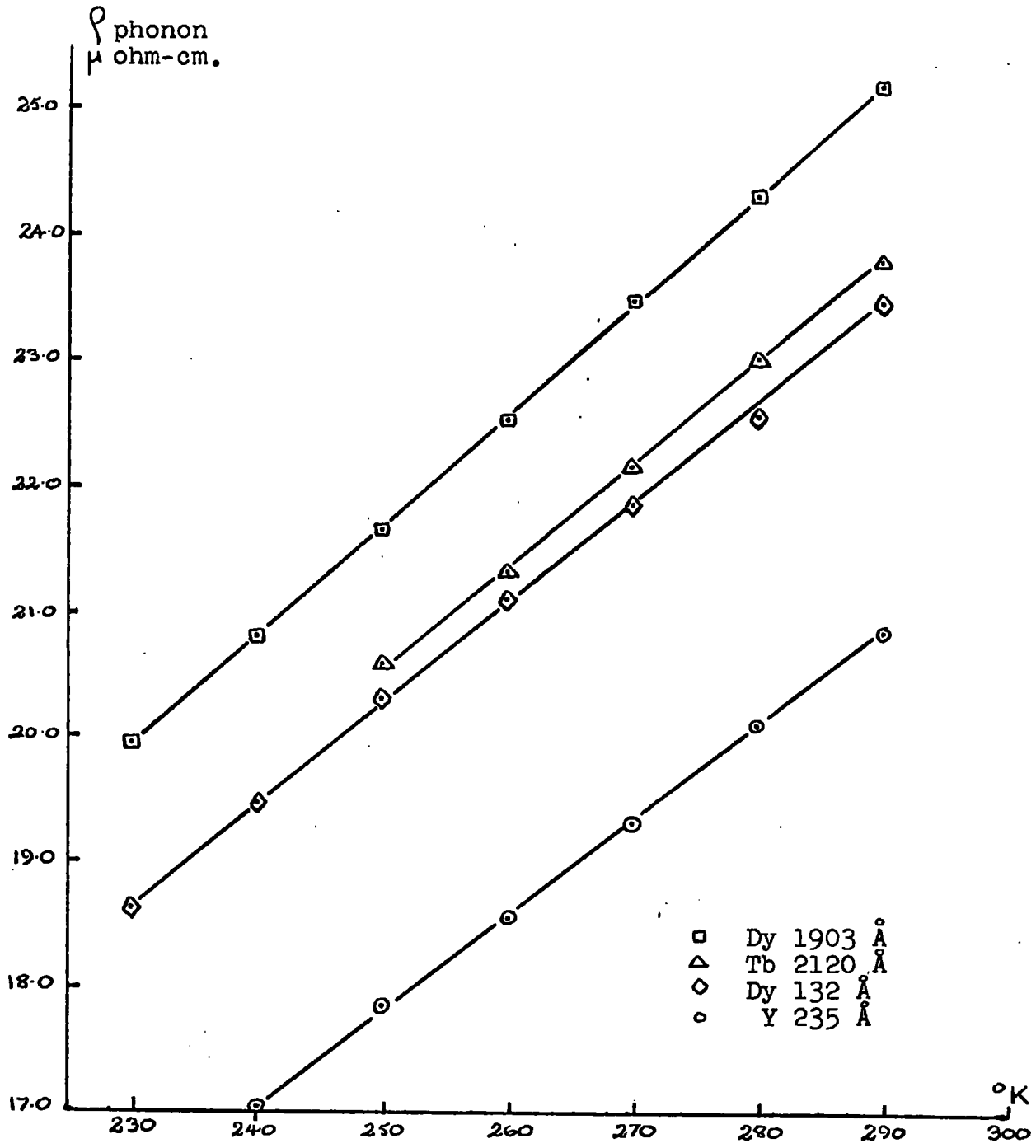

Fig. 6.8

Phonon resistivities of Dy, Tb, and Y films in the paramagnetic temperature region.

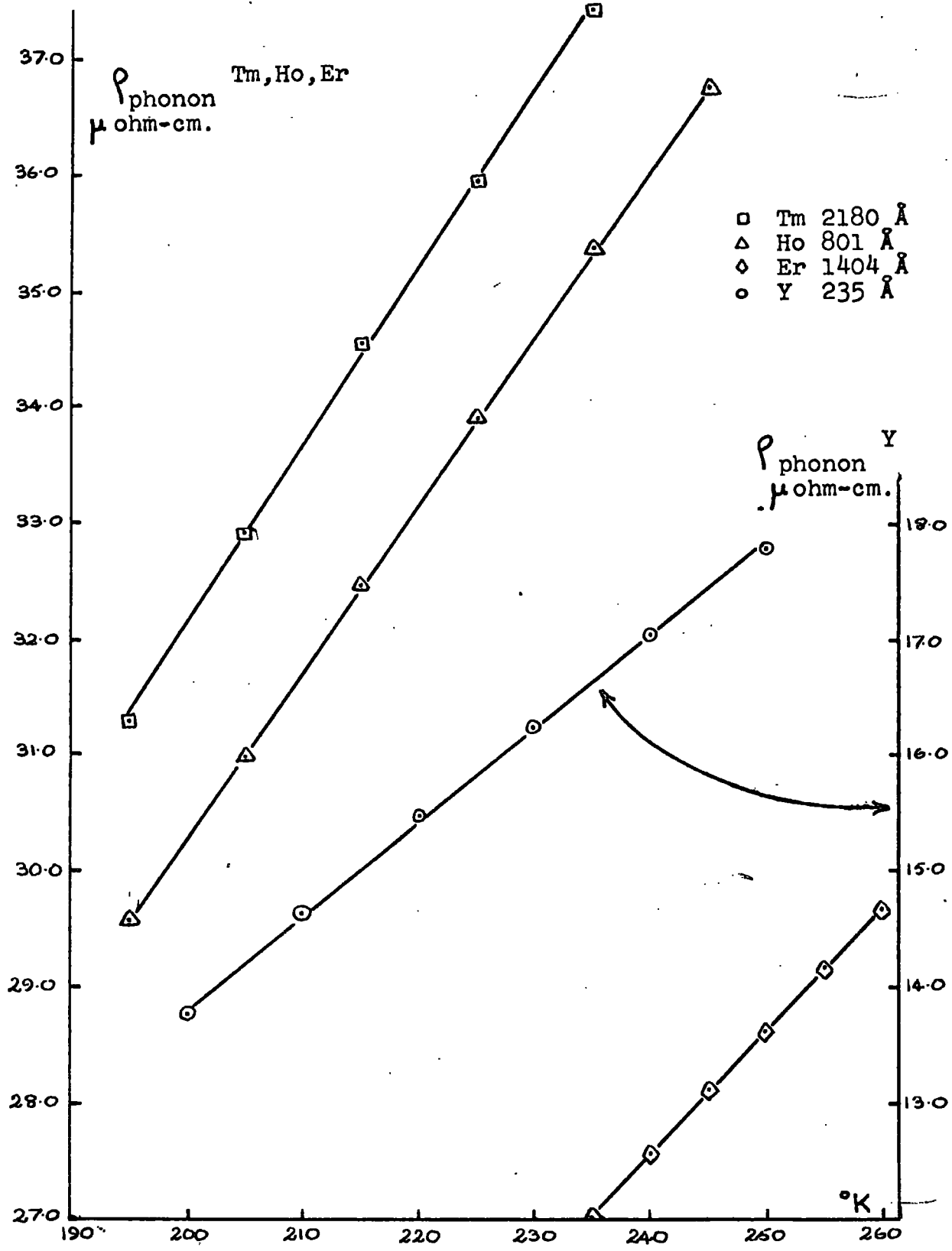

Fig. 6.9 Phonon resistivities of Tm, Ho, Er and Y films in the paramagnetic state.

Yttrium has a similar crystal structure and a similarity in the outer electronic shell configurations to the heavy rare earth metals. Its electrical resistance arises only from the residual and phonon contributions (equation 3.13) and its resistivity can therefore be used for direct comparison with the phonon resistivities of the heavy rare earth metals.

Although yttrium proved very difficult to evaporate successfully, a film of 235 Å was grown. Table 6.1 shows that the derivative of the resistivity of the yttrium film agreed closely with the values for the dysprosium and terbium films and in Figures 6.8 and 6.9 the phonon resistivities of several films in the paramagnetic state are compared with the resistivity of the yttrium film.

h) Magnetoresistance.

The effect on the electrical resistance of a uniform magnetic field applied parallel and perpendicular to the direction of the electric field in the film has been investigated. Figure 6.10a shows the variation with temperature of the negative transverse magnetoresistance of the Dy 1903 Å film, in the region of the Néel point. A constant field of 10 KOe was applied perpendicular to the face of the film and at this magnitude of field, the only marked effect appeared in the neighbourhood of the Néel point,

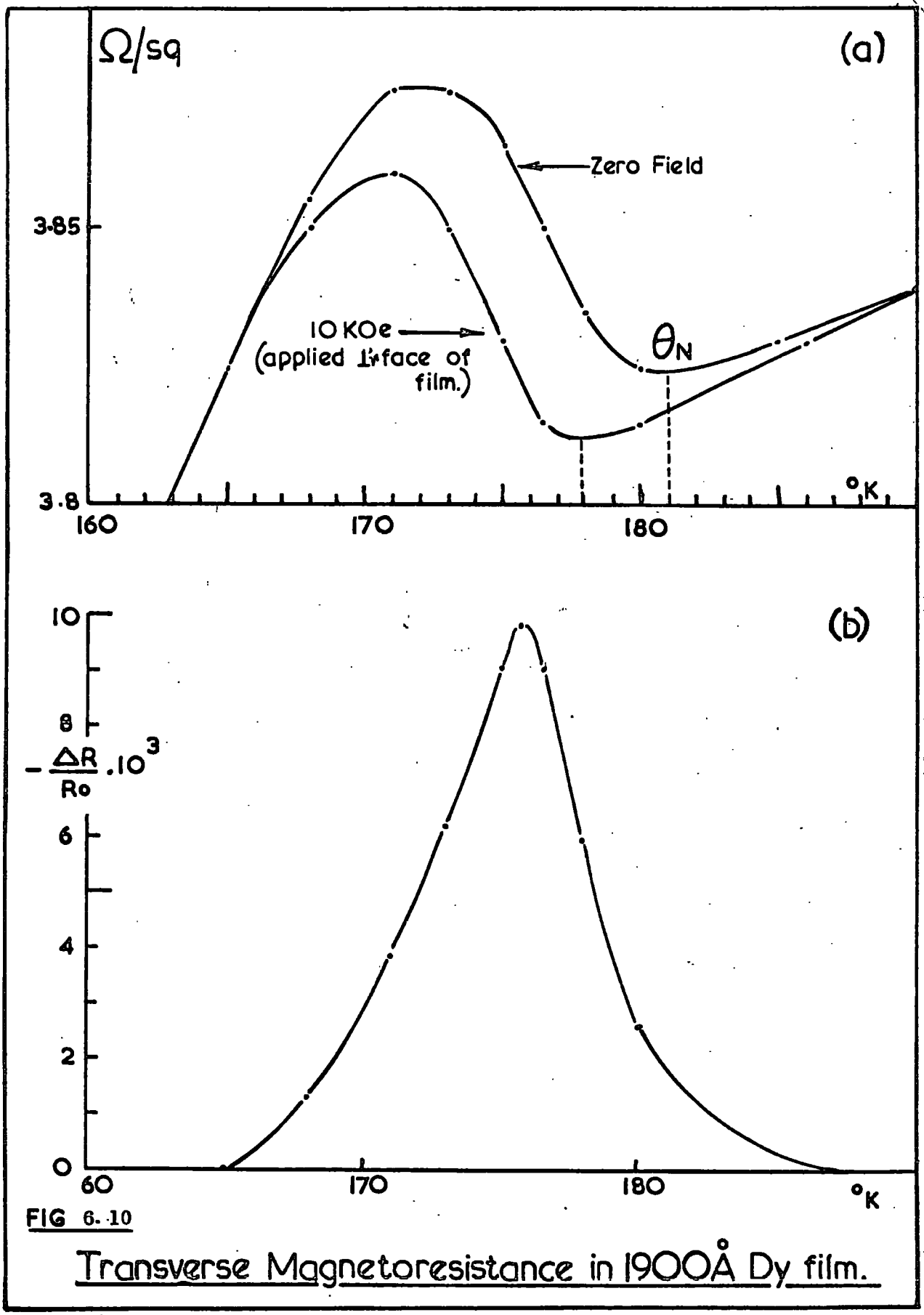

FIG 6.10

Transverse Magnetoresistance in 1900Å Dy film.

where the anomalous peak in the zero-field resistance was suppressed and the Néel point itself was reduced by about 3°K. No magnetoresistive effect was observed above 190°K in the paramagnetic region and Figure 6.10b shows the variation of $\Delta R/R_o$, which reaches a maximum at 176°K. Below 165°K, no magnetoresistive effect was detected, although this was undoubtedly due to the upper limit of 10 KOe which was available at the time. Subsequent to these measurements being taken, a field of 15 KOe became available and it was fortunately possible to obtain several isothermal measurements on the Dy 1903 Å film in the anti-ferromagnetic region. As has been previously mentioned (section 5.2e), this film was re-examined eight months after growth, during which time its electrical parameters had not changed at all.

In between changes of the magnitude and direction of the applied field, the film is allowed to regain the paramagnetic state to destroy any remanent effects of magnetization in the ferromagnetic or anti-ferromagnetic states. The curves which were obtained are shown in Figure 6.11 and it can be seen that except for the 177°K isotherm, where the critical field is obviously very small, the magnetoresistive effect occurs largely above the limits of the earlier measurements.

From the results of Behrendt et al. (97), of the variation of the critical field of dysprosium with temperature, the values

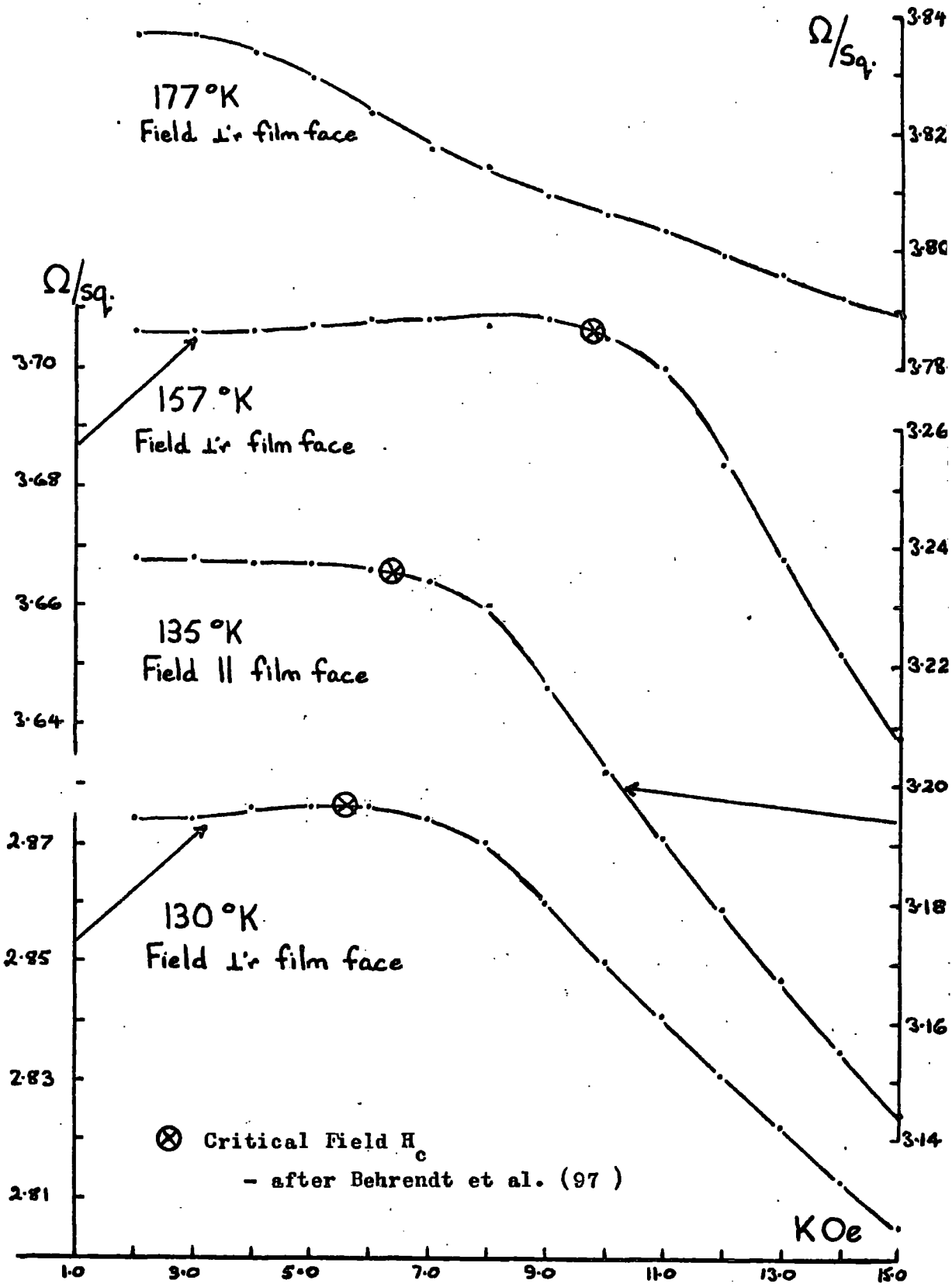

Fig. 6.11 Magnetoresistance Isotherms for the Dy 1903 Å film.

of the critical fields which correspond to the isothermal temperatures have been marked on the graphs, and it can be seen that in all cases, the region of critical field as indicated by the magnetoresistive measurements agrees well with the results of Behrendt.

The application of a magnetic field perpendicular to the surface of a thin film will introduce a demagnetizing field effect through the film owing to the proximity of the opposite surfaces of the film. The specimen was turned through 90^{o} at $135^{o}K$ in order to investigate the magnitude of the demagnetizing field. Compared to a 2.4% value of $\left(\Delta R/R_o\right)_{max}$ at $130^{o}K$ when the field was perpendicular to the surface, a value of 2.9% for $\left(\Delta R/R_o\right)_{max}$ was observed at $135^{o}K$, which indicates the presence of a demagnetizing field of about 16%. Finally, no longitudinal magnetoresistance was detected between $77^{o}K$ and room temperature, with a field of 10 KOe applied along the direction of the primary current.

The observation of a critical field effect, together with the anomaly in the resistivity near the Néel point, would indicate that the micro-crystallites of the film possess some degree of preferred orientation, with the c-axis of the crystallites lying in the plane of the film.

Figures 6.12a and 6.12b reproduce the negative transverse

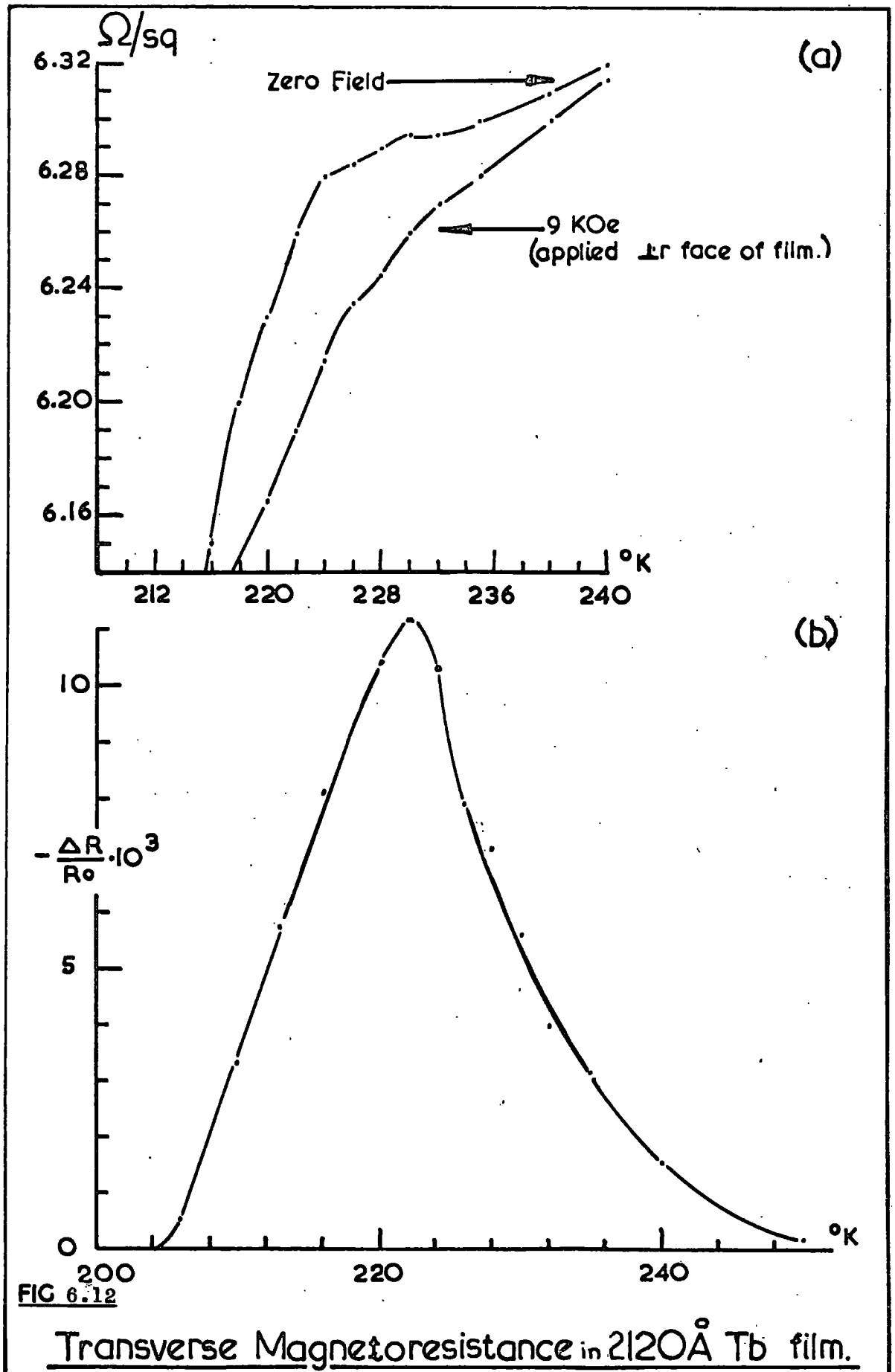

FIG 6.12

Transverse Magnetoresistance in 2120Å Tb film.

magnetoresistance at 9 KOe for the Tb 2120 Å film, which appears below 250°K in the paramagnetic region for the strength of field applied. The Néel point anomaly is almost completely suppressed and $\Delta R/R_o$ reaches a maximum at 222°K, just below the zero-field Curie temperature. Once again, at this field, the magnetoresistance quickly died out below the Curie point, only persisting down to about 204°K in the ferromagnetic region. Longitudinal magnetoresistance study produced no observable effect.

The unique feature of the magnetoresistance of thulium, shown in Figure 6.13a, is that it exhibits a positive peak at the ferromagnetic Curie point. The origin of this anomaly must lie in the collapse of the anti-phase spin structure at the Curie point, but the qualitative explanation of this is not fully understood. The two smaller peaks are similarly tentatively ascribed to spin structure changes which occur at 38°K and 56°K in thulium.

The small transverse magnetoresistance isotherms for gadolinium are shown in Figure 6.13b. As expected, there is no effect in the paramagnetic region and the greatest negative magnetoresistance is seen in the region of the Curie point, below which it again decreases.

Finally, Ho 801 Å did not show any marked transverse magnetoresistance effect, the greatest value of $-\Delta R/R_o$ being less than 0.1% at the Néel point. Erbium did not possess any observable

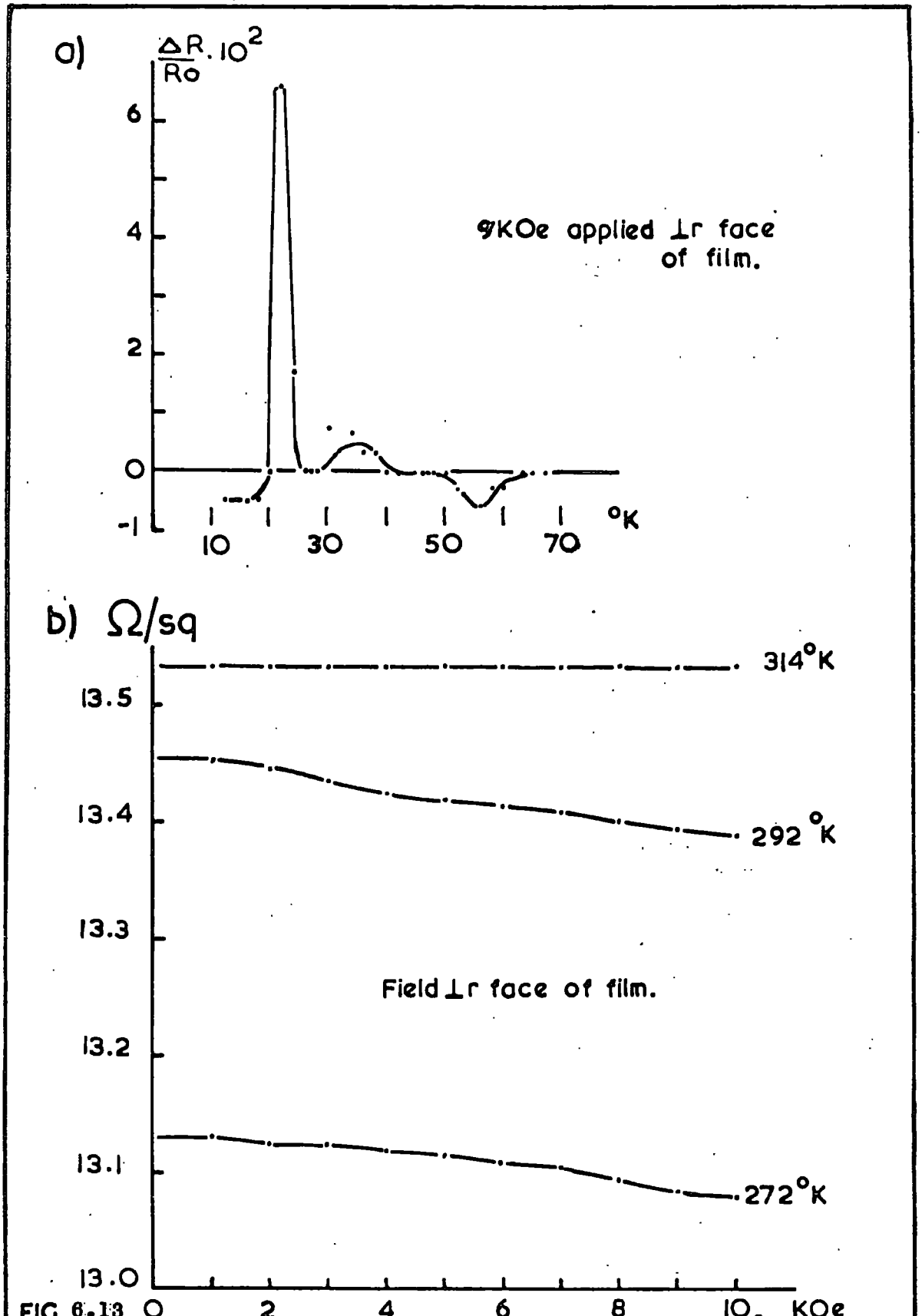

FIG 6.13

a) Transverse Magnetoresistance in 2180Å Tm film.

b) Magnetoresistance Isotherms in 1614Å Gd film.

magnetoresistance, which was undoubtedly due to the magnitude of the critical field of erbium in its anti-ferromagnetic region.

6.2 Discussion.

a) Film parameters.

The magnetic transition temperatures of the films, shown in Table 6.1, quite clearly show variations from the bulk values and in some instances, these variations are quite considerable.

There is a consistent decrease in the Néel point temperature Θ_N in dysprosium and holmium and overall, there appears to be a decrease in Θ_N with thickness. The 'thick' films have Néel temperatures which compare well with the bulk values. The ferromagnetic Curie points Θ_C appear to lie slightly above the accepted bulk values, with the exception of dysprosium. No change of Θ_C with thickness is observed in this latter metal.

It is difficult to obtain the exact values of the magnetic transition temperatures from examination of the R(T) curves and the estimated error in Θ_N and Θ_C in Table 6.1 is $\pm$ 1°K.

Unlike the case of dysprosium, it was not possible to associate any feature in the R(T) curves of the remaining metals with the paramagnetic Curie temperature Θ_P. This must cast doubt on the interpretation of Θ_P in dysprosium, and the changes shown in Table 6.1 in Θ_P may arise from changes in the

detailed spin structure. However, in the analysis of the exchange energy and effective mass (section 6.2b), the maximum change in is only 8% compared to a change of 55% in ρ_{spin}, which is the predominant factor involved.

It has been shown by Hoffman (98) that thin films may be subject to very large internal stresses, arising from their mode of formation, which can be interpreted in the form of compressive or tensile forces, the former for discontinuous films and the latter for continuous films. These stress forces have been shown to be capable of profoundly affecting the physical properties of thin films and since it is the lattice structure which is primarily involved, electrical and magnetic properties are also affected by stress effects. Milton and Scott (99) have investigated the effects of pressure on dysprosium and have found that $d\Theta_N/dP$ $-0.5^{\circ}K/k.bar$. This would imply that compression forces of about 20 k.bars exist in the thinnest films of dysprosium and a force of this magnitude is considerably larger than those normally found (100,101). Further, this fails to account for the consistency of the ferromagnetic Curie point of the dysprosium films, which is achieved in the bulk metal with only about 5 k.bars pressure according to Milton and Scott. Also, tensile stresses would be expected to be present, if the films are continuous.

However, stress forces, if present, must influence the

film parameters to some extent. The resistance ratios are a clear indication of the presence of stresses, although the distribution of stress arising from tensile stress in the surface is unknown. The very thin films possess smaller resistance ratios, even though the impurity concentration is unlikely to be greater than in the thicker films. To substantiate this, there is the prediction in section 5.3b that the rate of deposition is better than 250 times that of residual gas bombardment. Aside from the stress concept therefore, it is not obvious why the film values of θ_c in dysprosium should be lower than the bulk value of 85°K, although Schuler (102) has reported a value of 82°K in a 2200 Å dysprosium film.

Finally, Table 6.1 lists the derivatives of the phonon resistivity, which were obtained from the computed least-squares fit to the experimental points. Very little variation with thickness is seen, although a gradual increase down the series is observed. A larger concentration of impurity in the thinner films would be expected to produce correspondingly greater lattice scattering and hence a larger value of $d\rho_{ph.}/dT$. The consistency in the values of the phonon resistivity also indicates that the thinnest films are still continuous in structure, rather than an array of discrete islands. The conduction mechanisms of such an array in an evaporated metal film have been examined by

Neugebauer and Webb (103) and Hartman (104) who found that the conductivity depends exponentially on reciprocal temperature.

b) Thickness dependence of the spin-disorder resistivity of dysprosium.

Figure 6.7 shows the observed variation with thickness of the spin-disorder resistivity ρ_{spin} of dysprosium, which exhibits a sharp fall-off with thickness below about 400 Å.

In seeking to account for this observation, we must turn to the theories of ferromagnetism of thin films, of which some mention has been made earlier, (section 3.5). While no specific theoretical prediction exists of the thickness dependence of the spontaneous magnetization of a hexagonal close-packed structure, some inferences on the behaviour of the spin-disorder resistivity, which is intrinsically linked to the behaviour of the spontaneous magnetization, may be drawn from these results.

Klein and Smith (44) first calculated the spontaneous magnetization for films of simple cubic structure using spin-wave theory and this work was later extended to body-centred and face-centred cubic structures by Glass and Klein (45), whose results are shown in Figure 6.14. They differ from those of simple cubic films only in detail and the general form of these results is unchanged by the change in lattice type.

However, later work by Corciovei (47), who applied the Holstein-Primakoff (48) formulation to thin ferromagnetic films, and Pearson (42), who used the Bethe-Peierls-Weiss approximation of the molecular field approach, concluded that the saturation magnetization of a ferromagnetic thin film will fall below the bulk value only in films of less than about 40 Å thickness. Experimentally, Neugebauer (105) has obtained results in close agreement with this postulate by using ultra-high vacuum techniques to grow continuous films of nickel less than 100 Å thick. This contrasts with earlier experimental work by Crittenden and Hoffman (106) in which reduced values of the magnetization were obtained below about 400 Å thickness.

Figure 6.15 shows the variation of the reduced spin-disorder resistivity term ρ_{spin}/ρ_{bulk} of dysprosium with film thickness (t Å). It is interesting to observe the similarity to the family of curves of Glass and Klein in Figure 6.14 and also that the extrapolated region where $t < 200$ Å passes through the origin. Owing to this linearity and its approach to zero, it is proposed that the observed variation with thickness of the spin-disorder resistivity of dysprosium is a real effect, related to the magnetization of the films, since the possibility of impurity has been dealt with.

Following the investigations of previous workers (107),

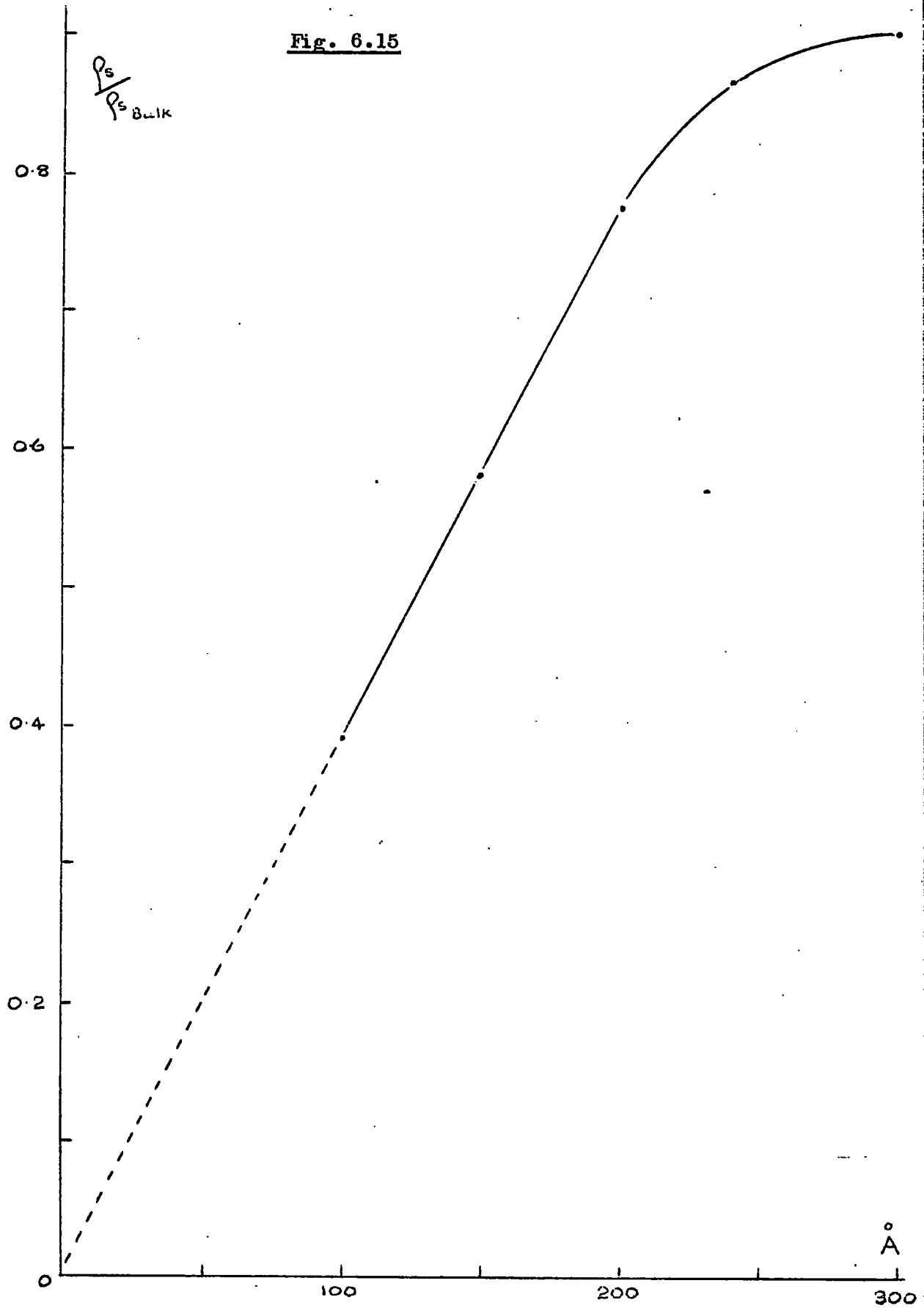

Reduced spin disorder resistivity of Dysprosium

Rocher's analysis (65) of the indirect exchange interaction, which leads to the derivation of equations 3.33, 3.34 and 3.35, may be used to examine the behaviour of the effective mass m* and the exchange energy G.

Accordingly, m* and G were evaluated for the dysprosium films from equations 3.34 and 3.35 using the experimental results of ρ_{spin} and the paramagnetic Curie temperature θ_p. The values of m* and G are listed in Table 6.2 and the variation with thickness of G is shown in Figure 6.16. As expected, in the thicker films, there is no deviation from the bulk value of G. It is possible however, that equations 3.34 and 3.35 are not directly applicable to the case of very thin films, owing to the increasing influence of the surface states, which may result in a modification of the exchange interaction. Also, there is now considerable doubt (108) about the validity of the derivation of equations 3.33, 3.34 and 3.35 from the R-K-K-Y interaction itself and therefore the apparent thickness dependence of G and m* below about 500 Å must be viewed with some uncertainty.

c) <u>The temperature dependence of the spin-disorder resistivities.</u>

The variations of $\rho_{spin}(T)$ of the various metals as obtained from the experimental results using Matthiessen's rule

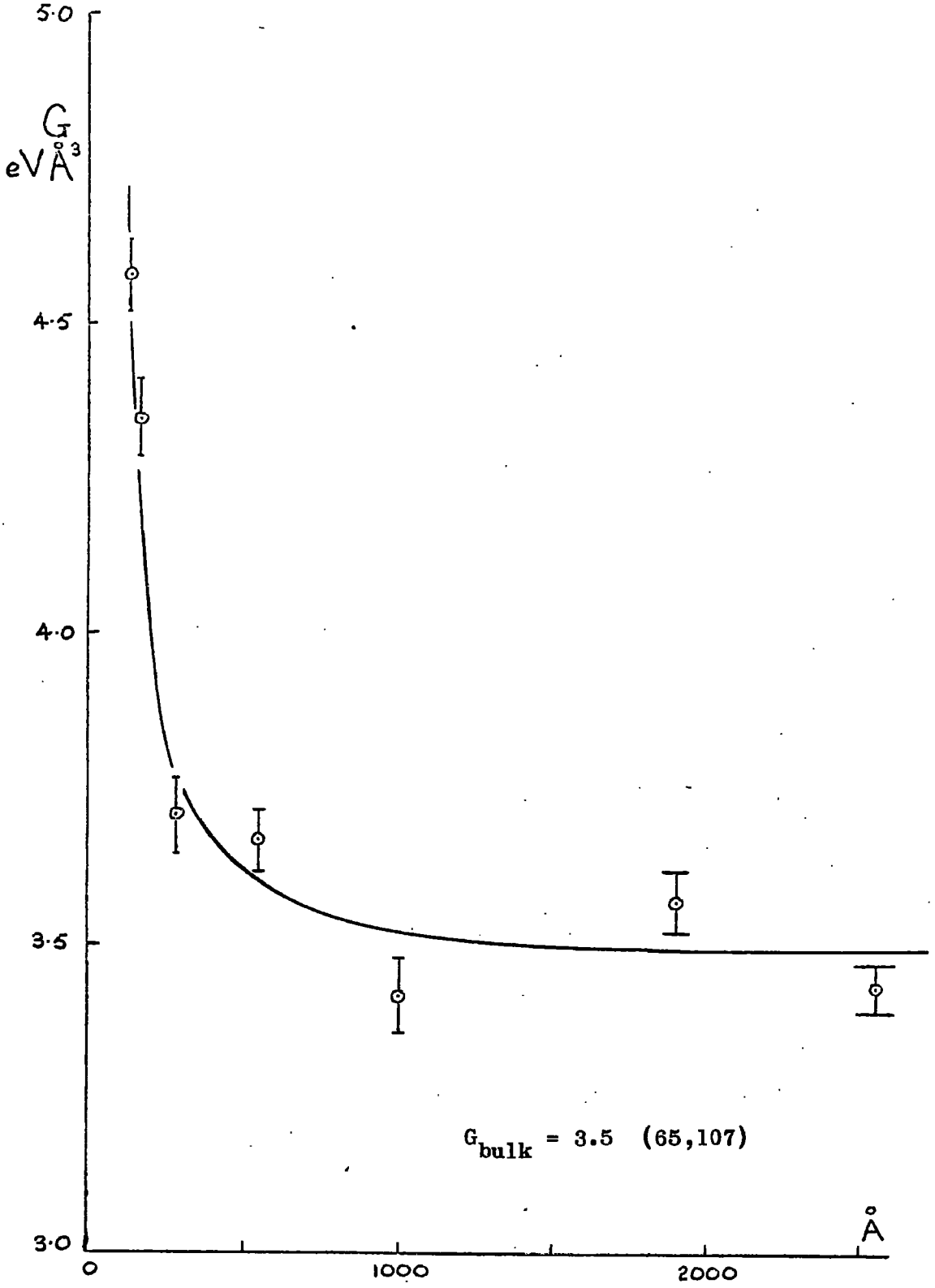

Fig. 6.16

Variation with film thickness of the exchange energy for Dysprosium.

(equation 3.16) are shown in Figures 6.17 and 6.18. It can be seen that $\rho_{spin}(T)$ of Gd, Tb and Dy vary as T^2 in a low temperature region and as $T^{3/2}$ in a higher temperature region. The behaviour of $\rho_{spin}(T)$ of holmium is very similar to that of Tb 2120 Å and consequently is not shown. Two examples of $\rho_{spin}(T)$ from the dysprosium series are depicted in Figure 6.18 and this behaviour is apparent in all the dysprosium films. $\rho_{spin}(T)$ in Gd 1614 Å follows a $T^{3/2}$ proportionality from a lower temperature than in Tb, Dy and Ho. The $T^{3/2}$ region in these metals commences in the temperature region 65 - 75°K and persists until about 110°K. Tb 405 Å uniquely exhibits a T proportionality above 100°K. In the low temperature region, departure from the T^2 behaviour commences below 35°K but Gd continues as T^2 to approximately 22°K.

The $\rho_{spin}(T)$ term of Er 1404 Å shows a very close fit to $T^{5/2}$ between 36°K and 54°K but $\rho_{spin}(T)$ of Er 475 Å was not successfully analysed owing to its small magnitude, which made a reliable separation of ρ_{spin} at intermediate temperatures impossible.

In Tm 2180 Å, $\rho_{spin}(T)$ varies as T^{10} between 26°K and 32°K. Above this temperature, as the Néel point is approached, no temperature proportionality is discernible.

Table 6.3 lists the constants of proportionality for $\rho_{spin} \propto T^n$ (where $n = 1, 2, 3/2, 5/2$) which are obtained by

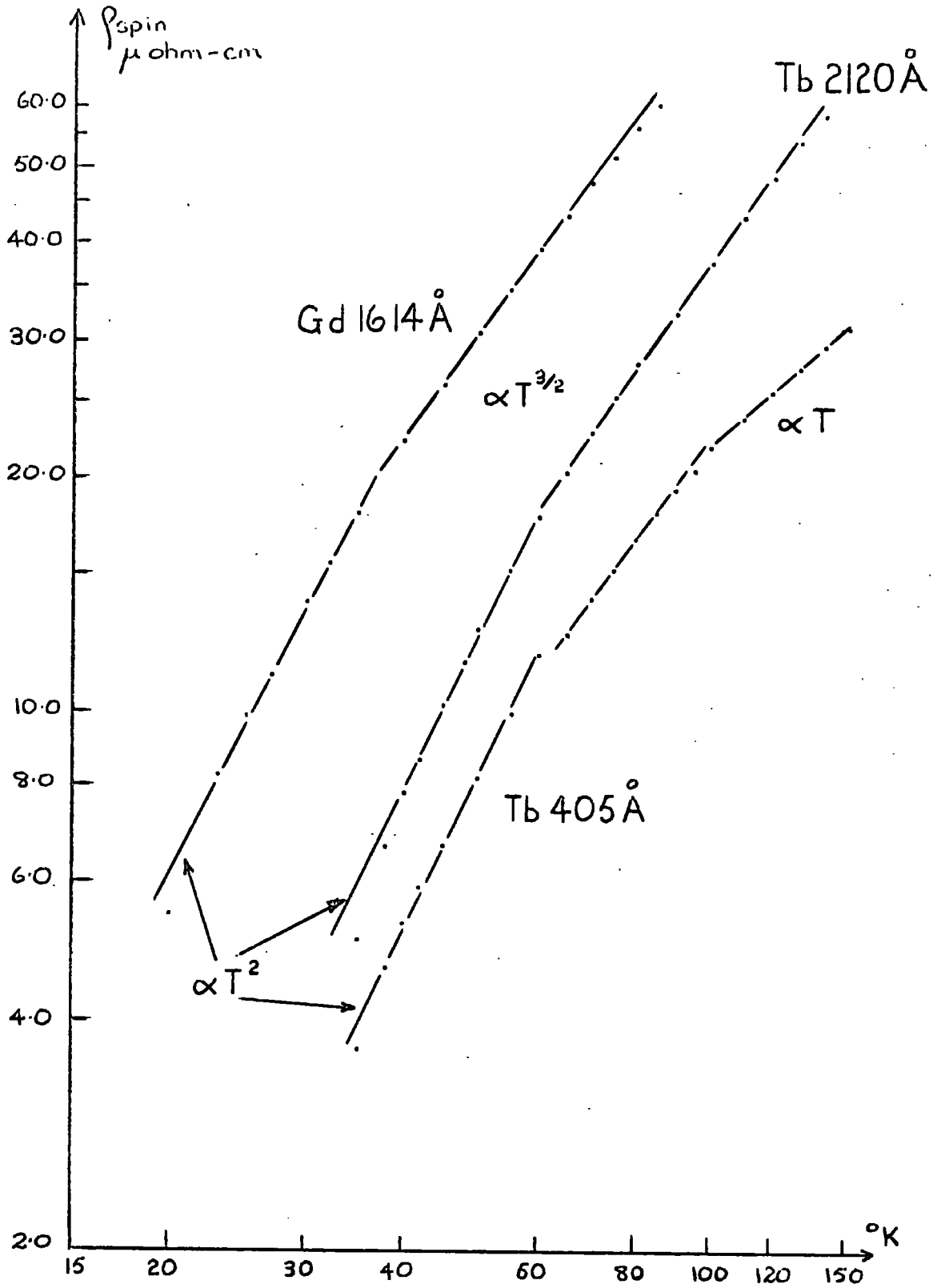

Fig. 6.17 ρ_{spin} Vs. Temperature on a log-log scale for Tb and Gd films.

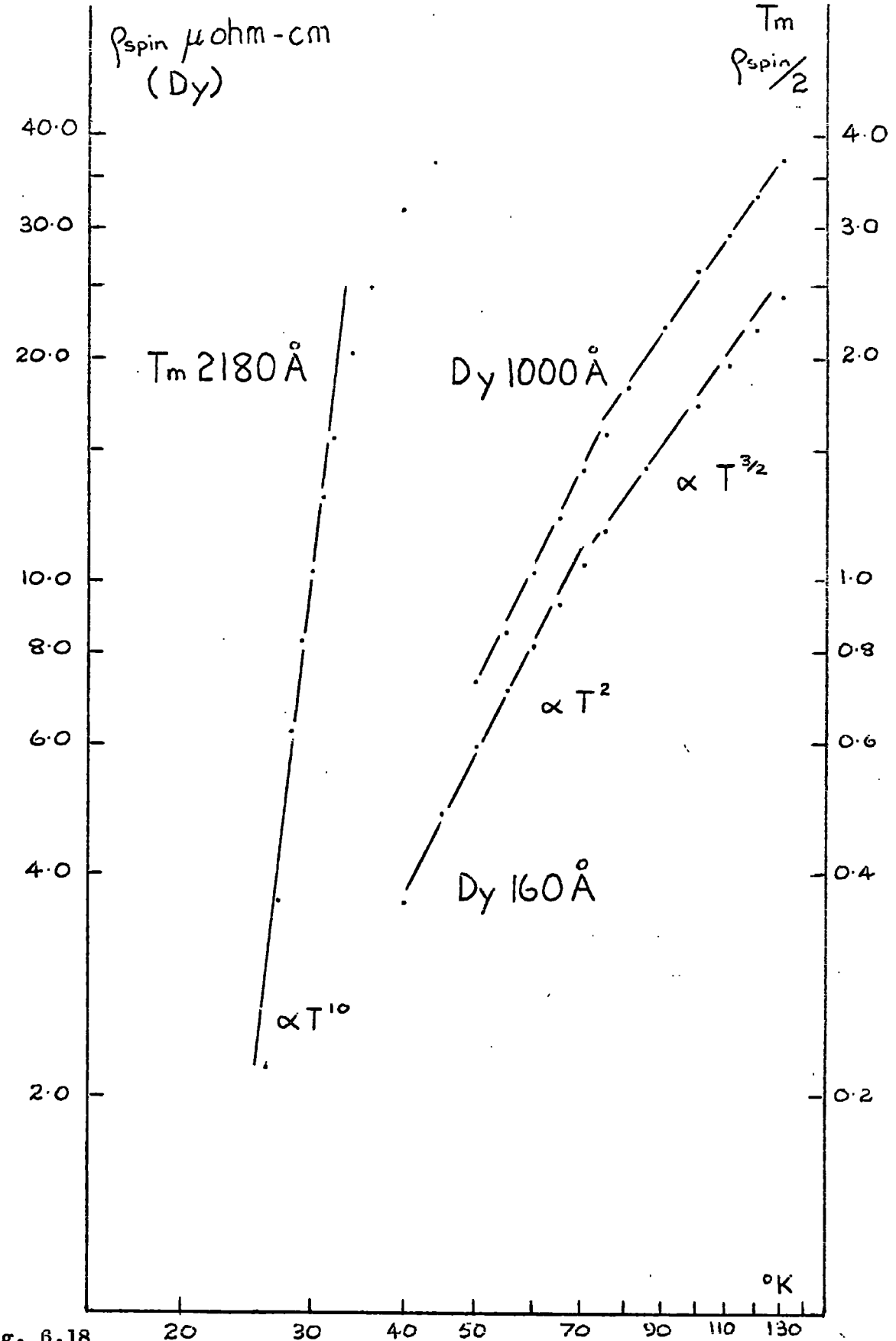

Fig. 6.18 ρ_{spin} Vs Temperature on a log-log scale for two Dy films and Tm

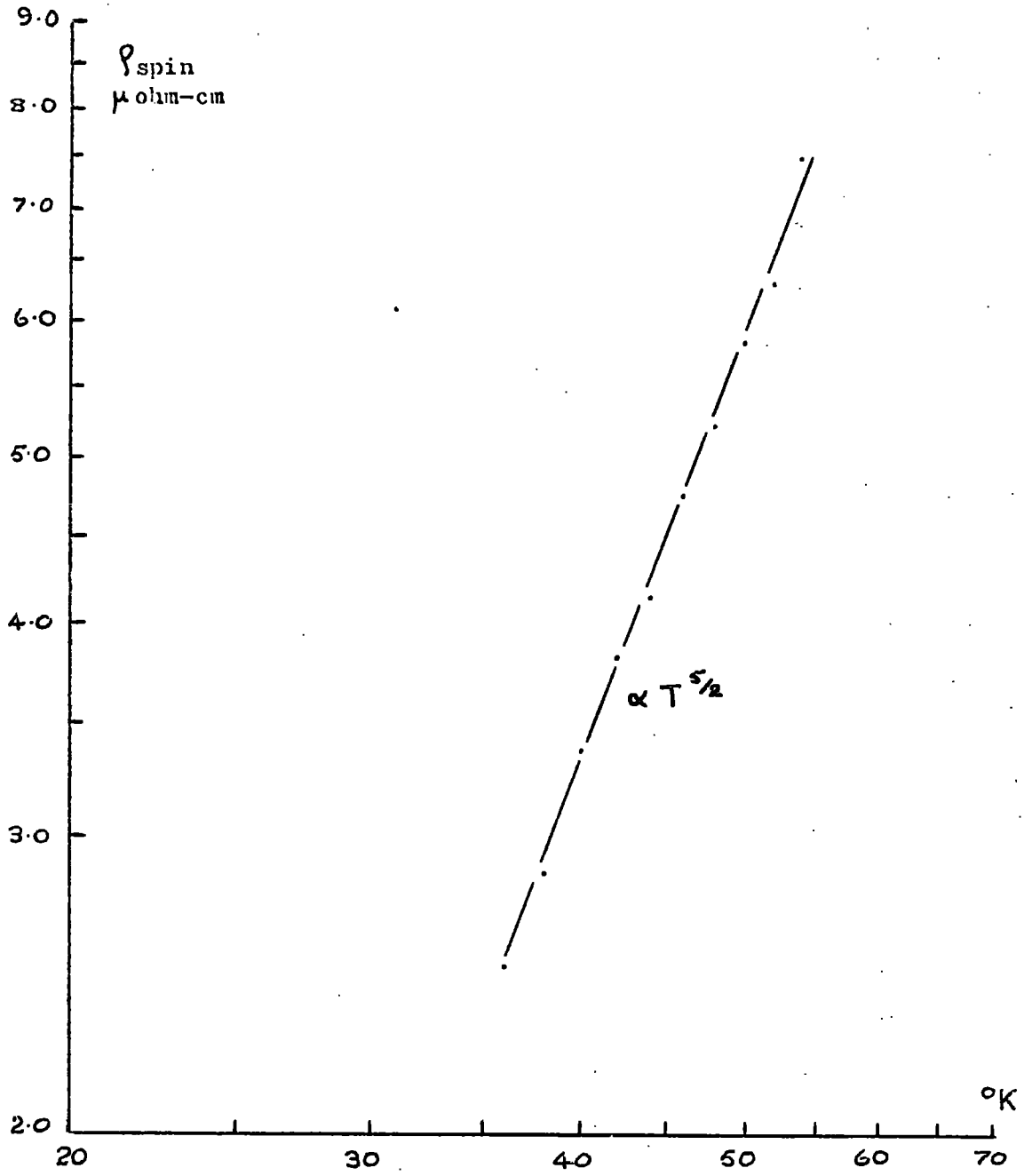

Fig. 6.19

ρ_{spin} vs. temperature on a log-log scale for 1404 Å Er.

plotting ρ_{spin} versus T^n on a linear scale. The T^2 constants of Tb, Dy and Ho show a decrease with thickness, which is undoubtedly due to the change in magnitude of the spin-disorder resistivities, since the variation of the magnitude of the constants follows these changes closely. The behaviour of the $T^{3/2}$ constants is more difficult to understand however, since no regular variation exists, as in the T^2 case. It was not possible to obtain the constant of $\rho_{spin} \propto T^{10}$ for thulium.

It is now well established that in ferromagnetic materials, the scattering of electrons by disordering of the spin system can be analysed in terms of the spin-wave spectrum. Kasuya (31) and Mannari (32) have shown that for simple ferromagnets, this term can be written (see equation 3.18)

$$\rho_{spin} = C.T^2 \qquad 6.1$$

while Mackintosh (91) has argued that in ferromagnets with high anisotropy, the spin resistivity will involve a term in the spin-wave excitation energy Δ . The contribution then becomes

$$\rho_{spin} = C.T^2 \exp(-\Delta/kT) \qquad 6.2$$

where Δ is given by $\Delta = (K_2 K_6')^{\frac{1}{2}}/k$ where K_2 and K_6' are respectively the c-axis and basal plane anisotropy energies and k is Boltzmann's constant.

In order to obtain a good fit to the observed magnetization

curve, Niira (109) assumed a value of $\Delta/k = 20^{\circ}K$ for dysprosium. Since in the low temperature ferromagnetic phase, terbium is very similar to dysprosium, Mackintosh assumed an energy gap of similar magnitude and found a good fit for the experimental values of the resistivities of polycrystalline dysprosium and terbium obtained by Colvin et al. (53). Recent measurements by Sze et al. (110) on a single crystal of terbium orientated along the c-axis demonstrate the existence of this energy gap at $21.5^{\circ}K$.

In order to check the validity of this approach for the thin films of dysprosium and terbium, the results were re-plotted as ρ_{spin}/T^2 against $1/T$. Figure 6.20, on a log-linear scale, shows the experimental points of the terbium films in the T^2 region of Figure 6.17 which are adequately described by equation 6.2 in the T^2 region with $\Delta/k = 20^{\circ}K$. Similarly all of the dysprosium films are describable by equation 6.2 with $\Delta/k = 23 \pm 2^{\circ}K$. Figure 6.21 typically shows the result for the Dy 542 Å film. Unfortunately, the width of the T^2 section of the ρ_{spin}-T observations was never more than $30^{\circ}K$ and often less than this, consequently, it was not possible to obtain more accurate values of Δ.

It can be seen in Figures 6.20 and 6.21 that below about $35^{\circ}K$, the experimental points deviate from the fitted result; this is due to the fact that in the analysis of ρ_{spin}, the

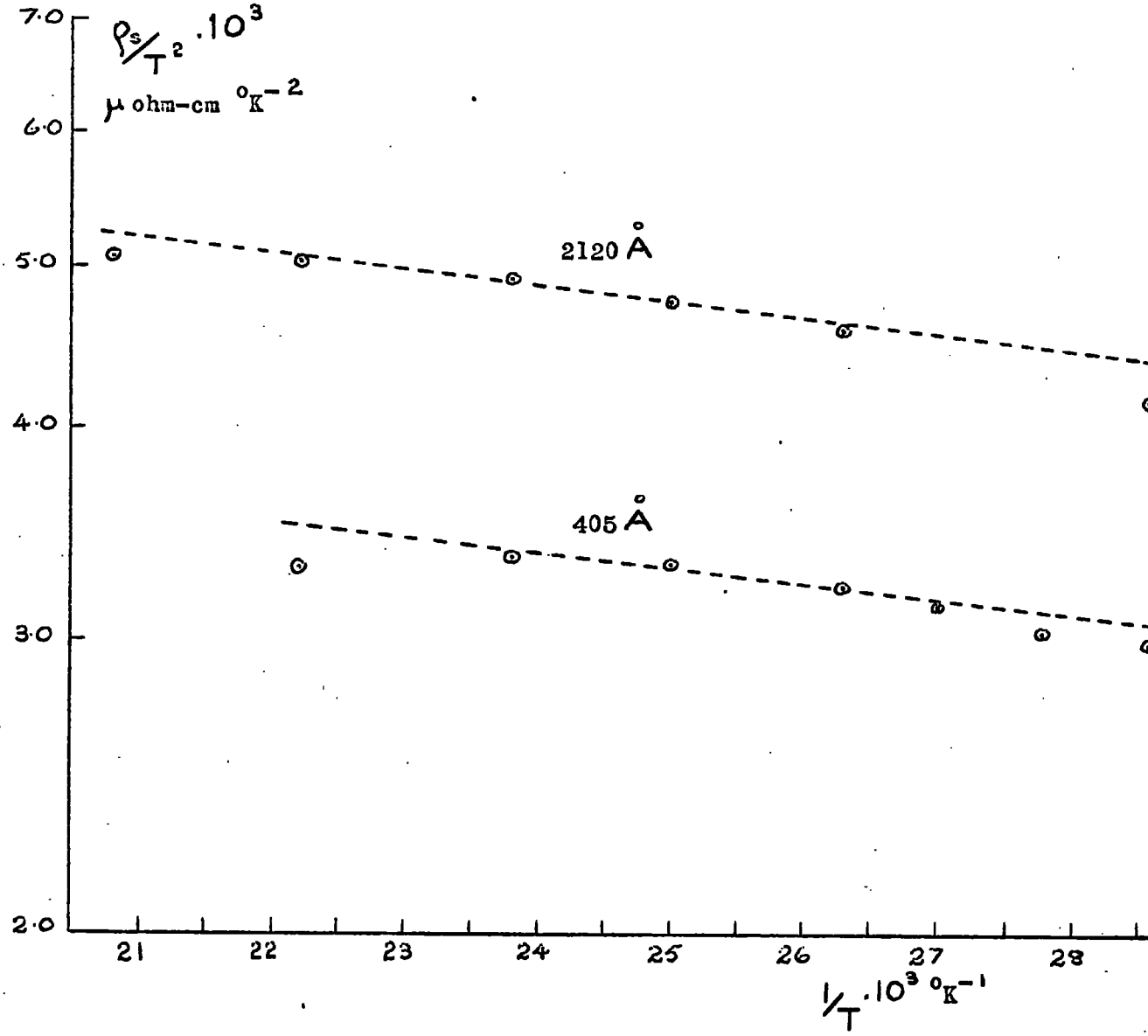

Fig. 6.20

Fit of $\rho_{spin} = CT^2 \exp(-\Delta/kT)$ with $\Delta/k = 20^oK$ to Terbium; on a log-linear scale.

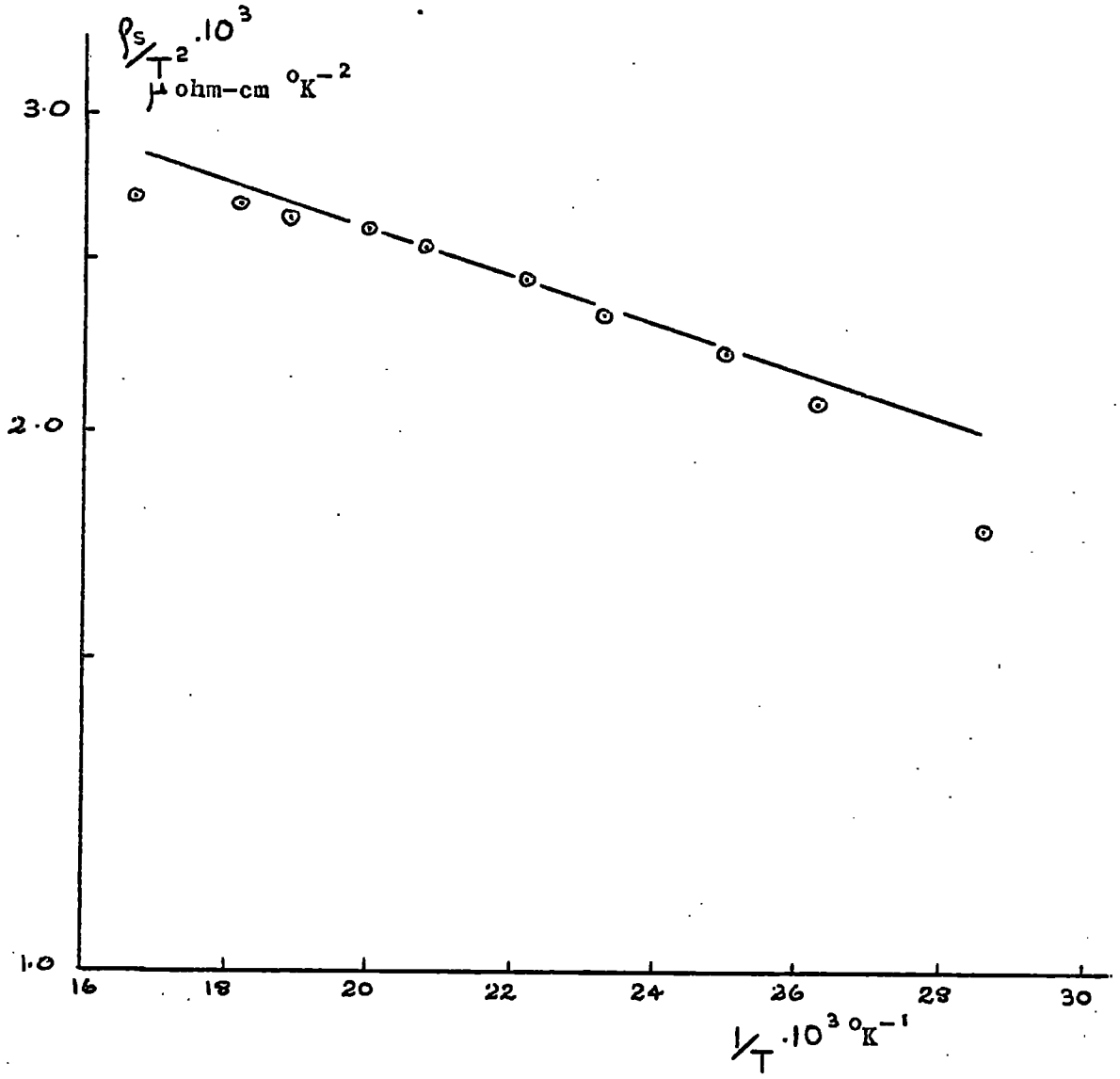

Fig. 6.21

Fit of $\rho_{spin} = CT^2 \exp(-\Delta/kT)$ with $\Delta/k = 25^oK$ to Dy 542 Å on a log-linear scale.

linearity of the paramagnetic region of the phonon resistivity is also assumed to be true at very low temperatures, when in fact in these regions, the phonon resistivity varies as T^5, according to equation 3.15. This is shown to be the case in Figure 6.22, where the experimental values of ρ_{phonon} for Dy 2550 Å are compared with the values predicted from the equation

$$\rho_{phonon} = \rho_{total}(T) - \rho_{residual} - C.T^2 \exp(-\Delta/kT) \qquad 6.3$$

It is found that the phonon resistivity derived from equation 6.3 has a T^5 proportionality between 30°K and 40°K, thus verifying that the discrepances observed in Figures 6.20 and 6.21 are due to the neglect of the low temperature dependence of the phonon resistivity.

Yosimori (111) and Kaplan (112) have shown that the spin-wave dispersion law in spiral structures and in ferromagnetic spirals is linear, while anisotropy can produce an energy gap. Niira has also shown that a linear spin-wave dispersion law indicates a T^2 magnetization curve. On this basis, Mackintosh has predicted that the spin-disorder resistivities of holmium and erbium, which are examples of ferromagnetic spirals with anisotropy, should be proportional to $T^4 \exp(-\Delta/kT)$. However, no such dependence was observed in the spin-disorder resistivities of these metals.

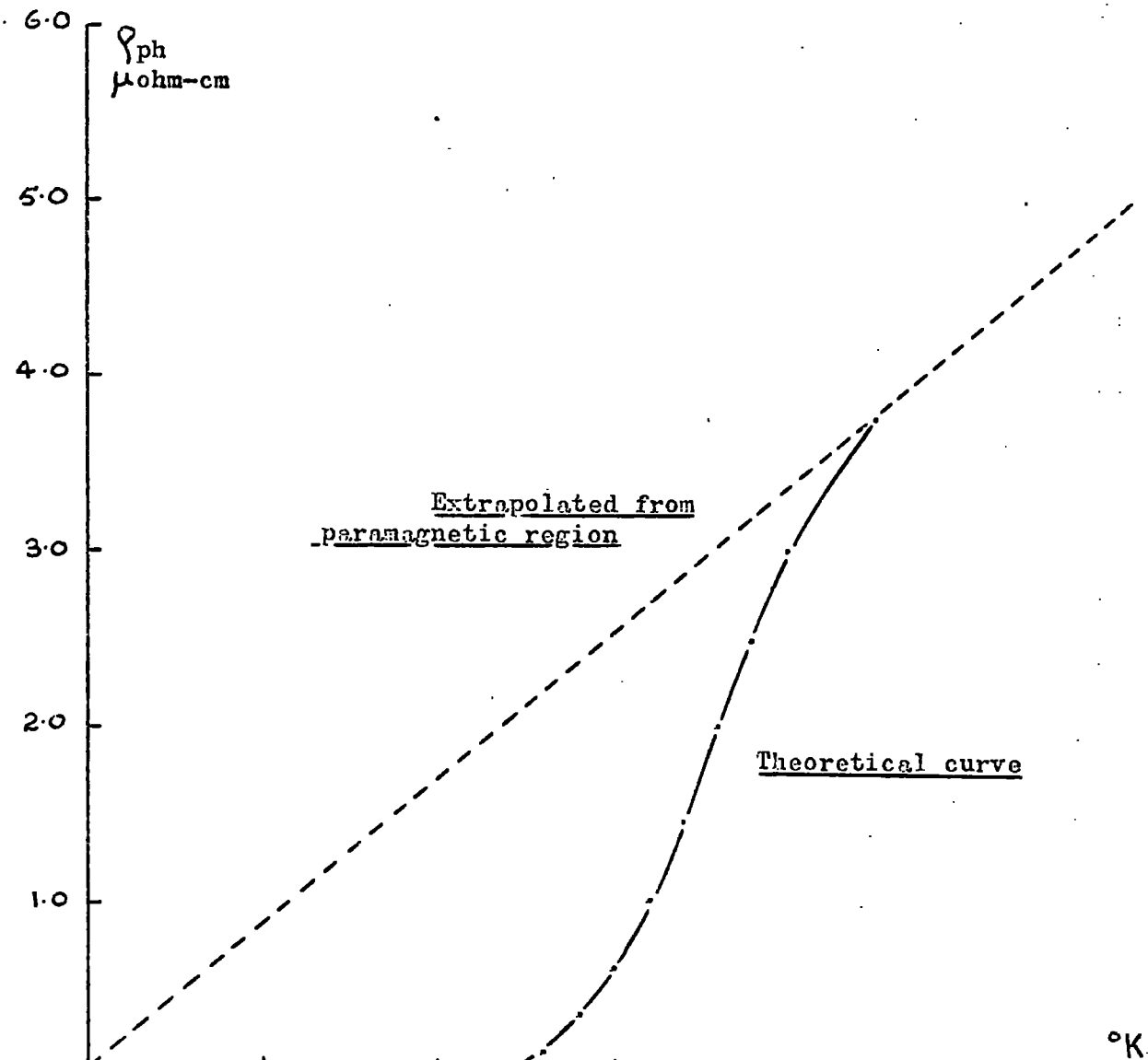

Fig. 6.22

The theoretical curve of the phonon resistivity below 40°K compared to the extrapolated estimation.

The change from the T^2 to the $T^{3/2}$ dependence in Gd, Tb, Dy and Ho occurred in all the films of these metals and also in the bulk polycrystalline dysprosium sample which was examined. Investigations of the basal plane anisotropy constants which have been derived for dysprosium and terbium by Rhyne and Clark (113) and for gadolinium by Graham (114), have shown that in dysprosium and terbium, K_6^6 is falling rapidly in the region 60 - 70^{0}K, while for gadolinium, K_6^6 begins to fall sharply from about 30^{0}K. Consequently, above these temperatures, we are probably dealing with the low anisotropy case of Mannari rather than a spin-wave model requiring a spin-wave excitation energy.

However, while the fall of the anisotropy energies of Gd, Tb and Dy appears to be connected to the observed change in the temperature dependence of the spin-disorder resistivity, it does not explain the reason for this change and it is therefore necessary to examine other associated phenomena for an interpretation of the observations.

The calculated dependence of the anomalous Hall coefficient R_s upon the spontaneous magnetization and upon temperature has been discussed earlier (section 3.7), with reference to the particular case of the rare earth metals. It has also been established both qualitatively and quantitatively that there is an inter-dependence of the spin-disorder resistivity ρ_{spin} and R_s

and following from this, a dependence of ρ_{spin} on the spontaneous magnetization. These dependencies are shown in equations 3.41, 3.42 and 3.43.

In an effort to explain the observed dependence of $\rho_{spin}(T)$ of the rare earth thin films, an attempt was made initially to measure the Hall effect in a dysprosium film, in order to verify equation 3.41 but this was unsuccessful owing to the small size of the Hall emf ($\sim 10^{-7}$ V.cm/Amp). It is therefore necessary to analyse the results of previous work for corroborative information.

For gadolinium, Kikoin and Igosheva (74) report a linear dependence of R_s on ρ_{spin} above about $50^{\circ}K$, while analysis of the results of Volkenshtein et al. (115) on a single crystal specimen of gadolinium indicated that R_s measured in the direction of the b-axis has a $T^{3/2}$ dependence over a similar temperature range. Volkenshtein also found good agreement with equation 3.42 for these results. Measurements taken by Lee and Legvold (116) on single crystal gadolinium compare favourably with those of Volkenshtein.

Further, examination of the magnetization results for polycrystalline gadolinium of Elliott et al. (117) shows that on a log-log scale $\left[M_s^2(0) - M_s^2(T) \right] \propto T^{3/2}$ above about $30^{\circ}K$ (Figure 6.23).

The most informative results for R_s of dysprosium have recently been carried out by Rhyne (75) on single crystal specimens.

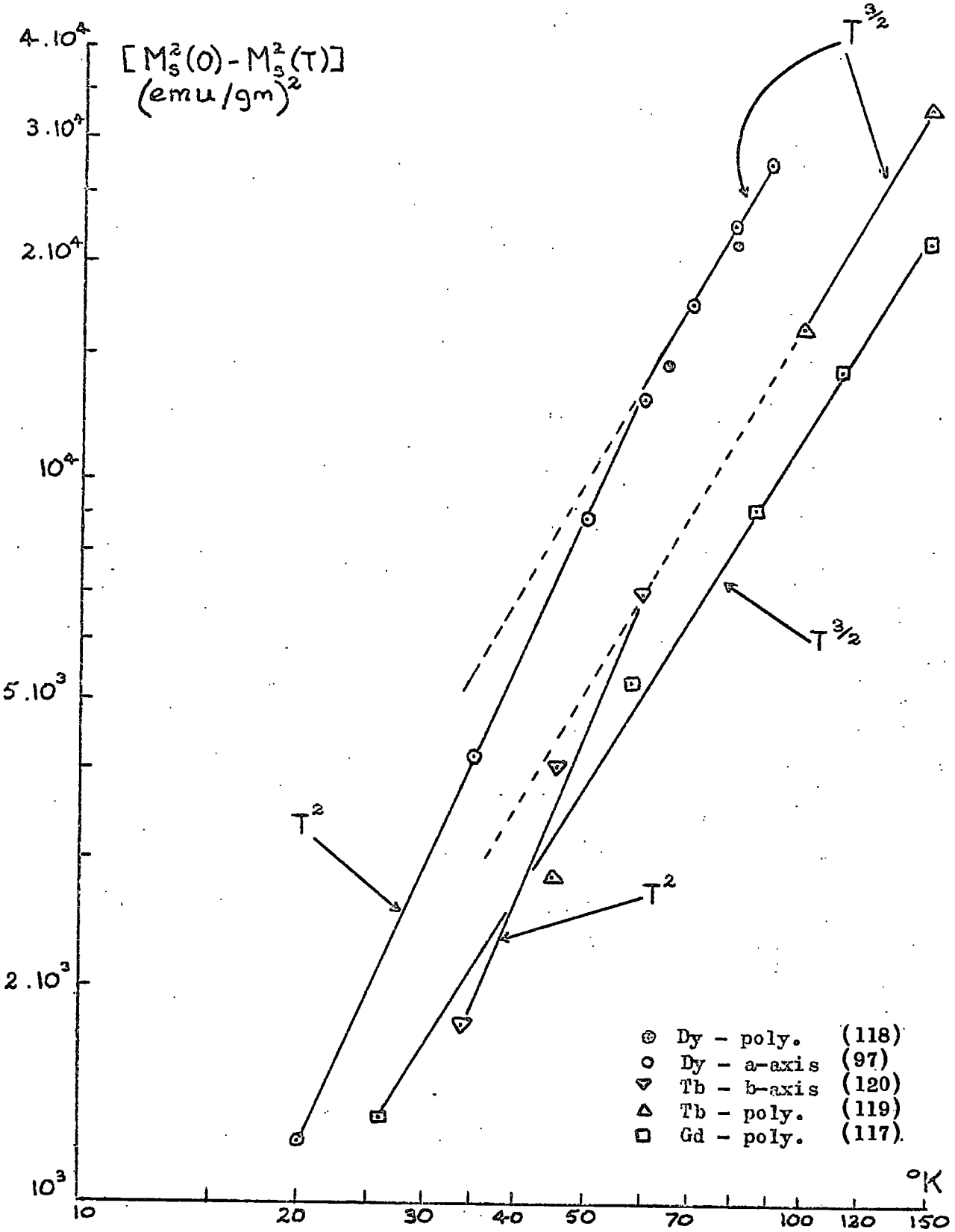

Fig. 6.23

Variation of $\left[M_s^2(0) - M_s^2(T)\right]$ with temperature on a log-log. scale.

It is found that R_s is proportional to ρ_{spin} between about $30^{o}K$ and $100^{o}K$ and also that R_s varies as T^2 at low temperatures (Figure 6.24a) and is dependent upon the square of the reduced magnetization, also at low temperatures (Figure 6.24b). Further examination of the results shown in Figure 6.24a reveals that above about $60^{o}K$, R_s varies as $T^{3/2}$ up to about $110^{o}K$, as shown in Figure 6.25.

The dysprosium single crystal magnetization data of Behrendt et al. (97) and the polycrystalline data of Elliott et al. (118) has been used to ascertain that at low temperatures $\left[M_s^2(0) - M_s^2(T)\right] \propto T^2$ while above about $60^{o}K$, there is a change to a $T^{3/2}$ proportionality (Figure 6.23).

Also shown in Figure 6.23 are the magnetization results of polycrystalline terbium from Thorburn et al. (119) and the single crystal terbium results of Hegland et al. (120). These results show good agreement with each other and the high temperature points fit a $T^{3/2}$ slope, while below $60^{o}K$, there is clearly a change of dependence to a higher order of T and a T^2 fit to these points is shown. However, the observed change at $100^{o}K$ to a variation linear with T in the Tb 405 Å film is not seen in the magnetization data analysis and the reason for this second slope change is not understood.

In Figure 6.26 is shown the variation of ρ_{spin} of films of

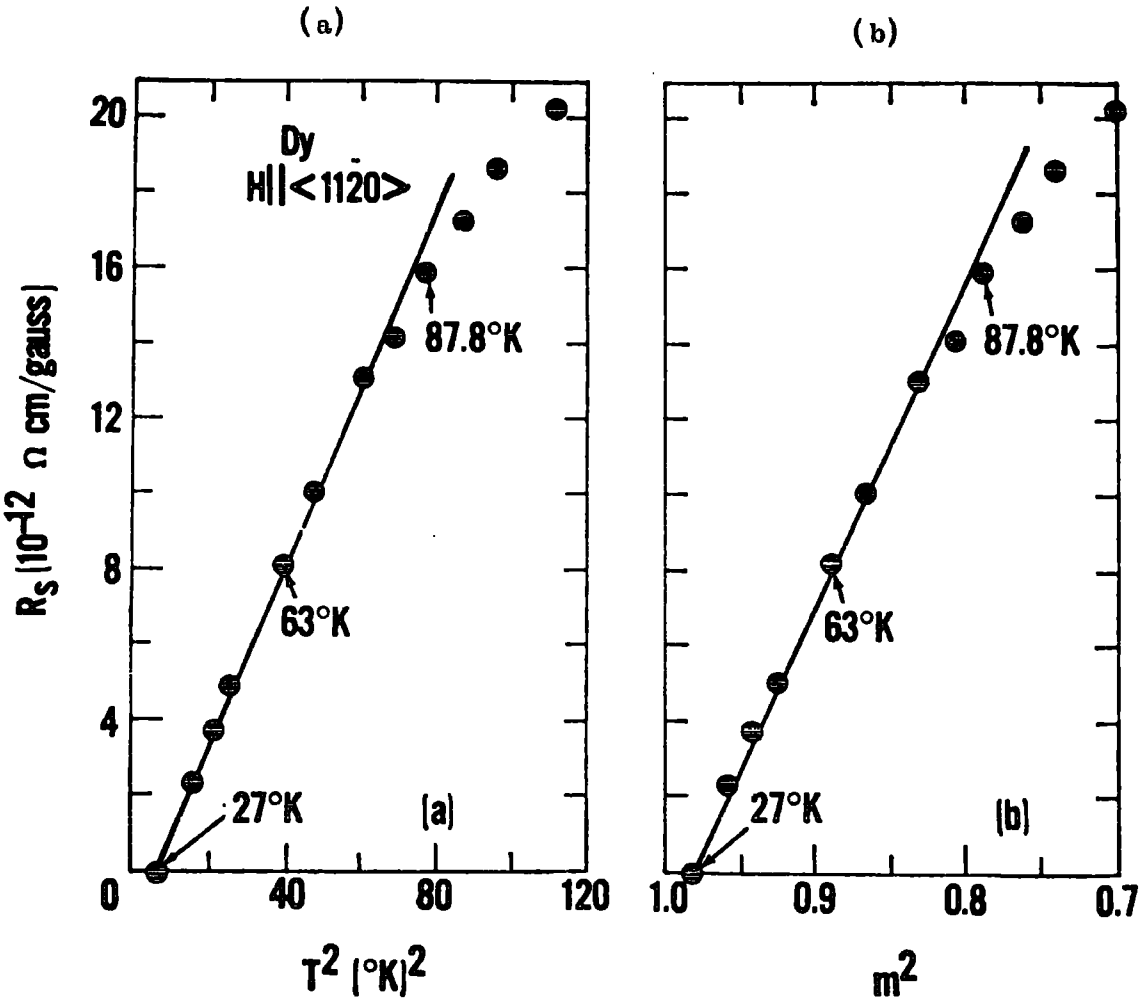

Fig. 6.24

Rhyne's results for the behaviour of the anomalous Hall coefficient in single-crystal Dysprosium (75).

(a) The dependence of R_s on T^2 at low temperatures.

(b) The dependence of R_s on the square of the reduced magnetization $\frac{M(T)}{M(0)}$.

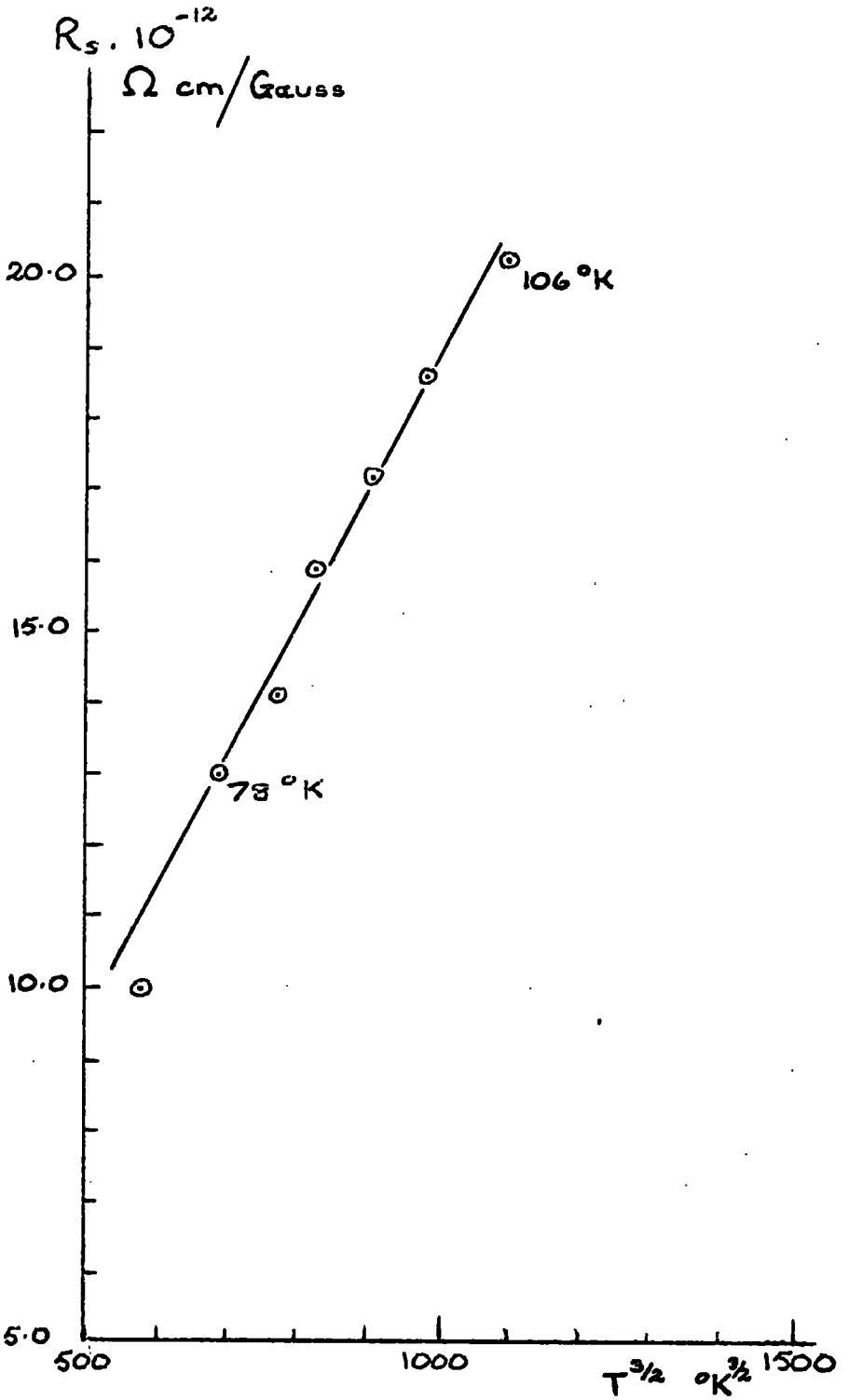

Fig. 6.25

Anomalous Hall coefficient R_s vs. $T^{3/2}$ for Dy [after Rhyne (75).]

Dy, Gd and Tb with $\left[M_s^2(0) - M_s^2(T)\right]$ for these metals as determined from other authors (97,117,120). It is apparent that equation 3.43 is obeyed fairly well and it therefore appears from the foregoing results from gadolinium, terbium and dysprosium that there is experimental corroboration of the quantitatively established relationships between ρ_{spin}, R_s and the spontaneous magnetization and that it is possible to explain the variation of $\rho_{spin}(T)$ of these metals on this basis.

Since the $\rho_{spin}(T)$ curves of holmium are very similar to those of terbium and dysprosium, the behaviour of $\rho_{spin}(T)$ of holmium is almost certainly due to the same cause; unfortunately, the data of Strandburg et al. (121) on the magnetization of single crystal holmium and that of Rhodes et al. (122) on polycrystalline holmium, are too brief to permit analysis, while Volkenshtein and Fedorov (123) were not able to achieve the separation of R_s from their measurements of the Hall effect of holmium.

The singular behaviour of the spin-disorder resistivities of the Er 1404 Å film, which has a $T^{5/2}$ proportionality between 36°K and 54°K and the Tm 2180 Å film, which varies as T^{10} between 26°K and 32°K, has not been explained in the same way as has the behaviour of the spin resistivities of Gd, Tb, Dy and Ho.

The spin resistivity of the Er 1404 Å film does not follow

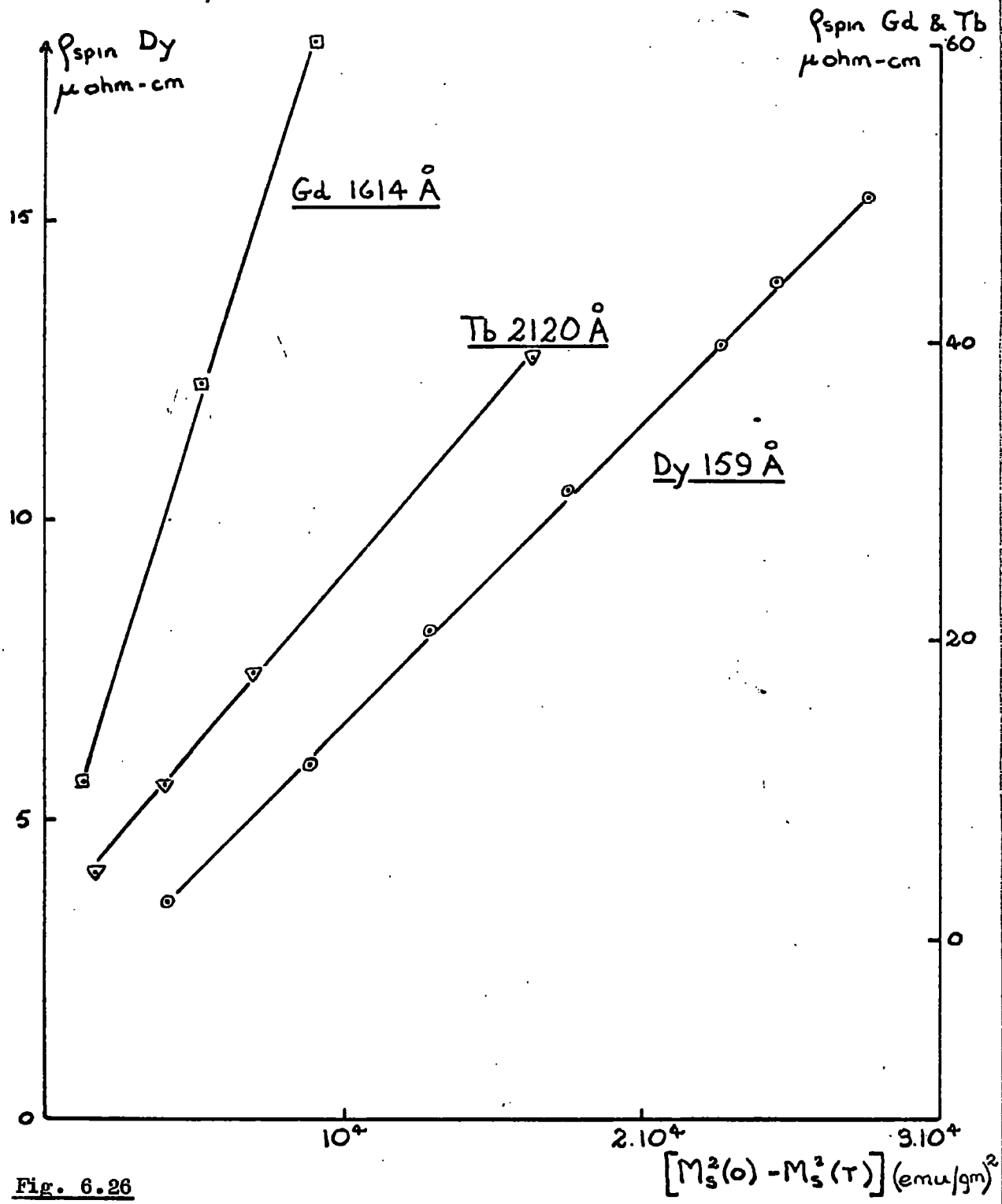

Fig. 6.26

Variation of ρ_s of films of Gd, Tb and Dy with $\left(M_s^2(0) - M_s^2(T)\right)$.

the prediction of Mackintosh (91) that $\rho_{spin} \propto T^4 \exp(-\Delta/kT)$ and so attempts have been made as before to explain the observations from the magnetization results on erbium single crystals of Green et al. (124) and the Hall effect measurements on polycrystalline erbium of Volkenshtein et al. (125). These failed however, owing to insufficient data.

Likewise, the Hall effect measurements of Volkenshtein et al. (126) and the magnetization measurements of Rhodes et al. (122) on polycrystalline thulium are not sufficiently detailed for analysis and so there is no substantiating evidence to account for the observed behaviour of the spin-disorder resistivities of erbium and thulium. However, it is certain that the peculiarities of the spin resistivities of these metals are in some complex way connected with those of their magnetic structures in the range of the magnetically ordered states and obviously, measurement of the anomalous Hall effect in single crystal specimens of these metals would provide further evidence for explaining this connection.

6.3 Summary of Results.

Owing to limitations in preparative techniques, it is found to be impossible to grow films of the rare earth metals to any specified thickness, except in the case of dysprosium, which proved

to be very easy to evaporate. Therefore, only in the case of dysprosium has it been possible to examine the electrical and associated magnetic parameters over a wide film thickness; the parameters of the remaining metals being examined in limited thickness ranges.

A film thickness dependence is generally observed in the Néel point θ_N and in the spin-disorder resistivity ρ_{spin}, although in the case of ρ_{spin}, the degree of variation does not appear to be consistent with thickness. The variation of ρ_{spin} of dysprosium is examined in greatest detail and it is suggested that the observed fall-off of spin resistivity with thickness, which can be extrapolated to zero at zero thickness, is related to the variation of magnetization with thickness in the films.

Associated with the thickness dependence of ρ_{spin}, equations derived by Rocher imply an associated dependence of the effective mass and the exchange energy and these equations are evaluated for the dysprosium results. However, some reservation is made about the validity of this approach on the grounds that the assumptions made by Rocher in the derivation of his equations may be incorrect.

The variation of $\rho_{spin}(T)$ of the films is examined. In the low temperature region, where spin-wave theory is applicable, Tb, Dy and Ho films are found to display a change in the

temperature dependence of ρ_{spin} between 60°K and 70°K. Below 60°K, the variation of $\rho_{spin}(T)$ of terbium and dysprosium is explained in terms of a spin-wave excitation energy Δ and the expression $\rho_{spin} \propto T^2 \exp(-\Delta/kT)$ best describes the behaviour of $\rho_{spin}(T)$. Above 60°K, a change to a $T^{3/2}$ dependency occurs and there is no quantitative explanation for this. However, it is shown that in agreement with theory, the behaviour of $\rho_{spin}(T)$ of Gd, Tb and Dy can be related to the temperature dependence of the spontaneous magnetization and additionally in the case of dysprosium, to the temperature dependence of the anomalous Hall coefficient. Owing to a lack of available data, no correlations can be made for holmium although the behaviour of $\rho_{spin}(T)$ is similar to that of terbium.

Erbium and thulium possess more complicated ordered magnetic structures and the behaviour of $\rho_{spin}(T)$ in these metals differs from the other metals. At the present time, this behaviour is not understood and the Hall effect measurements on single crystal specimens are needed for confirmation of the observed temperature dependence of ρ_{spin}.

Finally, magnetoresistive studies detected negative effects in Gd, Tb and Dy with fields applied transversely to the electric field. The anomalous peak at the Néel point is suppressed in Dy and Tb and a small demagnetizing field effect is observed in dysprosium.

6.4 Suggestions for Further Work.

Obviously, the preceding report is far from being a full investigation of resistance in thin films of the rare earth metals, because of the limitations in the thicknesses of the films and because the films were essentially disorientated deposits, although some evidence of a degree of preferential orientation was detected. The logical progression from work of this kind on partially orientated aggregates of crystallites is to the study of mono-crystalline films with single orientations.

In principle, it is now possible, by one or more of the several preparative techniques available, to grow epitaxial films of most materials which have been studied in bulk single crystal form. Moreover, epitaxy can provide new orientations, or crystalline layers with near perfect surface structures, which are very difficult to produce in bulk crystals.

Considerable theoretical and experimental research has been devoted to studies of size effects which, in randomly orientated deposits, influence electrical resistivity and magnetic properties as the film thickness decreases through a critical range. Analyses of such phenomena are complicated by incomplete knowledge of detailed film structure and could be simplified greatly by using epitaxial films with single orientations and atomically smooth surfaces. There is considerable scope in this field in the

evaluation of anisotropic electrical properties associated with directional ordering. Magnetoresistance of single crystal films is also one method of evaluating Fermi surface topology.

However, the epitaxial growth of films of the rare earth metals is an almost completely untouched field and the possible research potential is enormous. Even on polycrystalline films of rare earth metals, the scope for work is almost limitless but in the confines of the present study, clearly, magnetoresistance studies at higher fields would be of interest, while magnetization measurements may assist in resolving the observed thickness variations of the various electrical parameters. Extension of interest to alloy systems may also add to the knowledge of the behaviour of the spin resistivity in these thin films.

ACKNOWLEDGEMENTS.

I should like to express my sincere thanks to my supervisor Dr. K.N.R. Taylor, for his continual guidance and assistance on all stages of this project.

I am also grateful to Professor G.D. Rochester F.R.S., for the research facilities made available to me and to the staff of the Physics Department workshops for their technical assistance on apparatus construction.

An acknowledgement is also due to my fellow research students for many helpful comments and to my wife for her patience in typing this manuscript.

This work was performed during the tenure of a Research Studentship from the Science Research Council from 1966 to 1969.

F.M.K.L.

August 1969.

REFERENCES

1. Stoner E.C. Repts. Prog. Phys. 11, 43, (1948)
   Proc.Roy.Soc. A165, 372,(1938); A169, 339,(1939)
2. Slater J.C. Phys.Rev. 49, 537,(1936)
3. Ridley E.C. Proc.Camb.Phil.Soc. 56, 41,(1960)
4. Sternheimer R.M. Phys.Rev. 80, 102,(1950)
5. Judd B.R. & Lindgren I. Phys.Rev. 122, 1802,(1961)
6. Elliott R.J. & Stevens K.W.H. Proc.Roy.Soc. A219, 387,(1953)
7. Bleaney B. Proc.Phys.Soc. 68A, 937,(1955)
8. Freeman A.J. & Watson R.E. Phys.Rev. 127, 2058,(1962)
9. Kasuya T. Progr.Theor.Phys.(Kyoto) 16, 45,(1956)
10. Yosida K. Phys.Rev. 106, 893,(1957)
11. Liu S.H. Phys.Rev. 121, 451,(1960); Phys.Rev. 123, 470,(1961)
12. Kaplan T.A. & Lyons D.H. Phys.Rev. 129, 2072,(1963)
13. Ruderman M.A. & Kittel C. Phys.Rev. 96, 99, (1954)
14. Yosida K. Phys.Rev. 106, 893,(1957)
15. de Gennes P.G. J.Phys.Rad. 23, 510,(1962)
16. Kasuya T. in "Magnetism" ed. Rado & Suhl Academic Press Vol. 11b (1966)
17. Elliott R.J. ibid. Vol. 11a
18. Roth L.M., Zeiger H.J. & Kaplan T.A. Phys.Rev. 149, 519,(1966)
19. Bloch F. Z.Phys. 52, 555,(1928)
20. Kroll W. Z.Phys. 80, 50,(1933)
21. Kohler M. Z.Phys. 124, 772,(1948); Z.Phys. 125, 679,(1949)
22. Sondheimer E.H. Proc.Roy.Soc. A203, 75,(1950)
23. Ziman J.M. Proc.Roy.Soc. A226, 436,(1954)
24. Blatt F.J. "Physics of Electronic Conduction in Solids" McGraw-Hill (1968) Chapter 7
25. Mott N.F. Proc.Phys.Soc. 47, 571,(1935)
    Proc.Roy.Soc. A153, 699,(1936)
26. Wilson A.H. Proc.Roy.Soc. A167, 580, (1938)
27. Vonsovski S.V. Zh.Eksperim.i Teor.Fiz. 18, 219,(1948)
28. Turov E.A. Izv.Akad.Nauk.SSSR,Ser.Fiz. 19, 426, (1955)
29. Kasuya T. Progr.Theor.Phys.(Kyoto) 16, 58, (1956)
30. de Gennes & Friedel J. J.Phys.Chem.Solids 4, 71,(1958)
31. Kasuya T. Progr.Theor.Phys.(Kyoto) 22, 227, (1959)
32. Mannari I. Progr.Theor.Phys.(Kyoto) 22, 335, (1959)
33. van Peski-Tinbergen T. & Dekker A.J. Physica 29, 917,(1963)
34. Chopra K.L. & Bobb L.C. in "Single Crystal Films" ed. Francombe & Sato, Pergammon Press (1964)
35. Ennos A.E. Brit.J.Appl.Phys. 8, 113, (1957)
36. Lucas M.S.P. J.Appl.Phys. 36, 1632,(1965)

37. Fuchs K. Proc.Camb.Phil.Soc. 34, 100,(1938)
38. Sondheimer E.H. Adv.Phys. 1,1,(1952)
39. Mayer H. in "Structure and Properties of Thin Films" ed. Neugebauer, Newkirk & Vermilyea. Wiley (1959)
40. Kittel C. Phys.Rev. 70, 965,(1946)
41. Valenta L. Czech.J.Phys. 7, 127,136,(1957)
42. Pearson J.J. Phys.Rev. 138, A213,(1965)
43. Corciovei A. Czech.J.Phys. 10, 568, 917,(1960) J.Phys.Chem.Solids 20, 162,(1961)
44. Klein M.J. & Smith R.S. Phys.Rev. 81, 378,(1951)
45. Glass S.J. & Klein M.J. Phys.Rev. 109, 288,(1958)
46. Doring W. Z.Naturforschg. 16a, 1008,(1961); 16a, 1146,(1961)
47. Corciovei A. Phys. Rev. 130, 2223,(1963)
48. Holstein T. & Primakoff H. Phys.Rev. 58, 1098,(1940)
49. Wojtczak L. Rev.Roum.Phys. 12, 577,(1967)
50. Davis J.A. J.Appl.Phys. 36, 3520,(1965)
51. Szczeniowski S. & Wojtczak L. J.Appl.Phys. 39, 1377,(1968)
52. Valenta L. Phys.Stat.Solidi 2, 112,(1962)
53. Colvin R.V., Legvold S. & Spedding F.H. Phys.Rev. 120, 741,(1960)
54. Elliott R.J. Phys.Rev. 124, 346,(1961)
55. Kaplan T.A. Phys.Rev. 124, 329,(1961)
56. Yosida K. & Miwa H. Progr.Theor.Phys.(Kyoto) 26, 693, (1961)
57. Colvin R.V. Legvold S. & Spedding F.H. Phys.Rev. 120,741,(1960)
58. Nigh H.E. Legvold S. & Spedding F.H. Phys.Rev. 132, 1092,(1963)
59. Strandburg et al. Phys. Rev. 127, 2046, (1962)
60. Green R.W. et al. Phys. Rev. 122, 827, (1961)
61. Hall P.M. et al. Phys. Rev. 117, 971, (1960)
62. Boas W. & Mackenzie J.K. Progr.in Metal Phys. 2, 90, (1950)
63. Elliott R.J. & Wedgewood F.A. Proc.Phys.Soc. 81, 946, (1963)
64. Edwards L.R. & Legvold S. Phys. Rev. 176, 753, (1968)
65. Rocher Y.A. Phil.Mag.Suppl. 11, 233,(1962)
66. e.g. Kittel C. "Introduction to Solid State Physics" p.296
67. Pugh E.M. et al. Phys.Rev. 80, 688, (1950)
68. Karplus R. & Luttinger J.M. Phys.Rev. 95, 1154,(1954)
69. Kondo J. Progr.Theor.Phys. 27, 772, (1962)
70. Maranzana F.E. Phys.Rev. 160, 421, (1967)
71. Irkhin P. & Abel'skii Sh. Soviet Phys. Solid State 6,1283,(1964)
72. Kikoin I.K. et al. Soviet Phys. Doklady 4, 386, (1959)
73. Kagan Yu. & Maksimov L.A. Soviet Phys. Solid State 7,422, (1965)
74. Kikoin I.K. & Igosheva T.N. Soviet Phys. JETP 19, 48,(1964)
75. Rhyne J.J. Phys.Rev. 172, 523, (1968)
76. Pound G.M. et al. J.Chem.Phys. 22, 1215,(1954)
77. Sears G.W. & Cahn J.W. J.Chem.Phys. 33, 494, (1960)
78. Walton D. J.Chem. Phys. 37, 2182, (1962)
79. Rhodin T.N. & Walton D. Trans. 9th Natl. Vacuum Symp. L.A. 1962 Macmillan N.Y.

80. Levinstein H. J. appl. Phys. 20, 306, (1949)
81. Stahl H.A. J. appl. Phys. 20, 1, (1949)
82. Evans D.M. & Wilman H. Acta.cryst.Camb. 5, 731, (1952)
83. Koenig H. & Helwig G. Optik 6, 111, (1950)
84. Holland L. J. opt. Soc. Amer. 42, 686, (1952)
85. Barton D.M. Vacuum 3, 51, (1953)
86. Colbert W.H. & Weinrich A.R. U.S. Pat. 2383469 (1943)
87. Prutton M. in "Thin Ferromagnetic Films" p.12(Butterworth 1962)
88. Dean E.R. J. appl. Phys. 34, 2930, (1964)
89. Milgram A.A. & Lu C. J. appl. Phys. 39, (1968)
90. e.g. "Principles of Vacuum Engineering" by Pirani M. & Yarwood J. (Chapman & Hall, London 1961) p.514
91. Mackintosh A.R. Phys.Rev.Letters 9, 90, (1962)
92. Miwa H. Prog.Theor.Phys.(Kyoto) 28, 208, (1962)
93. Koehler W.C., Cable J.W., Child H.R., Wilkinson M.K. Wollan E.O. Phys. Rev. 158, 450, (1967)
94. Davis D.D. & Bozorth R.M. Phys.Rev. 118, 1543, (1960)
95. Bozorth R.M. & Gambino R.J. Phys.Rev. 147, 487, (1966)
96. Edwards L.R. & Legvold S. Phys.Rev. 176, 753, (1968)
97. Behrendt D.R. & Legvold S. Phys. Rev. 109, 1544, (1958)
98. Hoffman R.W. in "The Use of Thin Films in Physical Investigations" ed. Anderson J.C. (Academic Press 1966) p.270
99. Milton J.E. & Scott T.A. Phys.Rev. 160, 387, (1967)
100. Prütton M. Nature 193, 565, (1963)
101. Horikoshi et al. J. appl. Phys.(Japan) 1, 304, (1962)
102. Schuler C. Z.Angew. Phys. 15, 218, (1965)
103. Neugebauer C.A. & Webb M.B. J.appl.Phys. 33, 74, (1962)
104. Hartman T.E. J. appl. Phys. 34, 943, (1963)
105. Neugebauer C.A. Phys. Rev. 116, 1441, (1959)
106. Crittenden E.C. & Hoffman R.W. Rev.Mod.Phys. 25, 310, (1953)
107. Dekker A.J. J. appl.Phys. 36, 906, (1965)
108. Hennephof J. & Hoekstra G. Proc.Phys.Soc. 1, 1140, (1968)
109. Niira K. Phys. Rev. 117, 129, (1960)
110. Sze N.H., Rao K.V. & Meaden G.T. To be published.
111. Yosimori A. J.Phys.Soc.(Japan) 14, 807, (1959)
112. Kaplan T.A. Phys. Rev. 124, 329, (1961)
113. Rhyne J.J. & Clark A.E. J.appl.Phys. 38, 1379, (1967)
114. Graham C.D. J.appl.Phys. 38, 1375, (1967)
115. Volkenshtein N.V., Grigorova G.V. & Fyodorova G.V. Soviet Phys. JETP 19, 1003, (1966)
116. Lee R.S. & Legvold S. Phys. Rev. 162, 431, (1967)
117. Elliott J.F. Legvold S. & Spedding F.H. Phys.Rev. 91, 28, (1953)
118. Elliott J.F. et al. Phys. Rev. 94, 1143, (1954)
119. Thorburn W.C. et al. Phys. Rev. 112, 56, (1958)
120. Hegland D.E. et al. Phys. Rev. 131, 158, (1963)

121. Strandburg D.L. et al. Phys. Rev. 127, 2046, (1962)
122. Rhodes B.L. et al. Phys. Rev. 109, 1547, (1958)
123. Volkenshtein N.V. & Fedorov G.V. Soviet Phys. Solid State 8, 1500, (1966)
124. Green R.W. et al. Phys. Rev. 122, 827, (1961)
125. Volkenshtein N.V. & Fedorov G.V. Soviet Phys. JETP 17, 560, (1963)
126. Volkenshtein N.V. & Fedorov G.V. Phys. Metals Metallography 20, 28, (1965)